universität wien

MASTERARBEIT | MASTER'S THESIS

Titel | Title

Crosstalk between Enzymatic and Non-enzymatic Posttranslational Modifications: Analyzing the Interplay of Site-Specific Glycation and Ubiquitination of α-Synuclein

verfasst von | submitted by

Judith Görlich BSc

angestrebter akademischer Grad | in partial fulfilment of the requirements for the degree of

Master of Science (MSc)

Wien | Vienna, 2024

Studienkennzahl lt. Studienblatt | Degree programme code as it appears on the student record sheet:	UA 066 862
Studienrichtung lt. Studienblatt | Degree programme as it appears on the student record sheet:	Masterstudium Chemie
Betreut von | Supervisor:	Univ.-Prof. Dr. Christian Friedrich Wilhelm Becker
Mitbetreut von | Co-Supervisor:	Somnath Mukherjee BSc MSc PhD

Table of contents

Table of contents

Acknowledgement

First and foremost, I would like to sincerely thank Professor Dr. Christian Becker for giving me the opportunity to participate my Master's thesis in his research group and for his support and advice.

I would also like to thank my supervisor Dr. Somnath Mukherjee for mentoring me during my Master's thesis and teaching me the molecular biology methods and the practical aspects involved. I greatly appreciate his support, encouragement and patience and would especially like to thank him for always listening to my problems and questions.

I am also grateful to the entire research group for the friendly interaction I experienced inside and outside the lab.

Finally, I would also like to thank my family and friends who have always supported me in difficult times. I am eternally grateful.

Abbreviations

αS/αSyn	alpha Synuclein
ACN	Acetonitrile
AcOH	Acetic acid
AD	Alzheimer’s disease
AGEs	Advanced glycation end products
AMP	Ampicillin
APS	Ammonium persulfate
ATP	Adenosine triphosphate
BCA	Bicinchoninic acid assay
Boc	Tert-butyloxycarbonyl
CAM	Chloramphenicol
CEL	N-(Carboxyethyl)lysine
Cl-HOBt	6-Chloro-1-hydroxybenzotriazole dihydrate
CTD	C-Terminal domain
DB	Desulfurization buffer
DCM	Dichloromethane
DIC	N,N′-Diisopropylcarbodiimide
DIPEA	N,N-Diisopropylethylamine
DMF	N,N-Dimethylformamide
DMS	Dimethyl sulfide
DTT	Dithiothreitol
E.coli	*Escherichia coli*
EDTA	Ethylenediaminetetraacetic acid
EPL	Expressed protein ligation
EPR	Electron paramagnetic resonance
ESI-MS	Electrospray ionization mass spectrometry

Fmoc	Fluorenylmethoxycarbonyl
Gdn HCl	Guanidine hydrochloride
HATU	O-(7-Azabenzotriazol-1-yl)-N,N,N′,N′-tetramethyluronium-hexafluorphosphat
HEPES	4-(2-hydroxyethyl)-1-piperazineethanesulfonic acid
His_6	Hexahistidine
HPLC	High performance liquid chromatography
LB	Ligation buffer
LCMS	Liquid chromatography-mass spectrometry
MES	2-(N-morpholino)ethanesulfonic acid
MESNa	Sodium 2-mercaptoethanesulfonate
MG	Methylglyoxal
$mK_{6,10,12,21,23}$	CEL instead of lysine on sequence position 6,10,12,21 or 23
MOLD	Methylglyoxal-lysine dimer
MPAA	4-Mercaptophenylacetic acid
MS	Mass spectrometry
NAC	non-Aβ-component
NaPi	Sodium Phosphate Buffer
NCL	Native chemical ligation
Ni-NTA	Nickel-nitrilotriacetic acid
NMR	Nuclear magnetic resonance
nPTM	Non-enzymatic posttranslational modification
OtBu	Tert-butoxide
Oxyma	Ethyl cyanohydroxyiminoacetate
PBS	Phosphate-buffered saline
PD	Parkinson’s disease
PH	Peptide hydrazide

PPI	Protein-protein interaction
PTM	Posttranslational modification
RP	Reversed phase
SDS	Sodium dodecyl sulfate
SDS-PAGE	Sodium dodecyl sulfate polyacrylamide gel electrophoresis
SEM	Scanning electron microscopy
SNARE	Soluble N-ethylmaleimide-sensitive-factor attachment receptor
SPPS	Solid phase peptide synthesis
TBS	Tris-buffered saline
TCEP	Tris(2-carboxyethyl)phosphine
TE	Thioester
TEM	Transmission electron microscopy
TEMED	Tetramethylethylenediamine
TEV	Tobacco etch virus
TFA	Trifluoracetic acid
TIPS	Triisopropylsilane
ThT	Thioflavin T
Tris	Tris(hydroxymethyl)aminomethane
Ub	Ubiquitin
UPS	Ubiquitin-proteasome system
VA-044	2,2’-Azobis[2-(2-imidazolin-2-yl)propane] Dihydrochloride
Wt	Wild type

Abstract

α-synuclein (αSyn) aggregation is known to be associated with Parkinson's disease and other neurodegenerative disorders generally termed as synucleinopathies. The high number of lysine residues in this 140 amino acid long, intrinsically disordered protein makes it an obvious target for electrophilic metabolites, leading to the formation of advanced glycation end (AGE) products. Especially for a long-lived protein, such as αSyn, the propensity of formation of AGEs leading to aggregation and dysfunction seems to be a plausible route towards neurodegenerative etiologies.

In this thesis the interplay between enzymatic (ubiquitination) and non-enzymatic (glycation) posttranslational modifications of αSyn was analyzed. Expressed protein ligation was used to access site-specifically N_{ε}-(carboxyethyl)lysine (CEL) modified αSyn, to generate a library of homogeneously glycated αSyn, where the site of modification spans the N-terminal domain (K6, K10, K12, K21, K23). Therefore, the C-terminal part αS(30-140) was produced recombinantly having an N-terminal cysteine, while the N-terminal part αS(1-29) was produced synthetically with a C-terminal thioester utilizing Fmoc-SPPS. Six full-length αSyn variants were obtained utilizing ligation and metal-free desulfurization. The aggregation behaviour of all variants was compared utilizing ThT assay and SEM imaging. Whereby, the modified αSyn variants showed, on average, a lower ThT fluorescence response than the wild type protein, but no significant differences could be pointed out. The modified αSyn variants were then tested in an *in vitro* ubiquitination set-up to determine the impact of such site-specific CEL modification on the ubiquitination profile. The ubiquitination assay showed no significant differences between the variants. Which leads to the assumption that only one lysine position blocked by CEL does not have an influence on the overall ubiquitination as ubiquitin chains can attach to other positions, leading to differences in the ubiquitylation pattern (not analyzed here). All variants were ubiquitinated and monoubiquitination and diubiquitination were mainly found.

Zusammenfassung

Die Aggregation von α-Synuclein (αSyn) wird bekanntermaßen mit der Parkinson-Krankheit und anderen neurodegenerativen Erkrankungen in Verbindung gebracht, die allgemein als Synucleinopathien bezeichnet werden. Die hohe Anzahl von Lysinresten in diesem 140 Aminosäuren langen, intrinsisch ungeordneten Protein macht es zu einem offensichtlichen Ziel für elektrophile Metaboliten, die zur Bildung von fortgeschrittenen Advanced glycation end-product (AGE) führen. Insbesondere bei einem langlebigen Protein wie αSyn scheint die Neigung zur Bildung von AGEs, die zu Aggregation und Dysfunktion führen, ein plausibler Weg zu neurodegenerativen Ätiologien zu sein.

In dieser Arbeit wurde das Zusammenspiel zwischen enzymatischen (Ubiquitinierung) und nicht-enzymatischen (Glykierung) posttranslationalen Modifikationen von αSyn analysiert. Expressed Protein Ligation wurde verwendet, um Zugang zu ortsspezifisch Nε-(Carboxyethyl)lysin (CEL) modifiziertem αSyn zu erhalten, um eine Bibliothek von homogen glykiertem αSyn zu generieren, wobei sich der Ort der Modifikation über die N-terminale Domäne (K6, K10, K12, K21, K23) erstreckt. Dafür wurde der C-terminale Teil αS(30-140) rekombinant mit einem N-terminalen Cystein hergestellt, während der N-terminale Teil αS(1-29) synthetisch mit einem C-terminalen Thioester unter Verwendung von Fmoc-SPPS hergestellt wurde. Sechs αSyn-Varianten in voller Länge wurden durch Ligation und metallfreie Entschwefelung gewonnen. Das Aggregationsverhalten aller Varianten wurde mit Hilfe des ThT-Versuchs und der SEM-Bildgebung verglichen. Dabei zeigten die modifizierten αSyn-Varianten im Durchschnitt eine geringere ThT-Fluoreszenzintensität als das Wildtyp-Protein, es konnten jedoch keine signifikanten Unterschiede festgestellt werden. Die modifizierten αSyn-Varianten wurden dann in einem *in-vitro* Ubiquitinierungsversuch getestet, um die Auswirkungen einer solchen ortsspezifischen CEL-Modifikation auf das Ubiquitinierungsprofil zu bestimmen. Der Ubiquitinierungsversuch zeigte keine signifikanten Unterschiede zwischen den Varianten. Dies legt die Vermutung nahe, dass nur eine durch CEL blockierte Lysinposition keinen Einfluss auf die Ubiquitinierung hat, da Ubiquitinketten auch an anderen Positionen anhaften können, was zu Unterschieden im Ubiquitinierungsmuster führt (hier nicht analysiert). Alle Varianten waren ubiquitiniert und es wurden hauptsächlich Mono- und Diubiquitinierungen gefunden.

1 Introduction

1.1 Alpha Synuclein (αSyn)

The protein α-synuclein (αSyn) was independently discovered on multiple occasions.[1] Maroteaux et al. were the first to name and describe it in 1988 as a neuron-specific protein localized in the nucleus and the presynaptic nerve terminals.[2] αSyn, produced by the SNCA gene[3], is an intrinsically disordered protein prone to aggregation and implicated in different neurodevelopmental disorders.[4,5] It consists of 140 amino acids and can be divided into three domains (Figure 1): the N-terminal (residue 1-60), the central non-Aβ-component (NAC) domain (residue 61-95), and the C-terminal (residue 96-140).[6] The N-terminal contains highly conserved repeats forming an amphipathic alpha-helix, while the NAC domain is highly amyloidogenic, driving the protein's folding from coils into beta-sheet structures into fibrils.[1,7] The C-terminal is polar, phosphorylated, and less conserved.[1] It is a long-lived human protein containing 15 lysine residues (lysine-rich).[8,9] Recombinantly expressed, purified αSyn behaves in vitro like a natively unfolded protein, while binding to artificial membranes it forms an α-helix.[10,11]

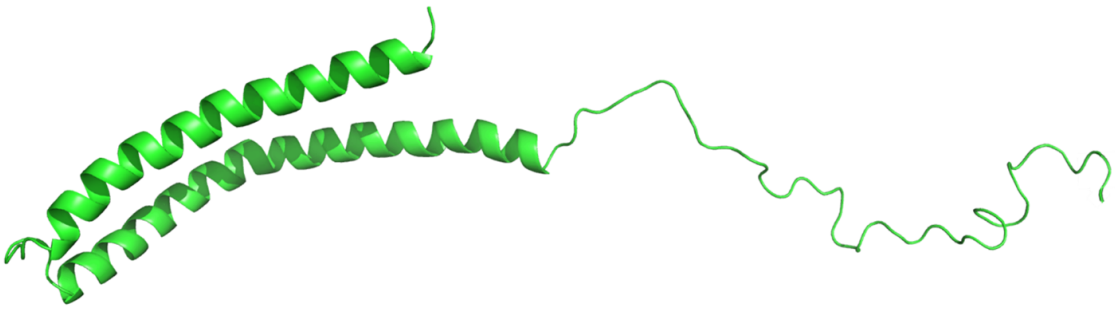

1	MDVFMKGLSK	AKEGVVAAAE	KTKQGVAEAA	GKTKEGVLYV	GSKTKEGVVH
51	GVATVAEKTK	EQVTNVGGAV	VTGVTAVAQK	TVEGAGSIAA	ATGFVKKDQL
101	GKNEEGAPQE	GILEDMPVDP	DNEAYEMPSE	EGYQDYEPEA	

Figure 1 top: predicted structure of alpha synuclein (PyMOL); bottom: Sequence of alpha synuclein (blue: N-terminal domain; black: non-Aβ-component (NAC) domain; red: C-terminal domain)[6,12].

The synuclein family includes alpha-, beta-, and gamma-synuclein. Alpha-synuclein is most significant for its role in neurodegenerative diseases, while beta-synuclein has neuroprotective properties, and gamma-synuclein is linked to certain forms of cancer.[13,14]

In its native state, αSyn is involved in synaptic transmission, acting as a chaperone for synaptic SNARE proteins, regulating neuronal redox balance, and inhibiting apoptosis.[13,15–17] However, its overexpression or misfolding leads to neurotoxicity and neurodegeneration.[13] Various post-translational modifications (PTMs), such as

phosphorylation, nitration, acetylation, ubiquitination, sumoylation or glycation, influence its aggregation and function.[18–20]

In Parkinson's disease (PD) and other synucleinopathies αSyn's misfolding and aggregation is a hallmark.[21] Understanding the precise mechanisms of αSyn aggregation and toxicity is crucial for developing effective therapeutic strategies against related neurodegenerative diseases.[21] Parkinson's disease (PD) is after Alzheimer's disease (AD) the second most important neurodegenerative disorder and is characterized by the formation of toxic aggregates of the protein αSyn.[6,22] Studies show that high levels of αSyn correlate with disease progression, emphasizing the importance of cellular mechanisms that degrade excess αSyn.[22] Injecting αSyn fibers into healthy mice brains resulted in PD-like pathology, demonstrating its role in disease causation.[23] Gene duplications and triplications are linked to early-onset PD and animal models overexpressing αSyn further suggest that its accumulation accelerates neurodegeneration.[22,24]

αSyn aggregates spread between neurons, contributing to Lewy body formation. Research indicates that this spread occurs through endocytosis, where donor cells with high αSyn levels (overexpression) transfer aggregates to neighboring neurons (without overexpression), leading to similar inclusions in recipient cells. Overall, maintaining proper αSyn levels is crucial in preventing its aggregation and the subsequent progression of neurodegenerative diseases.[22,25] Lewy bodies and Lewy neurites are αSyn aggregates which are found in PD and other synucleinopathies, leading to motor symptoms from dopaminergic neuron loss and various nonmotor symptoms due to broader neuronal deposition.[21,26,27] PD causes nonmotor symptoms such as depression, constipation, hyposmia, and rapid eye movement behavior disorder[27], and motor symptoms such as tremor, rigidity, progressive movement disability, and bradykinesia.[6]

αSyn also plays a role in multiple system atrophy and dementia with Lewy bodies, with differing cell-type deposition.[1,28] Its presence in Alzheimer's disease is noted in up to 60% of cases.[29] In addition to neurodegenerative diseases, αSyn is also associated with neurodevelopmental disorders, including autism spectrum disorder. Studies have detected αSyn in various body fluids and tissues, suggesting potential for early diagnosis of neurodevelopmental diseases.[13]

Research has shown that αSyn can be degraded through lysosomal, proteasomal and autophagic pathways, whereby the degradation process is influenced by the posttranslational modification of αSyn via monoubiquitination.[22,30] Mass spectrometry analysis revealed that αSyn can be monoubiquitinated at nine lysine residues (K6, 10, 12, 21, 23, 32, 34, 43, and 96), creating a heterogeneous mixture, whereby monoubiquitination at sites near the N terminus of αSyn tends to lead to proteasomal

degradation (26S proteasome), whereas sites closer to the center of the protein typically do not.[22]

Advanced glycation end-products (AGEs) play an important role as non-enzymatic posttranslational modification (nPTM) of αSyn.[18] Oxidative stress is considered an important pathogenic factor in Parkinson's disease that increases the formation of AGEs.[31] On LBs the most prevalent AGEs found are N_{ε}-(carboxyethyl)lysine (CEL) and methylglyoxal-lysine dimer (MOLD), which form when αSyn reacts with methylglyoxal (MG), a byproduct of glycolysis. This glycation alters the structure and function of αSyn, increasing its conformational heterogeneity and inhibiting its aggregation, but not disassembling preexisting fibrils, indicating that CEL formation occurs post-aggregation.[18] Glycation mainly affects the N-terminal domain of αSyn, impairing clearance, reducing its membrane binding, and promoting the accumulation of toxic oligomers, enhancing neurotoxicity.[21] These modifications are more pronounced in individuals with diabetes mellitus, potentially explaining the higher prevalence of PD in these patients. AGEs have a huge impact on the biophysical properties of αSyn and their potential role in PD pathogenesis.[18]

1.2 Synthesis Strategies for modified αSyn

1.2.1 Protein Expression

Protein expression is a critical biological process that allows the production of proteins often based on genetic manipulation of expression systems. Bacterial systems, especially *Escherichia coli* (*E. coli*), are widely used for producing recombinant proteins due to their fast growth, low cost, and well-understood genetics. However, protein expression in bacteria can be complicated by protein folding, the lack of post-translational modifications, and toxicity. To address these challenges, various strategies, including the co-expression of chaperones, fusion proteins, and optimized codon usage, are employed to enhance the yield and functionality of target proteins.[32] Different host organisms such as yeast, insect, and mammalian cells can be used to improve protein yield and functionality.[33]

Some heterologous proteins cannot be expressed in *E. coli* due to the presence of "rare" codons in the target mRNA, which are uncommon in *E. coli* but more frequent in human proteins.[34] This can lead to mistranslation, with lysine being inserted instead of arginine.[35] To overcome this issue, online tools like the rare codon calculator (RaCC, http://nihserver.mbi.ucla.edu/RACC/) can be used. Solutions include codon optimization of the gene for *E. coli* or using commercially available codon-optimized genes.[36] Alternatively, co-expressing rare tRNAs with the target gene or using specialized *E. coli* strains such as BL21 (DE3)-RIL/RP/RILP cells from Stratagene or

Rosetta cells from Novagen, containing plasmids for rare tRNAs can improve expression.[37,38]

Protein expression in *E. coli* has limitations in studying protein function, as it restricts to a limited number of amino acids that can be incorporated and makes precise post-translational modifications (PTMs) challenging. Total chemical synthesis of proteins provides a solution for this problem as Solid phase peptide synthesis (SPPS) allows specific modifications to the protein's structure, enabling the incorporation of any desired changes or labels. This is crucial for advanced biophysical spectroscopic methods like NMR, EPR, and laser Raman spectroscopy.[39,40]

1.2.2 SPPS

Solid phase peptide synthesis (SPPS) was developed by Robert Bruce Merrifield in 1963.[41] Originally, this technique was suited for the synthesis of peptides on small scales. Nowadays, strategies are used by which peptides can be synthesised on a large scale using SPPS.[41,42]

In SPPS, the C-terminal amino acid of a target peptide is bound to an insoluble polymer carrier. Further amino acids are then added by removing the N(α)-protecting group of polymer-attached amino acid, purifying the resin-bound residue by filtration and washing, and adding the next amino acid in its protected, activated form. After the formation of each new peptide bond, excess activated amino acids and soluble by-products are removed by filtration and washing. These steps are repeated until the protected peptide chain is completely built up. In the final step, all protecting groups are removed and the peptide chain is cleaved from the resin to obtain the crude peptide product (Figure 2). Purification by filtration and washing allows a large excess of activated amino acid to be utilised, allowing the reactions to proceed quickly and almost completely. As the product remains bound to the resin throughout the synthesis losses are minimised. If the synthesis is well planned and carried out, this leads to products with a high proportion of the desired peptide and a high yield. However, the maximum size of the synthesisable polypeptides is limited by accumulation of by-products resulting from incomplete reactions. Therefore, on average, peptides with a length of up to 50 amino acids can be produced in sufficient yield and purity.[39]

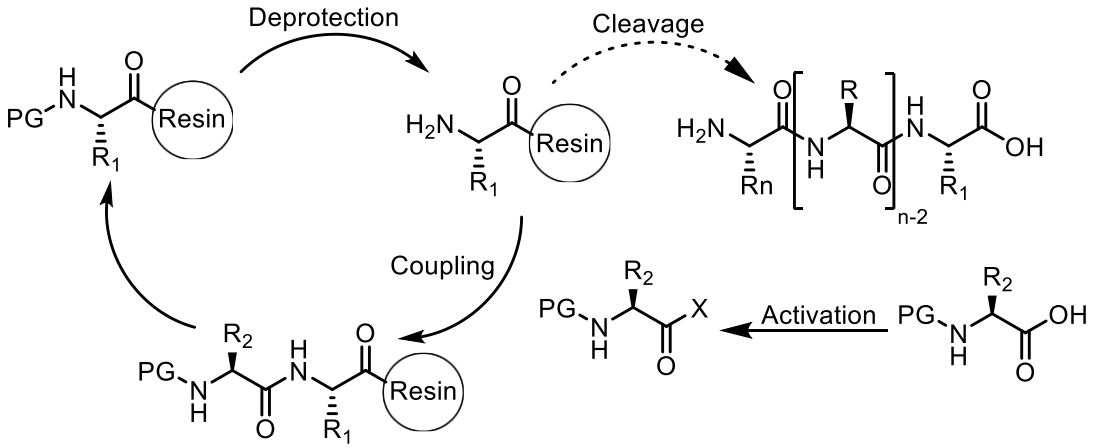

Figure 2 SPPS reaction scheme.

1.2.3 NCL

Native chemical ligation (NCL) is an important method for synthesis of peptides and proteins with more than 50 amino acids. It is a particularly mild and efficient method. This technique has greatly simplified the synthesis of proteins and peptides and expands the possibilities of protein research and development.[43] NCL has proven to be particularly valuable as it allows the synthesis of large and complex proteins that are difficult to access by conventional methods. The use of NCL has led to the production of numerous proteins that are important for biochemical studies and therapeutic applications.[44]

The NCL method, developed by Kent and colleagues in 1994[44], involves a selective reaction between two unprotected peptide segments, one with a C-terminal thioester and the other with an N-terminal cysteine (Cys) residue. This reaction occurs in aqueous conditions, typically at neutral pH and room temperature, with a chaotropic agent like guanidine to prevent the formation of secondary structures that could hinder the process. The ligation starts with a trans-thioesterification step, where the thiol group of the Cys residue attacks the thioester's carbonyl carbon, releasing a thiol and forming a new thioester intermediate. This intermediate then undergoes an S->N acyl shift, where the thiol segment’s terminal amine attacks the newly formed thioester, resulting in a native amide bond and restoring the Cys thiol side chain (Figure 3).[45]

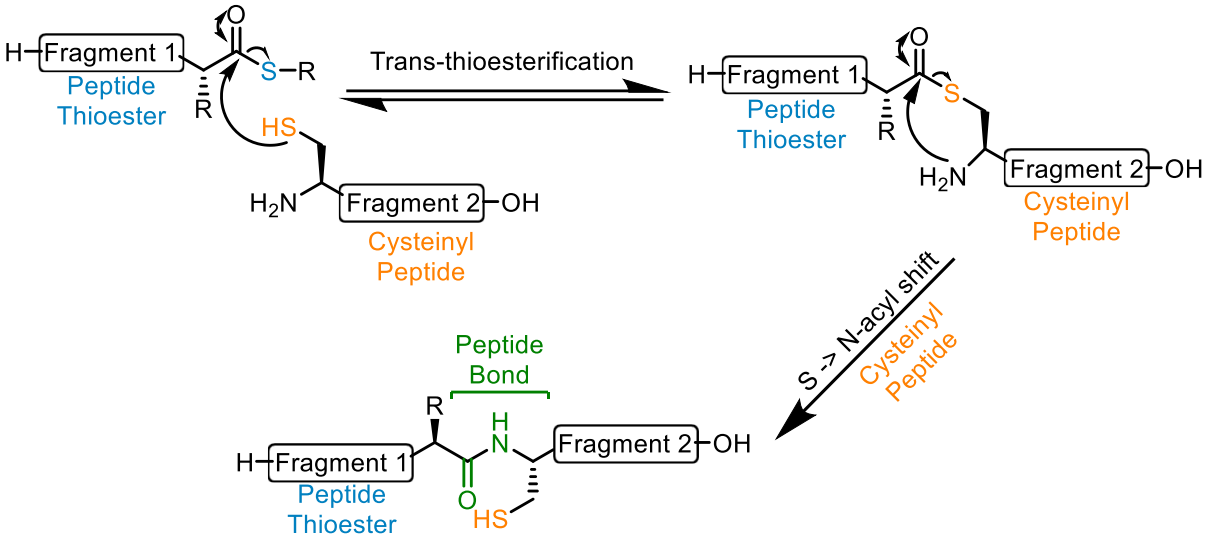

Figure 3 NCL reaction scheme (based on [45]).

Over the past 20 years, the ability to incorporate non-proteinogenic amino acids (such as D-amino acids or fluorescent labels) and post-translational modifications into proteins by connecting peptide segments has led to significant advances in peptide and protein research. Extensions to the original concept of NCL, included the development of thiol- and selenol-derived amino acids and methods for desulfurization and deselenization. The improved access to peptide thioesters, and the use of this method in combination with recombinantly expressed polypeptide segments (Expressed Protein Ligation, EPL) have helped to further expand the utility of the methodology.[45]

1.2.4 Inteins as tools for protein semisynthesis in EPL

Expressed protein ligation (EPL) is a technique used in protein semisynthesis, generally involving the reaction between a recombinant protein segment with a C-terminal thioesters and synthetic peptides containing an N-terminal cysteine in a chemoselective ligation process identical to NCL. The C-terminal thioesters of recombinant proteins are generated by utilizing natural inteins, which are protein segments that facilitate protein splicing.[46]

Applications of protein splicing include tagless protein purification, *in vitro* protein semi-synthesis, segmental isotopic labelling, protein and peptide cyclization, conditional protein splicing, and *in vivo* protein semi-synthesis.[47]

Inteins are self-processing segments found across all life forms which execute protein splicing, a multi-step biochemical reaction involving both the breaking and forming of peptide bonds. While their natural substrates are specific crucial proteins in host organisms, they can also function outside their usual context, allowing chemical modification of nearly any polypeptide chain. Because of this versatility, protein

chemists have used intein reactivity to modify proteins in numerous ways for biological research and potential therapeutic uses.[47]

An intein undergoes a distinctive autocatalytic process called protein splicing. During this process, it removes itself from a larger precursor polypeptide by cleaving two peptide bonds and simultaneously connecting the neighbouring extein (external protein) sequences through a new peptide bond. This rearrangement occurs after translation or sometimes during translation since intein genes are located within other protein-coding genes. Intein-mediated protein splicing occurs spontaneously and relies solely on the folding of the intein domain, without the need for external factors, energy, cofactors, or additional enzymes.[47] The process consists of four intramolecular reactions, the first three occurring at a single catalytic site within the intein. Mutations can modify protein splicing, transforming it into highly specific self-cleavage and protein ligation reactions that are valuable for protein engineering.[48] A distinction is made between cis and trans splicing, whereby cis splicing is performed by the more prevalent contiguous inteins, while trans splicing is performed by the rarer split inteins.[47]

During protein splicing (Figure 4), an acyl shift from N -> S or O occurs at the intein's N-terminal residue. Then trans(thio)-esterification to the residue at the C-terminal end of the intein happens, creating a branched intermediate. The C-terminal intein-extein bond gets cleaved by the intein's C-terminal asparagine, producing a succinimide product. The exteins then undergo an (S,O) -> N acyl shift, forming a native peptide bond.[49] In EPL, a thiol generates a thioester from a modified intein, which can then react with an N-terminal cysteine of a peptide through NCL (Figure 5).[46,49]

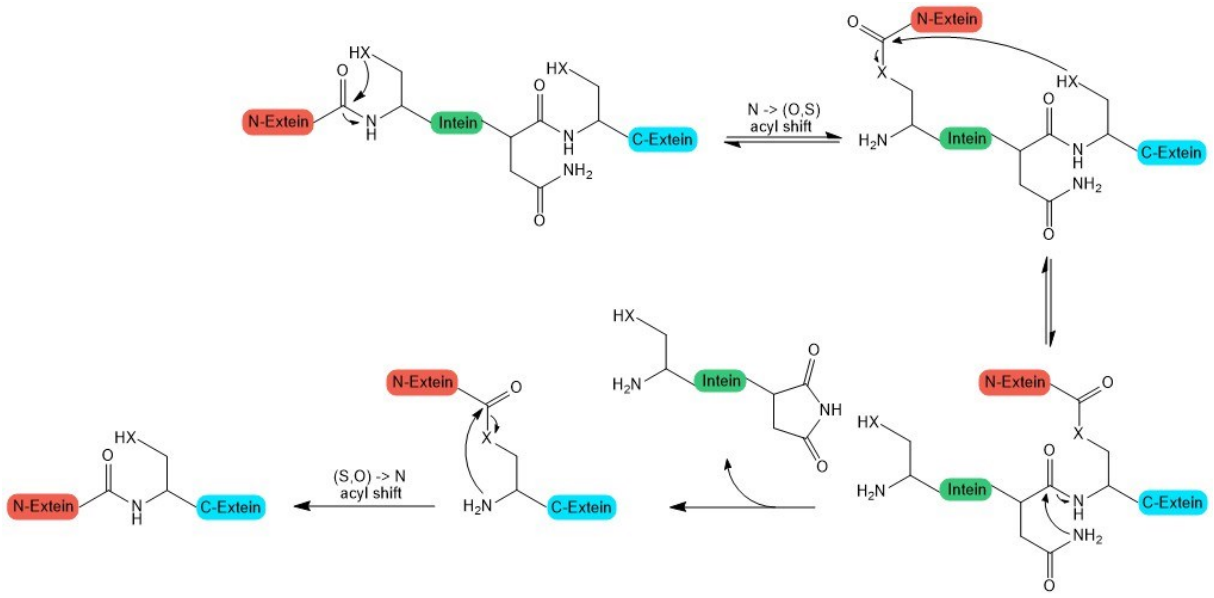

Figure 4 Mechanism of protein splicing; X= O, S (based on [49]).

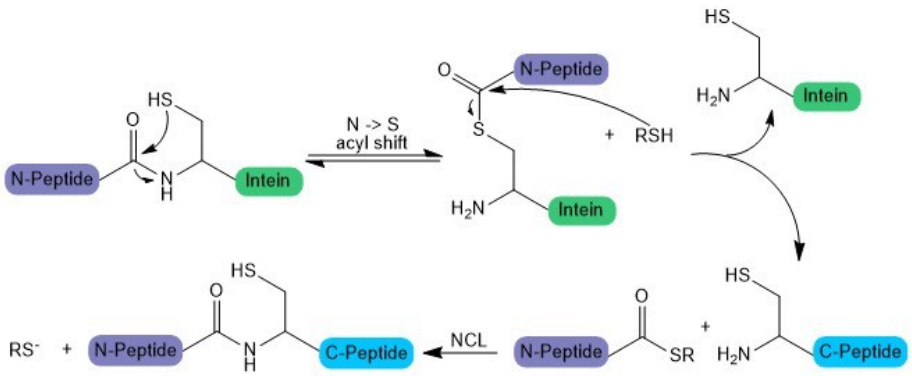

Figure 5 Mechanism of EPL; R = alkyl, phenyl, benzyl, $CH_2CH_2SO_3Na$ (based on [49]).

In EPL, a semi-synthetic method, a recombinant protein thioester, which is produced by the thiolysis of an intein fusion protein, reacts with a synthetic or recombinant peptide with an N-terminal cysteine to form a native peptide bond.[49] Since its introduction, this technique has been applied to various targets, enabling site-specific incorporation of biophysical probes, attachment to surfaces, polymers, or nanoparticles, and the creation of proteins that are toxic or challenging to express by other means. EPL has been extensively used to incorporate post-translational modifications and unnatural amino acids into proteins.[49,50] The use of EPL in studying protein structure and function has become increasingly sophisticated, helping to unravel the complexity of subcellular trafficking and signaling networks.[49]

The ability to chemically synthesize and precisely modify biomacromolecules offers opportunities for new biological discoveries and therapeutic methods. However, creating peptides and proteins with diverse functions requires highly selective and efficient chemical processes. Chemoselective transformation strategies are essential for easy access and precise modification of complex biomacromolecules. Specifically, desulfurization chemistry enhances chemical protein synthesis by expanding the use of cysteine-based peptide ligation.[51]

1.2.5 Desulfurization

NCL relies on the presence of a Cys residue in the ligation process, which has been exploited due to its prevalence in proteins, especially secreted proteins with multiple disulfide bonds. Cys residues, whether naturally occurring or engineered, often do not significantly disrupt protein structure or function. The cysteine thiolate is a valuable natural nucleophile for chemoselective modifications, allowing it to be converted into residues resembling natural amino acids. For instance, aminoethyl reagents can create lysine isosteres, and alkylation with iodoacetic acid or iodoacetamide can yield homoglutamate or homoglutamine analogs.[52]

A straightforward approach for synthesizing cysteine-free polypeptides while retaining the benefits of NCL involves converting the generated Cys residue to a naturally occurring amino acid, such as alanine. This method was first detailed in 2000 and involves hydrogenolytic desulfurization using catalysts like Raney nickel which were effective in biological studies. These catalysts facilitate the conversion of Cys to Ala, enabling ligation at Xaa-Ala sites and utilize the practical advantages of NCL. Up to now various reagents were tested, including Pd/C, $Pd/BaSO_4$, and PdO under hydrogen atmosphere. Raney nickel and Pd/Al_2O_3 (H_2) were the most sufficient catalysts. This efficient access to Xaa-Ala ligation sites has become a valuable technology in protein synthesis due to alanine's natural abundance in proteins and its tolerance to mutations without significant impact on protein properties.[53]

Despite the success of Raney nickel and Pd/Al_2O_3-mediated desulfurization, their heterogeneous nature poses challenges in controlling reaction stoichiometry. To address this, the Danishefsky laboratory developed a homogeneous desulfurization protocol using a radical induced reaction with tris(2-carboxyethyl)phosphine (TCEP) as a reducing agent which is stable in air, reactive over a wide pH range, and functions as phosphine source. This method involves treating a Cys peptide with a radical initiator, TCEP, and excess thiols like tBuSH and EtSH to increase the reaction rate. As radical initiator 2,2'-azobis[2-(2-imidazolin-2-yl)propane]dihydrochloride (VA-044) is suitable due to its water solubility and low decomposition temperature.[54,55] Effective thiols such as glutathione and sodium mercaptoethylsulfate (MESNA with DTT (dithiothreitol)) enable one-pot ligation/desulfurization, with minimal side reactions reported.[56–59] Native cysteine residues can be preserved by selective protection with an acetamidomethyl (Acm) group.[59]

The TCEP-based method represents the mildest and most selective cysteine desulfurization protocol developed so far. This new free-radical cysteine reduction technique, grounded in classical organic chemistry, is highly versatile and metal-free, making it suitable for various functional groups. It is expected to have broad applications in complex peptide and glycopeptide synthesis.[55]

The mechanism of the metal-free desulfurization is shown in Figure 6. When the radical initiator decomposes, it generates a thiyl radical from the cysteine. This thiyl radical then reversibly interacts with the phosphine, forming a phosphoranyl radical. The phosphoranyl radical undergoes β-scission, resulting in the formation of an alanyl radical, which can then extract a hydrogen atom from a (thiol) hydrogen source.[60]

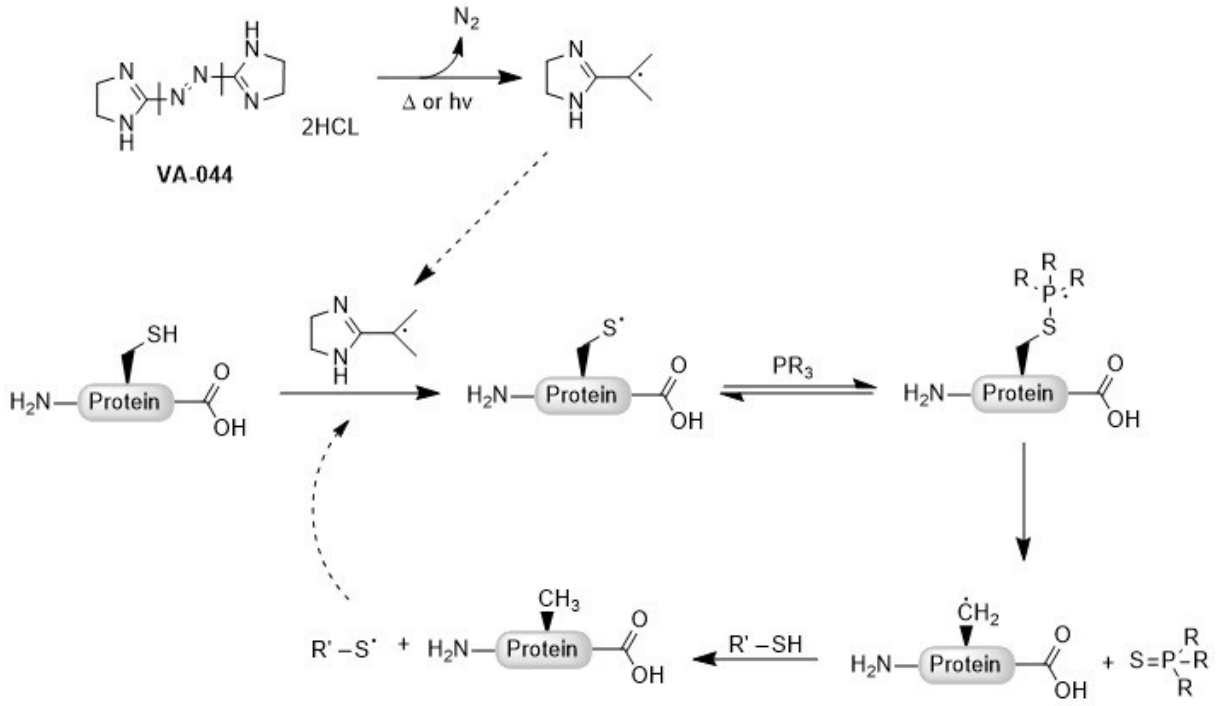

Figure 6 Mechansim of the metal-free desulfurization (based on [60]).

Xuechen Li and his team demonstrated another reagent highly compatible with NCL. Sodium tetraethylborate ($NaB(Et_4)$) is an effective reagent for rapidly desulfurizing Cys to Ala in polypeptides after they are assembled using NCL. The reaction occurs at room temperature within seconds due to sodium tetraethylborate acting as a source of ethyl radicals through its reaction with molecular oxygen.[61]

1.2.6 Protein Semisynthesis

Protein semisynthesis is defined as assembling recombinant and synthetic peptide segments into full length proteins to obtain site-selective modifications of such full-length proteins.[62] Therefore, the ligation of a recombinant building block with a synthetic peptide via EPL is the simplest strategy to gain a modified semisynthetic protein.[63]

With this method posttranslational modifications can be introduced within the N- or C-terminus of proteins. The C-terminal part of the protein of interest is produced recombinantly having an N-terminal cysteine, while the N-terminal part of the protein of interest is produced synthetically with a C-terminal thioester. This allows modifications on the N-terminus (Figure 7).[64]

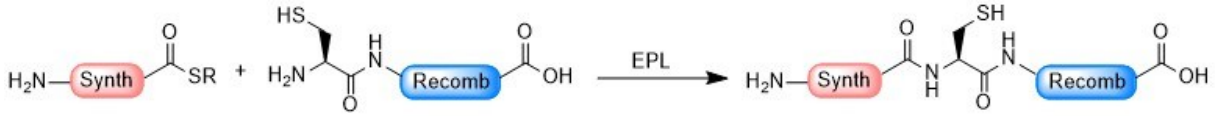

Figure 7 Protein assembly strategy to join peptide segments (one recombinant and one synthetic) with modifications incorporated at the N-terminus.

Methods to obtain proteins with a N-terminal cysteine require the designing of a precursor protein. A possible recombinant approach utilizes exogenous proteases. The recognition motif is introduced directly at the N-terminal cysteine. The tobacco etch virus (TEV) protease is frequently used, which recognizes a very specific hexapeptide sequence ENLYFQ and tolerates cysteine C-terminal of the cleavage site. After this treatment the desired peptide segment with an N-terminal cysteine is obtained.[65]

To obtain a peptide segment with a C-terminal thioester a frequently used method is Fmoc-SPPS, whereby a peptide hydrazide as precursor can be generated. Through $NaNO_2$ activation (oxidation under acidic pH) to the corresponding electrophilic azide and a thiolysis process utilizing an external thiol such as 4-mercaptophenylacetic acid (MPAA) the peptide hydrazide can be converted to a peptide thioester (epimerization-free) (Figure 8). Protecting groups for the side chain functionalities are not necessary since only the C-terminus is affected by this reaction.[66,67]

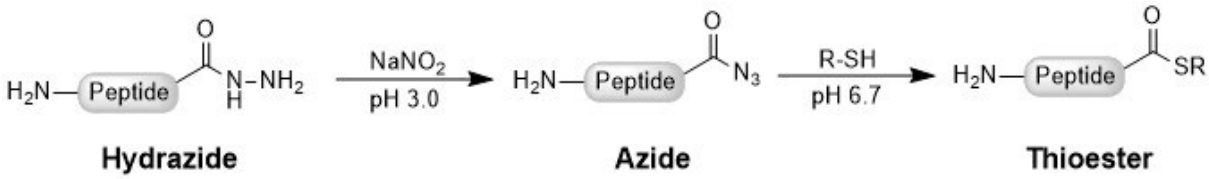

Figure 8 Conversion of a peptide hydrazide to a peptide thioester.

Through EPL the synthetic produced and the recombinant produced peptide segments can be ligated. If there is no native cysteine at the ligation site it is possible to desulfurize to alanine or modify by other means. The combined use of NCL/EPL and reductive desulfurization has proven to be a robust strategy for synthesizing proteins, particularly at Xaa-Ala sites, where ligation is rapid, and the starting materials are readily available.[59,65]

1.3 Glycation – a non-enzymatic PTM

Non-enzymatic posttranslational modifications (nPTMs) are enzyme independent reactions of metabolites with proteins and include for example glycation, carbamylation, nitrosylation, and carbonylation.[68] They are biomarkers for age-related as well as metabolic diseases (for example diabetes), neurological diseases, and others.[69,70] The impact of nPTMs on protein structure and function is complex and therefore still not completely understood. The most common nPTMs include ALEs (advanced lipoxidation end products) and AGEs (advanced glycation end products).[70]

Protein glycation is a natural process and involves the chemical alteration of amino acids with reactive amino and guanidine groups by sugars and reactive carbonyls derived from carbohydrates. The non-enzymatic glycation of proteins occurs through various simultaneous processes, including condensation, rearrangement,

fragmentation, and oxidation reactions and is called Maillard reaction (Figure 9).[71] α-oxoaldehydes, reducing carbohydrates, and their derivatives interact with the free amine groups of lysine and the guanidine groups of arginine in peptides and proteins. Schiff bases are formed which are unstable. A quick rearrangement occurs forming Amadori products (fructoselysine).[72] Several advanced glycation end products (AGEs), such as (carboxymethyl)lysine, pentosidine, and glucosepane, can be formed.[71] Oxidative reactions (metal-catalyzed) of Amadori intermediates lead to the irreversible formation of glyoxidation products such as N-ε-(carboxyethyl) lysine (CEL) or N-ε-carboxymethylated lysine (CML).[73] It should be mentioned that only a small part of the glycation process has been described here.

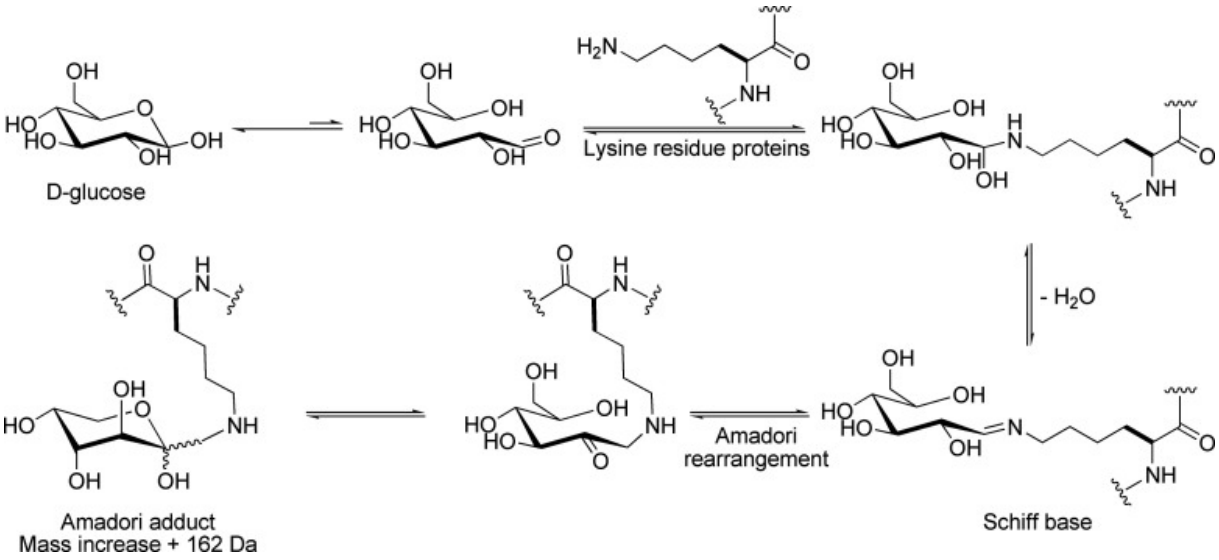

Figure 9 Glycation (nonenzymatic posttranslational modification (nPTM)) retrieved from[72].

After proteins are exposed to sugars they can become glycated (AGEs). Such modifications often accumulate in long lived human proteins. Proteins such as α-synuclein, amyloid β, and tau are glycated in patients with age-related neurodegenerative diseases such as Alzheimer's, Parkinson's and Huntington's disease. Studies indicate that patients' pathologies correlate with the degree of glycation, suggesting that AGEs contribute to the development of neurodegenerative diseases. An inflammatory response and localised oxidative stress are maintained in the brain as AGEs lead to abnormal deposition and accumulation of the respective proteins. This possibly leads to the development of neurodegenerative diseases. Strategies for the prevention and treatment of such diseases therefore also focus on researching the AGEs mechanisms that contribute to this neurotoxicity.[74]

Studies suggest that the degradation of AGE-modified proteins after ubiquitination relies on the ubiquitin-proteasome system (UPS), but glycation hinders the ability of ubiquitin and related enzymes to facilitate this process. The UPS is involved in breaking down AGEs, but glycated substrates degrade more slowly than unmodified ones.

Glycative stress also impairs UPS activity, leading to the accumulation of ubiquitin conjugates and AGEs in lysosomes.[75]

1.4 Ubiquitination

More than 400 different types of post-translational modifications (PTMs) are known.[76] Ubiquitination, glycosylation, phosphorylation, methylation, and acetylation are the most heavily investigated PTMs. Some are irreversible, such as proteolytic cleavages and some are reversible, such as phosphorylation involved in signalling pathways or glycosylation. PTMs serve a variety of purposes in different cellular processes and are important in the regulation of metabolism, cell signalling and gene expression, as they influence the function and localisation of proteins.[72] Ubiquitination is a PTM which modulates various physiological and cellular processes and plays an important role in the degradation of proteins.[77]

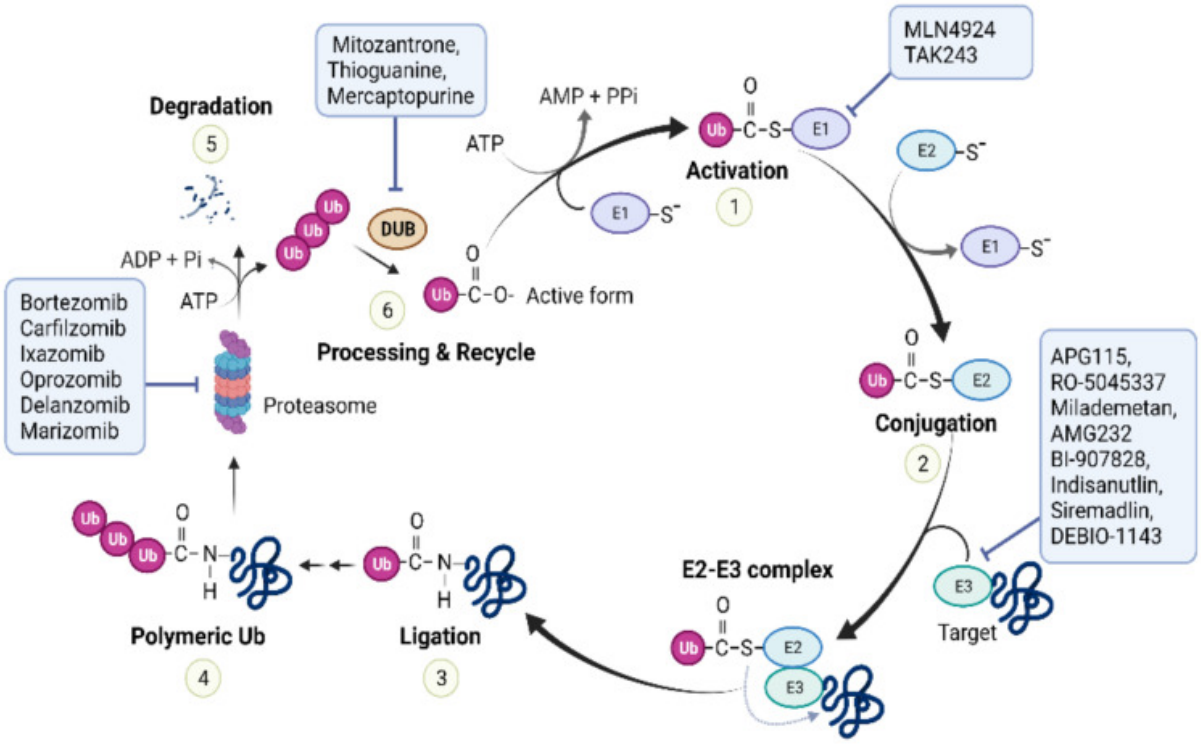

Figure 10 The ubiquitin-proteasome system (UPS) retrieved from[77].

The human genome encodes 2 Ub E1 enzymes, 38 Ub E2 enzymes and more than 700 E3 ligases.[77] Ubiquitin activating enzyme (E1), ubiquitin conjugating enzyme (E2) and ubiquitin ligase (E3) mediate the ubiquitination of proteins (Figure 10).[78] First, under ATP consumption ubiquitin is activated by E1, forming a E1-Ub-thioester. Then, ubiquitin is transferred to E2 forming a E2-Ub-thioester. Finally, E3 catalyses transfer of ubiquitin from E2 to a lysine (substrate target) forming an isopeptide bond.[77] Lysine and the N-terminus serve as anchoring point of poly-ub chains. Ubiquitin with 7 lysine

residues (K6, K11, K27, K29, K33, K48, and K63) and the N-terminus can also be a substrate for ubiquitination.[79] Repeating these steps can lead to the generation of a poly-ubiquitin chain. This then can lead to the digestion by the 26S proteasome as part of proteasomal degradation of targeted proteins.[77] Poly-ubiquitin chains K11- and K48-linked are mainly assigned to UPS.[80] The combination of E2 and E3 enzymes determines which kind of ubiquitin chain is generated and which protein is ubiquitylated.[78]

Since ubiquitination is involved in proteolysis as well as non-proteolytic processes such as DNA repair, inflammation, autophagy, activity regulation of enzymes, and protein complex formation, abnormalities of the UPS are associated with numerous diseases.[81] Thus, UPS defects are associated with cancer. For example, an abnormal UPS leads to the upregulation of oncogenic proteins and the downregulation of tumour suppressors. Therapeutic strategies are therefore being pursued in which proteasome inhibitors are used to treat cancer.[77]

Recent studies indicate that abnormal ubiquitin dependent pathways play a role in neurodegenerative diseases, such as Parkinson's disease, Huntington's disease, and Alzheimer's disease. The accumulation of misfolded or aggregated proteins leads to the formation of neurotoxic aggregates and, in turn, to neurodegeneration.[77,82] As UPS-associated enzymes play a role in neurodegenerative mechanisms, UPS inhibitors are being researched for the treatment of neurodegenerative diseases.[77]

2 The Outline of the Project

The goal of this master thesis was to produce 6 full-length αSyn variants via traceless semisynthesis. EPL was employed to access site-specifically CEL modified αSyn, to generate a library of homogeneously glycated αSyn, where the site of modification spans the N-terminal domain (K6, K10, K12, K21, K23). Therefore, the C-terminal part αS(30-140) was produced recombinantly having an N-terminal cysteine, while the N-terminal part αS(1-29) was produced synthetically with a C-terminal thioester utilizing Fmoc-SPPS. The full-length αSyn variants were obtained utilizing ligation and metal-free desulfurization. The aggregation of all variants was compared utilizing ThT assay and SEM imaging. The αSyn variants were then tested in an *in vitro* ubiquitination set-up to determine the impact of such site-specific CEL modification on the ubiquitination profile. αSyn was used as a model protein because it is a long-lived human protein with many lysine residues. *In vivo* it tends to form AGEs, which can lead to aggregation and dysfunction. It thus has an influence on proteasomal degradation via the UPS which tends to be a plausible pathway for the development of neurodegenerative diseases such as Parkinson's disease.[8,83]

3 Methods

All abbreviations for the peptide segments can be found in Figure 11.

3.1 Instruments

The SPPS was done on a Liberty Blue peptide synthesizer from CEM GmbH. The automated SPPS included microwave-assisted coupling and deprotection.

A Waters HPLC system (Water 2545 Quaternary Gradient Module, Waters Prep Inject, Waters 2489 UV/Vis Detector, Waters Fraction Collector) or Shimadzu HPLC system (FCV-200AL prep quaternary valve, CBM-20ACL communication bus module, LC-20AP prominence preparative liquid chromatograph, SPD-10A UV-Vis detector, FRC-10A fraction collector) was used for preparative HPLC. Either Kromasil C4/C18 reversed-phase semipreparative columns (300-10-C4/C18, 10 x 250 mm, 10 µm particle diameter, 300 Å pore size), or Kromasil C4/C18 reversed-phase preparative columns (300-10-C4/C18, 21.2 x 250 mm, 10 µm particle diameter, 300 Å pore size) were utilized.

LCMS and ESI-MS were performed on a system from Waters Corporation (2726 Sample Manager, 2545 Binary Gradient Modul, 515 HPLC Pump, 2489 UV/Vis Detector, and 3100 Mass Detector). Separation was achieved on a Kromasil C4 or C18 reversed-phase column (300-5-C4/18, 150 × 4.6 mm, 5 µm particle diameter) with a gradient ranging from 5% solvent B (ACN + 0.08% TFA) in solvent A (H2O + 0.1% TFA) to 65% solvent B in 10 min at a flow rate of 1 mL/min. The mass spectrometer was run in positive mode.

Analytical HPLC was done either on a Vanquish Flex UHPLC System or a Dionex Ultimate 3000 HPLC system (Thermo Fischer Scientific) on a Kromasil C4 or C18 reversed-phase column (300-5-C4/18, 150 x 4.6 mm, 5 µm particle diameter). The linear gradient ranged from 5% solvent B (ACN + 0.08% TFA) in solvent A (H2O + 0.1% TFA) to 65% solvent B in 40 min at a flow rate of 1 mL/min. The HPLC was monitored at 214 nm and 280 nm.

To measure the optical densities of cell cultures and concentrations of the protein construct before TEV cut a NanoDrop UV/VIS spectrophotometer from Thermo Scientific was used. For the purification of the protein construct an equilibrated Ni-NTA affinity column (for soluble proteins, 5 mL HisTrap™ High Performance column from GE Healthcare) was used, utilizing an ÄKTAprime plus (GE Healthcare) FPLC system.

For the BCA Protein Assay (Thermo Scientific) and the ThT Assay a Synergy Mx Microplate Reader from BioTek was used.

3.2 Chemicals

Unless otherwise noted, all chemicals and solvents were obtained from commercial sources and used without further purification. Deionized Water (Milli-Q Reference A+) was used for all buffer preparations and experiments.

For SPPS standard orthogonally protected Fmoc-amino acid building blocks were either purchased from Novabiochem, Sigma Aldrich or Iris Biotech GmbH. The chemicals and solvents used for SPPS were purchased from Sigma Aldrich, Novabiochem, GL Biochem, Biosolve, Iris Biotech GmbH and Thermo Fischer Scientific. Fmoc-L-CEL(OtBu)(Boc)-OH was purchased from Iris Biotech GmbH. The Cl-TCP(Cl) ProTide resin (CTC-resin) was purchased from CEM GmbH. Chemicals form Sigma Aldrich and Fluorochem were used for various applications.

The plasmid HisTEV-αS in a pET-21a(+) bacterial vector, which encodes the C-terminal domain (αS(30-140)) was obtained from Gene Universal. For the expression and purification of the recombinant αSyn part chemicals from PanReac Applichem, Gerbu, Roth and Sigma Aldrich were purchased.

For the ligation chemicals from Sigma Aldrich were ordered. The chemicals for desulfurization were purchased from Sigma Aldrich, Fluorochem and TCI Chemicals.

The ThT Assay was performed with chemicals from Sigma Aldrich, J.T.Baker, PanReac Applichem and VWR Chemicals. 96 well microplates (black, non-binding, flat bottom, chimney well, polystyrol) were ordered from Greiner Bio-One.

For the ubiquitination assay the chemicals were ordered from Roth, PanReac Applichem, J.T.Baker and Sigma Aldrich.

Mini-PROTEAN TGX Precast Gels (4-20%) were ordered from Bio-Rad Laboratories Ges.m.b.H.. ATP (25 µmol, 100 mM, pH: 7.5) was purchased from Thermo Scientific. Recombinant Human NEDD 4 (Ubiquitin Ligase E3) was ordered from BostonBiochem. The BCA Protein Assay Kit was from Thermo Scientific and the 96 well plates (pureGrade, clear, flat bottom, polystyrol) used for the BCA Assay were from Brand GmbH.

The ubiquitin-activating (E1) enzyme (UBA1 (*Yue-20200121*)), the ubiquitin-conjugating (E2) enzyme (Ubch5B) and ubiquitin (PP011) as well as a protocol for the ubiquitination assay were generous gifts from Dr. Luca Ferrari, Max Perutz Labs, Vienna, Austria.

3.3 Media, Buffers, Stock Solutions, and Gels

LB-medium	10 g/L Tryptone, 5 g/L Yeast extract, 10 g/L NaCl
2YT-medium	16 g/L Tryptone, 10 g/L Yeast extract, 5 g/L NaCl
TBS buffer	50 mM Tris, 150 mM NaCl (pH: 7.4 or 8.0)
2x SDS buffer	500 mM Tris (pH: 6.8), 6% (w/v) SDS, 35% Glycerin, 3.55% β-Mercaptoethanol, 0.05% (w/v) Bromophenol blue)
Coomassie-Staining solution	0.1% Coomassie R250, 10% acetic acid, 45% methanol
Destaining solution	10% acetic acid, 40% methanol in ddH_2O
Separating gel buffer	1.5 M TrisHCl, 0.4% (w/v) SDS, pH 8.8
Stacking gel buffer	0.5 M TrisHCl, 0.4% (w/v) SDS, pH 6.8
10x Laemmli buffer	250 mM Tris, 2 M glycine, 1% (w/v) SDS
SDS Separating gel (for 12 gels)	12.5 mL ddH_2O, 13.5 mL separating gel buffer, 26 mL Acrylamide (30 %), 550 µL SDS (10 %), 550 µL APS (10 %), 18 µL TEMED
SDS Stacking gel (for 12 gels)	12.5 mL ddH_2O, 2.5 mL stacking gel buffer, 3.5 mL Acrylamide (30 %), 185 µL SDS (10 %), 185 µL APS (10 %), 18 µL TEMED
Gdn HCl solution	6 M Gdn HCl (pH: ca. 3.0)
Ligation buffer	200 mM NaPi, 6 M Gdn HCl (pH: 7.2)
Desulfurization buffer	200 mM NaPi, 6 M Gdn HCl (pH: 6.8-7.2)
Aggregation reaction buffer	137mM NaCl, 2.7 mM KCl, 10 mM Na_2HPO_4, 1.8 mM KH_2PO_4 (pH: 7.4) and 0.05% NaN_3
ThT stock solution	10 mM ThT
PBS buffer	137 mM NaCl, 2.7 mM KCl, 10 mM Na_2HPO_4, 2 mM KH_2PO_4 (PH: 7.4)
Tris-Cl buffer	1 M Tris-Cl (pH: 7.5 or 6.8)
$MgCl_2$ buffer	1 M $MgCl_2$
Ubiquitination buffer (10x)	250 mM Tris-Cl (pH: 7.5), 1200 mM NaCl, 10 mM $MgCl_2$, 3 mM DTT (added freshly)

DTT stock solution	1 M DTT
E1 (UBA1) stock	4.07 µM E1 (UBA1), 25 mM HEPES, 150 mM NaCl, 1mM DTT (added freshly)
MES running buffer	50 mM MES hydrate, 50 mM Tris, 1 mM EDTA, 0.1 % (w/v) SDS (pH: 7.3)
SDS loading dye (5x)	5 % β-Mercaptoethanol, 0.02 % (w/v) Bromophenol blue, 30 % Glycerol, 10 % (w/v) SDS, 250 mM Tris-Cl (pH: 6.8)
Nedd4 stock	25 µM Nedd4, 50 mM HEPES (pH: 8.0), 100 mM NaCl, 5 mM DTT, 1 mM EDTA
Fixation solution	40 % Ethanol, 10 % Acetic Acid in ddH_2O
Incubation solution	30 % Ethanol, 68 mg/mL NaOAc, 2 mg/mL Na-Thiosulfate
Silver nitrate solution	0,001 g/mL $AgNO_3$, 0.6 µL/mL 36 % Formaldehyde
Developing solution	0.02 g/mL Na_2CO_3, 0.3 µL/mL 36 % Formaldehyde
Stop solution	0,04 M EDTA (pH: 8.0), 10 % Glycerol

3.4 Transformation and Expression of HisTEV-αS(30-140)

The plasmid encoding His_6-ENLYFQC-αS(30-140) was transformed into *E. coli* BL21(DE3) Gold and *E. coli* BL21(DE3) Rosetta 2 cells using the heat shock method. 5 µg plasmid was dissolved in 50 µL of ddH_2O. 10 µL (for *E.coli* Gold) or 15 µL (for *E.coli* Rosetta 2) of the plasmid solution was added to 100 µL suspension of each competent *E. coli* strain. The cells were kept on ice for 10 minutes. Then, the cells were incubated for 90 s at 42°C and afterwards cooled with ice. 1 mL sterile LB-medium (10 g/L tryptone, 5 g/L yeast extract, 10 g/L NaCl) was added and the cells were incubated at 37°C for 60 minutes with gentle shaking. Afterwards, the cells were centrifuged for 2 min at 14000 rpm. The supernatant was removed, the cell pellet was resuspended in 100 µL of sterile ddH_2O, plated onto LB-agar plates containing appropriate antibiotics and incubated at 37°C overnight. On the next day, from each plate a single colony was picked and transferred into 3 mL sterile LB-medium containing antibiotics (100 µg/mL ampicillin for *E. coli* BL21(DE3) Gold; 100 µg/mL ampicillin and 30 µg/mL chloramphenicol for *E. coli* BL21(DE3) Rosetta 2). The incubation was continued overnight at 37 °C and 170 rpm. From the overnight culture a 150 mL primary culture was prepared (37 °C, 160 rpm, incubation overnight) by diluting it with 2YT-medium

(16 g/L Tryptone; 10 g/L Yeast extract; 5 g/L NaCl) containing antibiotics. Glycerol stocks were prepared for both *E. coli* strains by mixing 500 µL glycerol (40% in H_2O) and 500 µL of the primary culture. They were stored at -80 °C. A Nanodrop UV/VIS spectrophotometer was used to determine the optical densities at 600 nm (OD_{600}) of the primary cultures. Based on the optical densities the primary cultures were diluted with 2YT-medium containing antibiotics to obtain 1 L (Test-expression) of secondary culture with an OD_{600} of 0.2 (Formula 1).

$$V = \frac{V_{desired} * OD_{desired}}{OD_{measured}}$$

Formula 1

The secondary cultures were incubated at 37 °C (150 rpm) until the OD_{600} reached between 0.6 and 0.8 (after about 1 h). Then the protein expression was induced with 1 mM isopropyl-β-D-1-thiogalactopyranoside (IPTG) and the cells were incubated at 37 °C (160 rpm) for 4 h. The OD600 was checked every hour and gel samples were prepared. With Formula 2 the volume for the gel sample was calculated.

$$V = \frac{200\ \mu L}{OD_{measured}}$$

Formula 2

The volume was taken, centrifuged (2 min, 14000 rpm), the supernatant removed, and the pellets stored at -20 °C. The cells were harvested after 4 h by centrifugation at 15 °C at 6000 rpm for 17 min. The supernatant was removed, and the pellets stored at -80 °C until the next day. Then the pellets were resuspended in 100 mL TBS buffer (50 mM Tris, 150 mM NaCl, pH = 8.0) and homogenized utilizing an ultra turrax (IKA GmbH, 79219 Staufen, Germany). A cell disruptor (Constant Systems Limited, Northants United Kingdom) was used for cell lysis (1.9 kBar, 3 cycles), and the lysate was centrifuged (45 min, 15 °C, 18000 rpm). The supernatant, the pellet and the protein expression samples were analysed by SDS-PAGE. Therefore, a small piece of each pellet was resuspended in 10 µL H_2O and 10 µL 2x SDS buffer (500 mM Tris (pH: 6.8), 6% SDS, 35% Glycerin, 3.55% β-Mercaptoethanol, 0.05% Bromophenol blue). 10 µL of the soluble fraction was mixed with 10 µL 2x SDS buffer. All samples were boiled at 95 °C for 5 min and 10 µL from each was loaded onto a gel. A Lämmli buffer (10x) was diluted (to 1x) and used as running buffer. The gel was run for 37 min with constant voltage of 250 V. Afterwards, the gel was stained with Coomassie staining solution (0.1% Coomassie R250, 10% acetic acid, 45% methanol) for 30 min and destained with destaining solution (10% acetic acid, 40% methanol) for 20 min and kept in water overnight. The pellet was discarded because the protein construct was only found in the supernatant. The supernatant of the *E. coli* Gold strain and the *E. coli* Rosetta 2 strain were combined since both showed the same outcome in the gel.

Since the outcome of the expression was the same for both *E. coli* strains, for later expressions only *E. coli* BL21(DE3) Gold was used, as fewer antibiotic was needed compared to Rosetta 2. For later expressions the scale was 4 L secondary culture instead of 1 L.

3.5 Preparation of αS(30-140)

About 100 mL (per run) of the combined supernatant was loaded onto a TBS buffer (pH: 8.0) equilibrated Ni-NTA affinity column for soluble proteins (5 mL HisTrap™ High Performance column from GE Healthcare). An ÄKTA prime plus (GE Healthcare) FPLC system was used. Proteins lacking a His_6-Tag were washed away with TBS buffer (pH: 8.0). A linear gradient from 0 to 500 mM imidazole with a flow rate of 1 mL/min was used (60 min) to purify construct **F1**. The fractions of interest were analysed via SDS-PAGE and fractions containing the protein construct were combined. To remove the imidazole, the pool was dialyzed against 4 L of TBS buffer (pH: 8.0) at 4 °C overnight. UV/Vis spectrometry was used to check the protein concentration. The solution was diluted 1:3 with TBS (pH: 8.0) to get a concentration of 1 mg/mL. TCEP (a small amount) and TEV-Protease (TEV:protein = 1:10; w/w) was added and the solution incubated at 4 °C with gentle shaking for 6 h (or overnight). The TEV-Protease was utilized to remove the His_6-Tag. The outcome of the TEV-cut was checked via SDS-PAGE. To remove proteins still having a His_6-Tag as well as the TEV protease itself, a Ni-NTA-batch column was used. Therefore, the column was washed with TBS buffer (pH: 8.0), the protein solution was loaded and stirred for 1 h. The flow-through was collected and purified utilizing a preparative RP-HPLC with a Kromasil C4 column (300-10-C4, 21.2 x 250 mm, 10 µm particle diameter, 300 Å pore size). A linear gradient was used, ranging from 25-70% solvent B (ACN + 0.08% TFA) in solvent A (H2O + 0.1% TFA) in 30 min at a flow rate of 20 mL/min after a 20 min desalting phase at constant 5% solvent B. The fractions of interest were analysed by ESI-MS. Fractions containing product (**F2**) were combined, lyophilized, and stored at – 20°C.

The Ni-NTA-batch columns were on several occasions proved to be more challenging to work with for practical reasons. Therefore, instead of the batch column, the equilibrated Ni-NTA affinity ‘pre-packed’ column (5 mL HisTrap™ High Performance column from GE Healthcare) on an ÄKTAprime plus (GE Healthcare) FPLC system was used. The protein solution was slowly loaded (1.5 mL/min) and the flow-through (containing the protein of interest) was collected, and the following steps carried out like described above.

3.6 Solid Phase Peptide Synthesis

3.6.1 Synthesis of Ala-N_2H_4-CTC

The Cl-TCP(Cl) ProTide resin (CTC-resin; 0.42 mmol/g) was loaded with hydrazine and the C-terminal amino acid (Fmoc-Ala-OH). Therefore, in a polypropylene syringe

(20 mL) equipped with a polystyrene frit 1 g CTC-resin was weight in. To swell the resin it was rotated with 15 mL anhydrous DCM for 30 min. Then, the resin was treated with 15 mL hydrazine hydrate solution (5 % in DMF) and rotated for 1 h. Afterwards, it was washed (three times) with DMF. The unreacted sites were capped by the treatment with a mixture of MeOH and DMF (1:1; containing three drops of DIPEA) for 25 min. The hydrazine resin was washed with DMF (three times) and the C-terminal amino acid (Fmoc-Ala-OH) was coupled (5.0 equiv Fmoc-Ala-OH, 4.76 equiv HATU, 5 equiv Cl-HOBt, 10 equiv DIPEA in DMF) during a 30 min rotation step. Then, the resin was washed with DMF (three times) and the coupling step repeated like described above. Afterwards, the resin was washed with DMF (two times), DCM (two times), DCM-MeOH (1:1; two times), and MeOH (two times). Finally, it was dried in a vacuum desiccator overnight. The next day the loading was checked. Therefore, 12 mg of the resin was treated with 1 mL of piperidine (20 % in DMF) for 20 min. In this step the Fmoc protection group was cleaved and the dibenzofulvene–piperidine adduct (in the supernatant) was formed. 50 µL of the supernatant was diluted with 950 µL piperidine (20 % in DMF) and the UV absorbance was measured at 301 nm. Formula 3 was used to determine the loading of the resin (determined to be 0.27 mmol/g in our case). A_{301} is the measured absorbance at 301 nm, V is the sample volume (mL), F_D is the dilution factor, ε is the molar extinction coefficient (7800 mL/(mmol*cm) for Dibenzofulvene), m_{Resin} is the mass of the used resin (mg) and w is the width of the cuvette (cm).

$$Loading\ [mmol/g] = \frac{A_{301} * V * F_D}{\varepsilon * m_{Resin} * w}$$

Formula 3

Finally, the resin was stored at -20 °C till further usage.

3.6.2 Synthesis of αS(1-29)^{WT}-TE

The peptide hydrazide **E1a** was synthesized automatically (scale: 0.1 mmol) by microwave assisted SPPS using a Liberty Blue peptide synthesizer (CEM) using Fmoc-strategy. The synthesis was started from the pre-loaded hydrazine linked Cl-TCP resin prepared in section 3.6.1. Upon activation with DIC/Oxyma, the amino acids were coupled for 4 min with microwave assistance (150 W, Tmax = 95 °C). The microwave-assisted (150 W) deprotection steps were conducted for 1.2 min. Pseudoproline building blocks at position L-S and K-T were also utilized.

From the batch of fully synthesized peptide hydrazide a test cleavage and a final cleavage were performed. For the test cleavage a small portion (5-10 mg) of the peptide hydrazide was treated with 1 mL cleavage cocktail (87.5 % TFA, 5 % DMS, 5 % TIPS and 2.5 % H2O) for 3 h. Then, the cleaved peptide was precipitated with cold diethyl ether and centrifuged down (8 min, 4300 rpm, 4 °C). The diethyl ether was

removed and the pellet was dissolved into ACN:H_2O (1:1 containing 0.1 % TFA) and analysed via LCMS. For the final cleavage (global deprotection) the resin was split in two parts and for each, 8 mL cleavage cocktail (87.5 % TFA, 5 % DMS, 5 % TIPS and 2.5 % H2O) was used. The procedure was the same as for the test cleavage. Afterwards, the crude peptide hydrazide was lyophilized. The peptide hydrazide was then dissolved in ACN:H_2O (1:1 containing 0.1 % TFA) and purified by preparative RP-HPLC using a Kromasil C18 column (300-10-C4, 21.2 x 250 mm, 10 µm particle diameter, 300 Å pore size) with a linear gradient from 25 % solvent B (ACN + 0.08% TFA) in solvent A (H_2O + 0.1% TFA) to 70 % solvent B in 30 min at a flow rate of 20 mL/min and a desalting phase of 20 min. As the peptide hydrazide was hydrophilic and the result of the first used gradient was not good, for all other peptide hydrazide purifications only water was used to dissolve the crude peptide and a linear gradient from 5 % solvent B (ACN + 0.08% TFA) in solvent A (H_2O + 0.1% TFA) to 50 % solvent B in 30 min at a flow rate of 20 mL/min and a desalting phase of 20 min was used. The fractions were analysed by ESI-MS, the ones containing the product of interest were combined and lyophilized.

The protocol of Liu[66] was used as a guideline for the transformation of the peptide hydrazide **E1a** to the peptide thioester **E2a**. Therefore, 50 mg of the crude peptide hydrazide was dissolved in 5 mL Gdn-buffer (6M Gdn HCl; pH 3.0) and cooled down to -12 °C. 1.2 mL $NaNO_2$ solution (1 mg/mL in water) was added dropwise, and the mixture stirred for 15 min at -12 °C. Then, 3.3 mL MESNa solution (9.5 mg/mL in 6M Gdn HCL, pH 3.0) was added dropwise, the pH adjusted to 6.7 and the mixture stirred for 20 min at room temperature. The reaction progress was monitored by LCMS. When the reaction was finished the crude peptide thioester was purified by preparative RP-HPLC using a Kromasil C18 column (300-10-C4, 21.2 x 250 mm, 10 µm particle diameter, 300 Å pore size) with a linear gradient from 5% solvent B (ACN + 0.08% TFA) in solvent A (H2O + 0.1% TFA) to 50% solvent B in 30 min at a flow rate of 20 mL/min and a desalting phase of 20 min. The fractions were analysed by ESI-MS and the ones containing the product of interest (**E2a**) were combined, lyophilized, and stored at – 20°C. For the generation of all other peptide thioesters the crude peptide hydrazide was directly transformed into the peptide thioester without any additional purification step. For the transformation to the thioester, the crude lyophilized peptide hydrazide was treated in the same manner as above. The crude peptide thioester was then purified as described above.

3.6.3 Synthesis of αS(1-29)^{mK6,10,12,21,23}-TE

The syntheses of the modified peptide hydrazides (**E1b-f**) were caried out like described in section 3.6.2. Instead of Fmoc-Lys-(Boc)-OH, the modified amino acid Fmoc-L-CEL(OtBu)(Boc)-OH was coupled at the desired position. The transformation

to the desired peptide thioesters (**E2b-f**) was caried out like described in section 3.6.2. For the synthesis of αS(1-29)^{mK21}-TE (**E2e**) no pseudoproline on position K-T was used. For all modified versions the crude peptide hydrazide was transformed directly, without purification, to the peptide thioester.

3.7 Ligations

3.7.1 Ligation of αS(1-29)^{wt}-TE and αS(30-140)

For the protein synthesis the strategy of combining native chemical ligation with metal free desulfurization was followed. This strategy is described in papers by Philip E. Dawson[59] and Samuel J. Danishefsky[55]. For the ligation, 1 equivalent (5 mg) protein construct αS(30-140) (**F2**), prepared in section 3.5, was dissolved in degassed ligation buffer (200 mM NaPi, 6 M Gdn HCl, pH 7.2) containing 50 mM TCEP and 200 mM MPAA, to reach a protein concentration of 1 mM. 2.1 equivalent (2.8 mg) of peptide thioester (**E2a**) was added and the mixture was shaken at 600 rpm at 37°C for 5h. The reaction progress was monitored by LCMS, by analytical RP-HPLC, and by SDS-PAGE after 0.5h, 2h, and 5h. For the SDS-PAGE the guanidine hydrochloride needed to be removed by the treatment with cold ethanol. A small piece of each pellet was resuspended in 10 µL H_2O and 10 µL 2x SDS buffer (500 mM Tris (pH: 6.8), 6% SDS, 35% Glycerin, 3.55% β-Mercaptoethanol, 0.05% Bromophenolblue). All samples were boiled at 95 °C for 5 min and 10 µL from each was loaded onto a gel. A Lämmli buffer (10x) was diluted (to 1x) and used as running buffer. The gel was run for 37 min with constant voltage of 250 V. Afterwards, the gel was stained with Coomassie staining solution (0.1% Coomassie R250, 10% acetic acid, 45% methanol) for 30 min and destained with destaining solution (10% acetic acid, 40% methanol) for 20 min and washed with water overnight. The ligation product was purified by semipreparative RP-HPLC using a Kromasil C4 column (300-10-C4, 10 x 250 mm, 10 µm particle diameter, 300 Å pore size) and a linear gradient from 25% solvent B (ACN + 0.08% TFA) in solvent A (H2O + 0.1% TFA) to 70% solvent B in 30 min at flow rate of 5 mL/min, with a desalting phase of 20 min (at 5% solvent B). The fractions were analysed by ESI-MS and the ones containing the pure product of interest (**G1a**) were combined, and lyophilized. As the ligation was very fast for the later ligations the reaction time was kept shorter.

3.7.2 Ligation of αS(1-29)^{mK6,10,12,21,23}-TE and αS(30-140)

The ligation products (**G1b-f**) were obtained by the ligation of the modified thioesters (**E2b-f**) with the protein construct αS(30-140) (**F2**). The ligation was carried out like described in section 3.7.1.

3.8 Desulfurization

3.8.1 Desulfurization of αS(1-140)^{wt}

The ligation product (**G1a**) prepared in section 3.7.1 was dissolved in degassed desulfurization buffer DB (200 mM NaPi, 6 M Gdn HCl, pH 6.8-7.2) (100 µL per mg). The same volume of neutralized TCEP solution (500 mM TCEP in DB, neutralized with 28 µL Et_3N per 100 µL DB, pH 6.5-7.0) was added. Then, MESNa (130 mM final concentration) and VA-044 (0.4 M in degassed water; diluted to 25 mM final concentration (6.7 µL stock solution / 100 µL reaction volume)) were added, the pH was checked, and the mixture shaken at 600 rpm, at 37 °C for 2h. The reaction progress was monitored by LCMS. Then, the product was purified by semipreparative RP-HPLC using a Kromasil C4 column (300-10-C4, 10 x 250 mm, 10 µm particle diameter, 300 Å pore size) and a linear gradient from 25% solvent B (ACN + 0.08% TFA) in solvent A (H2O + 0.1% TFA) to 70% solvent B in 30 min at flow rate of 5 mL/min, with a desalting phase of 20 min (at 5% solvent B). The fractions were analysed by ESI-MS and the ones containing the pure product of interest (**G2a**) were combined, lyophilized, and stored at – 20°C. As the desulfurization in our first attempt took more than 3h, for the other desulfurizations 50 mM final concentration of VA-044 (radical initiator) was used.

3.8.2 Desulfurization of αS(1-140)^{mK6,10,12,21,23}

To obtain the desired desulfurization products (**G2b-f**) the desulfurization of the modified variants (**G1b-f**) was performed as described in section 3.8.1. A final concentration of 50 mM VA-044 was used.

3.9 ThT Assay and SEM Measurements

For the ThT (thioflavin T) assay, an approach was first followed in which the aggregation reaction was carried out for more than 7 days and the alpha synuclein aggregation of different time points was then quantified by thioflavin T fluorescence. The papers by Pratt[84] and Pratt[85] were used as a template.

The experiment was first only tried out for the wild type alpha synuclein (**G2a**). Therefore, about 500 µg αS(1-140)^{wt} was dissolved in 350 µL Aggregation reaction buffer (10 mM PBS, 0.05% sodium azide, pH 7.4) by bath sonication. Then, the solution was centrifuged (14000 rpm, 4 °C, 20 min) to remove any pre-formed aggregates (debris). The supernatant was transferred in a new tube. The concentration was determined using a BCA Protein Assay Kit from Thermo Scientific. The protein solution was diluted with aggregation reaction buffer and aliquoted into triplicate reactions (100 µL per Tube) with a final alpha synuclein concentration of 50 µM. The samples were incubated at 37 °C with constant agitation (1000 rpm) in a Thermo-Shaker TS-100

(Biosan) for at least 7 days. After different lengths of time aliquots were taken for analysis by ThT fluorescence. The aggregation assay was also tried out with 100 µM αSyn concentration instead of 50 µM, and with a higher volume (150 µL instead of 100 µL). By Thioflavin T fluorescence the degree of alpha synuclein aggregation was quantified. Therefore, the samples from the aggregation assay reaction mixture were diluted in a 96-well plate (microplate, black, non-binding) with aggregation reaction buffer (10 mM PBS, 0.05% sodium azide, pH 7.4, containing 10 µM ThT) to a final αSyn concentration of 1.25 µM. Therefore, 100 µL of a 1 mM ThT solution was prepared from a 10 mM ThT stock solution. 5 µL of the timepoints were diluted with 193 µL aggregation reaction buffer, and 2 µL 1 mM ThT solution was added (final ThT concentration: 10 µM). Each well contained a glass bead for better mixing. A Synergy Mx Microplate Reader from BioTek was utilized and the plate was shaken on “fast” setting for 3 min, followed by data collection (λex = 450, 9 nm band path, λem = 482 nm, 9 nm band path, reading from top of the plate, gain = 100, read height = 5.00 mm). Data was measured in triplicates for all aggregation reaction conditions and the blank value (triplicate) was deducted from the fluorescence readings at each time point. The ThT assay was also tried out with a gain of 50 instead of 100.

As this method did not lead to a reasonable result, as the values were subject to strong fluctuations, an approach was chosen instead in which the aggregation and the ThT fluorescence measurement was set up directly in a 96-well plate (microplate, black, non-binding; glass bead in each used well). The reaction was first tried out for the wild type alpha synuclein (**G2a**) in a volume of 150 µL with a αSyn concentration of 50 µM and 100 µM. As the higher concentration of αSyn led to a more stable result the final ThT assay was performed with all alpha synuclein variants (**G2a-f**) with a volume of 150 µL and a αSyn concentration of 85 µM (in 10 mM PBS, 0.05% sodium azide, pH 7.4, containing 10 µM ThT). A Synergy Mx Microplate Reader from BioTek was utilized and the plate was shaken continuous on “fast” setting for a total of 7 days at 37 °C. The data collection (λex = 450, 9 nm band path, λem = 482 nm, 9 nm band path, reading from top of the plate, gain = 50, read height = 5.00 mm) happened every 30 min. Data was measured in triplicates for all aggregation reaction conditions and the blank value (triplicate) was deducted from the fluorescence readings at each time point.

A scanning electron microscope (SEM) was utilized for the imaging of samples of the final ThT assay with all alpha synuclein variants. For imaging of protein aggregates, the volume of each desired well was resuspended, a 10 µL (85 µM concentration) droplet from each desired aggregation experiment was deposited on formvar coated copper TEM (transmission electron microscopy) grid (3.05 mm, 200 mesh, Plano GmbH, clued on a sample holder) and after a waiting period of 3 min the excess liquid was removed with filter paper. The grids were washed with 10 µL water for 1 min, and the remaining liquid again removed with filter paper. The prepared grids were sputter-

coated with gold and imaged using a scanning electron microscope operated with different magnification values.

3.10 Ubiquitination

A provided protocol from Dr. Luca Ferrari (Max Perutz Labs, Vienna, Austria) was used. First, the exact concentration of all alpha synuclein variants (**G2a-f**) was determined using a BCA Protein Assay Kit from Thermo Scientific. The ubiquitination assay was first performed only for the wild type alpha synuclein variant (**G2a**) with and without E3 (Nedd4), with and without ATP (Table 1-3). Then, the ubiquitination assay was carried out for all alpha synuclein variants (**G2a-f**) at the same time (with ATP, with E3, Table 4). Therefore, the proteins were thawed on hand, spinned down (10 sec, 4 °C, 16000 rpm). In the meantime, 1 µL DTT (1M) was added to 0.333 mL of ubiquitination buffer (250 mM Tris-Cl (pH 7.5), 1200 mM NaCl, 10 mM $MgCl_2$) to get a 3 mM final DTT concentration. The reaction mix was prepared following Table 1-4 on ice. It was mixed by quick gentle vortex. The reaction mix was put on a heat block (30 °C, no shaking). After 0, 5, 15, 60, 240 minutes, and overnight 8 µL of the reaction mixture was taken and added to 2 µL Protein Loading Dye (5x). A Mini-PROTEAN TGX Precast Gels (4-20%) from Bio-Rad Laboratories Ges.m.b.H. was used. 5 µL sample solution per well was loaded and a MES buffer used as running buffer. The gel was run for 35 min with constant voltage of 200 V. Afterwards, the gel was stained with Coomassie staining solution (0.1% Coomassie R250, 10% acetic acid, 45% methanol) for 30 min and destained with destaining solution (10% acetic acid, 40% methanol) for 20 min and kept in water overnight. Since the Coomassie staining did not lead to good results, silver staining was used instead. Therefore, the gel was 30 min in 50 mL fixation solution, then 10 min in 50 mL incubation solution. The gel was washed three times with water for 5 min. Then, the gel was 10 min in 50 mL silver nitrate solution and washed three times for 20 sec. Finally, the gel was stained in 50 mL developing solution till the bands could be seen. Then, the developing solution was removed, and the gel put in 50 mL stop solution. This step needed to be carried out very fast, otherwise the gel would turn too dark to see the protein bands.

Table 1

without E3 and with ATP		wt
Reagent (in order of addition)	Final conc.	V (µL)
Water	-	47.11
Ubiquitination Buffer 10x*	25 mM	6 + vortex
E1 UBA1 (*Yue-20200121*, 40.7 uM)**	50 nM	0.73
Ubiquitin (PP011, 822 uM)	10 µM	0.73
alpha-Synuclein (XX uM)	1.5 µM	1.3
E2 UbcH5B (26.4 µM)	0.5 µM	1.13
ATP pH 7.5 100mM	5 mM	3

Table 2

without E3 and without ATP		wt
Reagent (in order of addition)	Final conc.	V (µL)
Water	-	50.11
Ubiquitination Buffer 10x*	25 mM	6 + vortex
E1 UBA1 (*Yue-20200121*, 40.7 uM)**	50 nM	0.73
Ubiquitin (PP011, 822 uM)	10 µM	0.73
alpha-Synuclein (XX uM)	1.5 µM	1.3
E2 UbcH5B (26.4 µM)	0.5 µM	1.13
ATP pH 7.5 100mM	5 mM	-

Table 3

with E3 and without ATP		wt
Reagent (in order of addition)	Final conc.	V (µL)
Water	-	48.91
Ubiquitination Buffer 10x*	25 mM	6 +vortex
E1 UBA1 (*Yue-20200121*, 40.7 uM)**	50 nM	0.73
Ubiquitin (PP011, 822 uM)	10 µM	0.73
alpha-Synuclein (XX uM)	1.5 µM	1.3
E2 UbcH5B (26.4 µM)	0.5 µM	1.13
E3 Nedd4 (25 µM)	0.5 µM	1.2
ATP pH 7.5 100mM	5 mM	-

Table 4

with E3 and with ATP		**wt**	**mK6**	**mK10**	**mK12**	**mK21**	**mK23**
Reagent (in order of addition)	Final conc.	V (µL)	V (µL)	V (µL)	V (µL)	V (µL)	V (µL)
Water	-	45.91	46,01	46.31	46.01	46.21	46.11
Ubiquitination Buffer 10x*	25 mM	6 + vortex	6 + vortex	6 + vortex	6 + vortex	6 + vortex	6 + vortex
E1 UBA1 (*Yue-20200121*, 40.7 uM)**	50 nM	0.73	0.73	0.73	0.73	0.73	0.73
Ubiquitin (PP011, 822 uM)	10 µM	0.73	0.73	0.73	0.73	0.73	0.73
alpha-Synuclein (XX uM)	1.5 µM	1.3	1.2	0.9	1.2	1.0	1.1
E2 UbcH5B (26.4 µM)	0.5 µM	1.13	1.13	1.13	1.13	1.13	1.13
E3 Nedd4 (25 µM)	0.5 µM	1.2	1.2	1.2	1.2	1.2	1.2
ATP pH 7.5 100mM	5 mM	3	3	3	3	3	3

4 Results and Discussion

Of αSyn a wildtype variant and five site-specifically CEL modified variants were synthesized (**G2a-f** - wt, mK6, mK10, mK12, mK21, mK23). The highlighted lysins in Fig. 11A (6, 10, 12, 21 and 23) mark the nPTM (CEL) positions.

The N-terminal peptide segments of αS(1-29) **E2a-f** were synthesized carrying a C-terminal alpha-thioester. Therefore, Fmoc-SPPS was used to generate the corresponding peptide hydrazides **E1a-f**. To create the necessary functionality in order to carry out a ligation the peptide hydrazides were transformed into peptide thioesters by subsequent treatment with $NaNO_2$ and MesNa (Figure 11, B).[66] Further information can be found in section 4.3.

The expressed C-terminal peptide segment αS(30-140) **F2** was obtained via expression in *E. coli* BL21(DE3) Gold. At the N-terminus, the fusion construct **F1** contained a His_6-Tag for affinity purification (Ni-NTA affinity chromatography) and a recognition sequence for the tobacco etch virus (TEV-cleavage site). To create a suitable ligation site, alanine 30 was mutated to cysteine (Figure 11, C). Further information can be found in section 4.1 and 4.2.

To generate the full-length alpha synuclein variants with a cysteine residue at position 30 **G1a-f** EPL was used. To this end, the recombinant C-terminal protein segment αS(30-140) **F2** and the desired N-terminal peptide segment αS(1-29) **E2a-f** were combined utilizing the chemoselective EPL chemistry.[54,59] Desulfurization was performed to convert the cysteine residue back to alanine in the natural sequence at position 30. This traceless semisynthesis led to the native full-length alpha Synuclein **G2a** and its site-specifically CEL modified analogs (nPTM) **G2b-f** (Figure 11, D). Further information can be found in section 4.4 and 4.5.

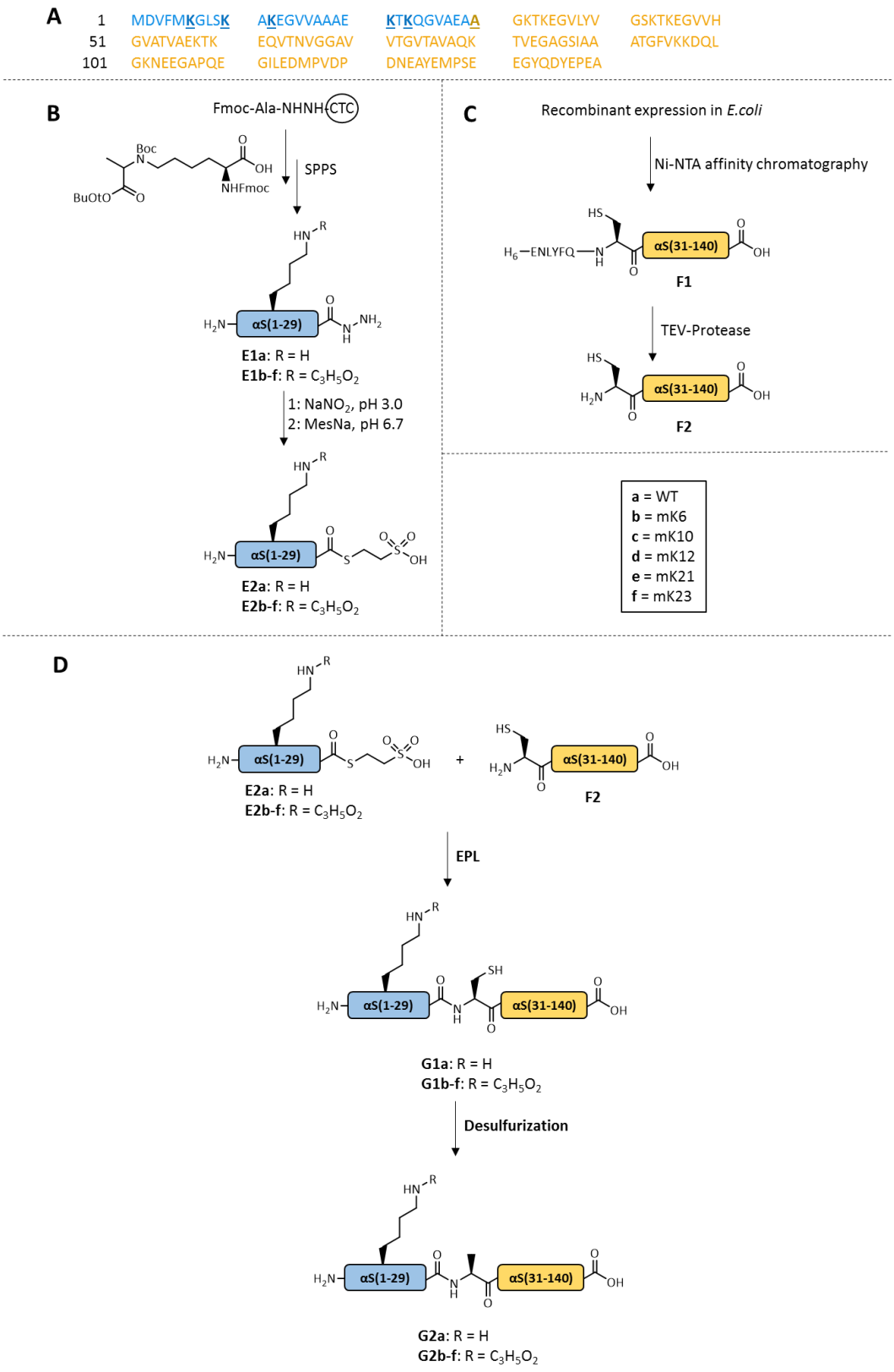

Figure 11 A: Sequence of α-Synuclein with the N-terminal segment (prepared by SPPS) in blue and the C-terminal segment (recombinantly expressed) in yellow. The highlighted lysins (dark blue - 6, 10, 12, 21 and 23) mark the nPTM (CEL) positions.For the ligation to take place, the alanine residue at position 30 was mutated to cysteine. B: Production route of the N-terminal segment of α-Synuclein. C: Production route of the C-terminal segment of α-Synuclein. D: Ligation and desulfurization strategy for the traceless semisynthesis of α-Synuclein.

4.1 Expression of HisTEV-αS(30-140)

The fusion construct **F1** (MW: 13.3 kDa) was successfully obtained via small-scale test expression in 2YT-medium (1 L). SDS-PAGE analysis (Figure 12) showed for the *E. coli* strains BL21(DE3) Gold and BL21(DE3) Rosetta 2 over-expression of the construct after 4 h of IPTG induction (1 mM). After harvesting, lysis and centrifugation the fusion construct was only found in the soluble fraction (TBS, pH 8.0). As the difference in the expression level of the construct was almost identical for both *E. coli* strains, *E. coli* BL21(DE3) Gold was used for the further large-scale expressions (4 L), since only one antibiotic needs to be used for this *E. coli* strain.

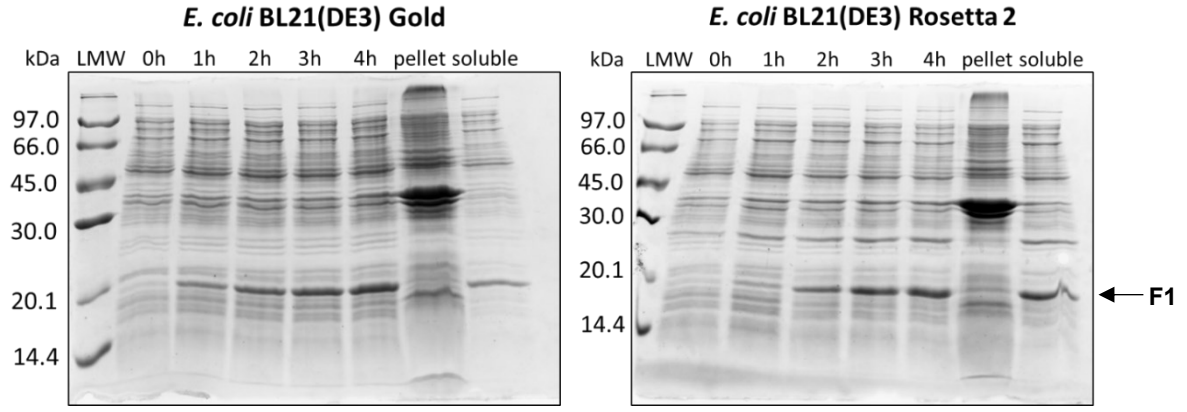

Figure 12 Test expression of the construct F1 (MW: 13.3 kDa) in E. coli strains BL21(DE3) Gold (left) and BL21(DE3) Rosetta 2 (right). The construct was found after induction with IPTG. After harvesting, lysis, and centrifugation the construct was only found in the soluble fraction but not in the pellet.

4.2 Preparation of αS(30-140)

Via the His_6-Tag the construct **F1** was bound to the Ni-NTA affinity column. Other proteins were washed away, and the desired construct was eluted by raising the imidazole concentration (Figure 13, Left). TEV-protease was used for the cleavage of the His_6-Tag (Figure 13, Right). Therefore, first the imidazole was removed via dialysis. The concentration of the fusion construct **F1** was measured showing expression levels of about 33 mg/L of 2YT medium. After TEV-protease cleavage and purification the amount of protein segment αS(30-140) **F2** (MW: 11.5 kDa) was about 12.5 mg/L of 2YT medium (38 %).

As the first used Ni-NTA-batch columns were often blocked, an equilibrated Ni-NTA affinity column for soluble proteins was used instead. It was also important to load the protein solution slowly. The flowthrough contained the desired protein segment **F2**.

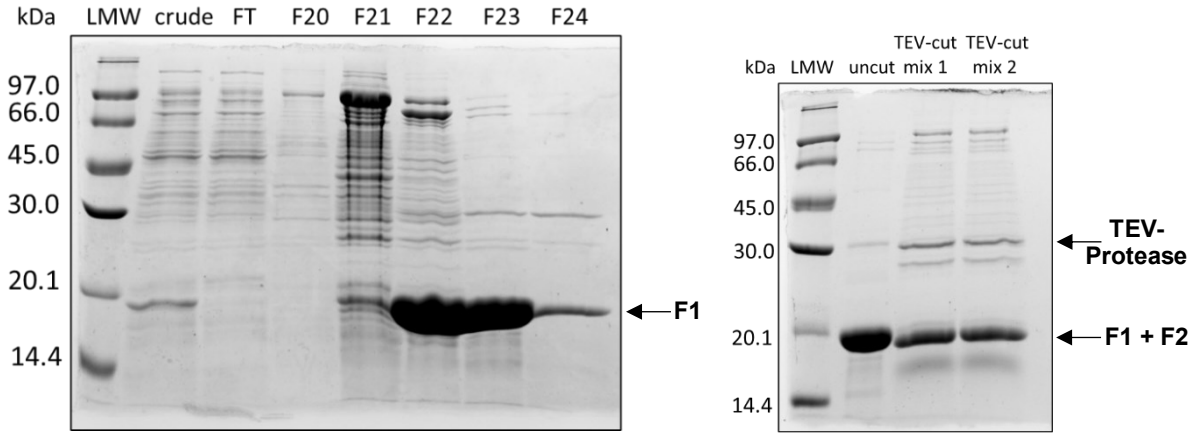

Figure 13 ***Left:*** *SDS-PAGE of the purification of construct* ***F1*** *by Ni-NTA affinity chromatography. The construct* ***F1*** *was eluted by raising the imidazole concentration. Crude: soluble fraction after centrifugation of the cell lysate; FT: Flowthrough during Ni-NTA affinity chromatography; F20-24: Fractions collected;* ***Right:*** *SDS-PAGE of the Cleavage (His_6-Tag) by TEV-Protease (MW: ~ 30kDa). About 38 % of construct* ***F1*** *was cleaved. The bands of* ***F1*** *(MW: 13.3 kDa) overlapped with the C-terminal protein segment* ***F2*** *(MW: 11.5 kDa).*

Segment **F2** from the flowthrough was desalted, purified by preparative RP-HPLC, and lyophilized. Analytical RP-HPLC, ESI-MS, and the deconvoluted mass of the protein are shown in Figure 14. There were several minor additional peaks observed, most likely thiazolidine adducts (Figure 14, C) which were, however, neglected for the further steps.

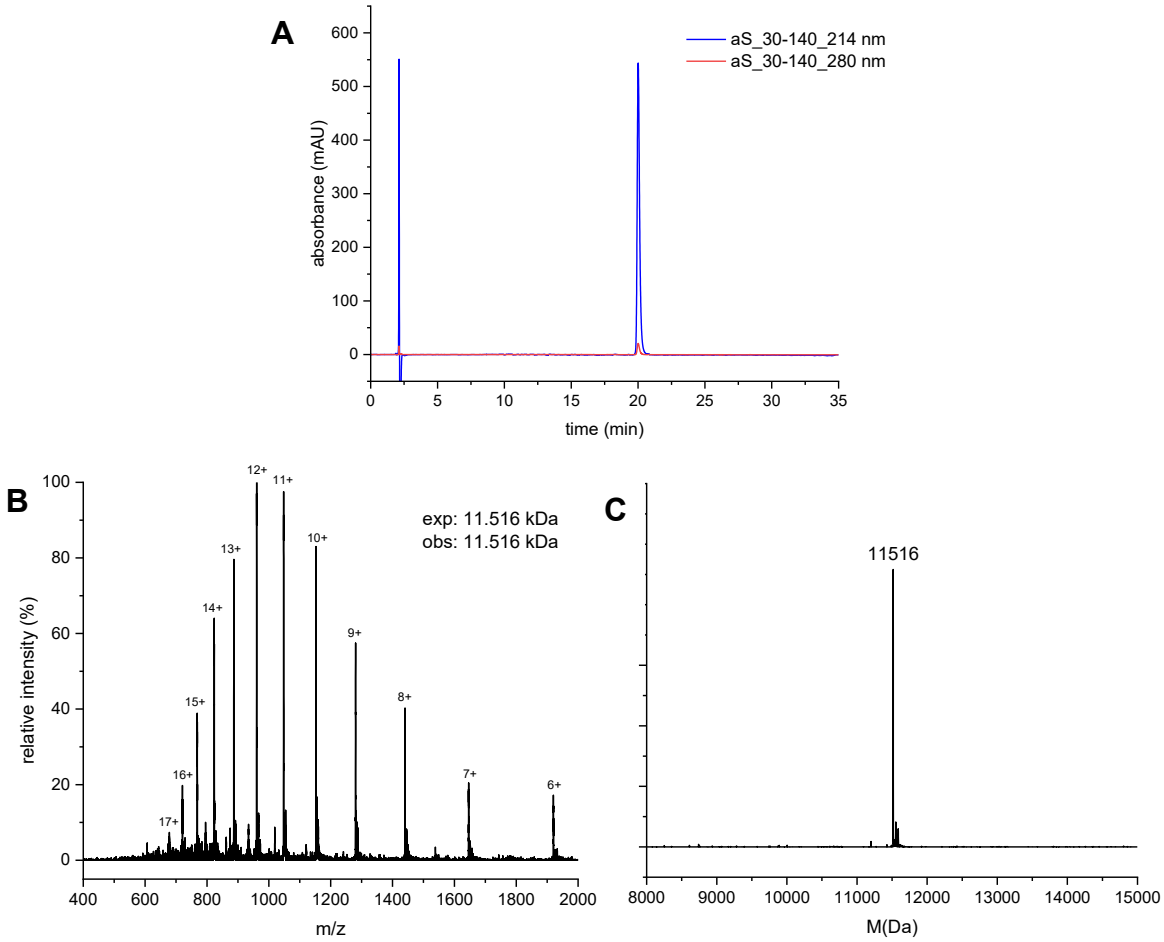

Figure 14 Characterization of C-terminal protein construct ***F2****;* ***A:*** *RP-HPLC analysis at 214 nm and 280 nm;* ***B:*** *raw ESI-MS;* ***C:*** *deconvoluted mass spectrum.*

4.3 Solid Phase Peptide Synthesis

4.3.1 Synthesis of αS(1-29)^{WT}-TE

The N-terminal peptide segment αS(1-29)^{WT}-TE **E2a** (wild type) was prepared using an automated microwave-assisted peptide synthesizer. After cleavage, precipitation, and lyophilization the desired crude peptide hydrazide was obtained. The yield was about 50 mg (17 % from 0.1 mmol scale). After purification via preparative RP-HPLC **E1a** was obtained. As the peptide hydrazide was hydrophilic and the first used gradient was not suitable, for all other peptide hydrazide purifications, the crude material was dissolved into neat water and a linear gradient from 5 % solvent B (ACN + 0.08 % TFA) in solvent A (H_2O + 0.1 % TFA) to 50 % solvent B in 30 min at a flow rate of 20 mL/min and a desalting phase of 20 min was used. After thioester conversion and purification, the desired peptide segment **E2a** was obtained with a yield of 6.4 mg (lost product during purification due to wrong gradient) (12 % from conversion; 2 % from 0.1 mmol synthesis scale) and 28.9 mg (second attempt) (56 % from conversion; 9 % from 0.1 mmol synthesis scale). Analytical RP-HPLC and ESI-MS are shown in Figure 15.

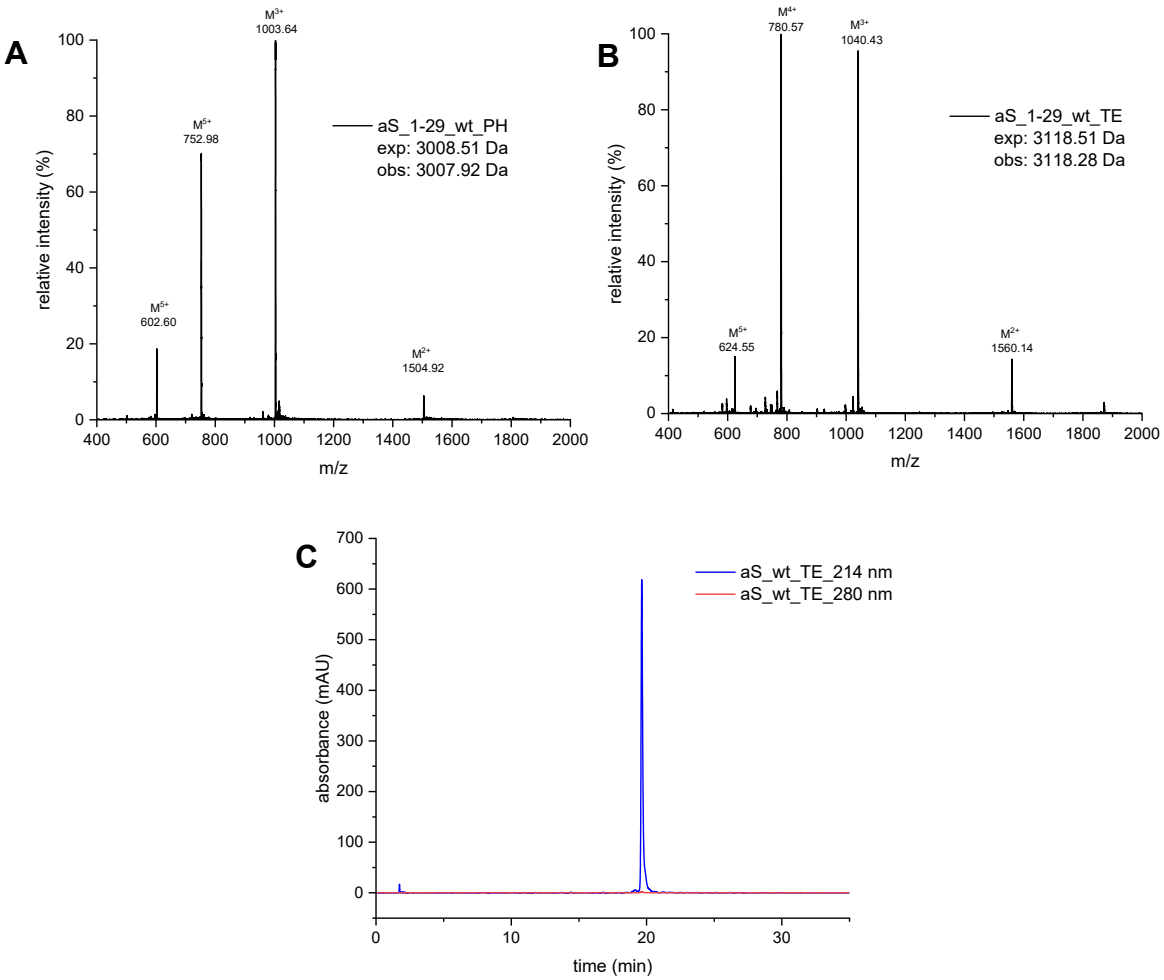

*Figure 15 Characterization of the N-terminal peptide thioester αS(1-29)^{WT}-TE **E2a**. **A:** ESI-MS of the peptide hydrazide **E1a**; **B:** ESI-MS of the peptide thioester **E2a**; **C:** Analytical RP-HPLC at 214 nm and 280 nm of **E2a**.*

4.3.2 Synthesis of αS(1-29)^{mK6,10,12,21,23}-TE

Instead of Fmoc-Lys-(Boc)-OH, the modified amino acid Fmoc-L-CEL(OtBu)(Boc)-OH was coupled at the desired position. For the generation of the peptide thioesters **E2b-f** the crude peptide hydrazides **E1b-f** were directly transformed into peptide thioesters without purification of the crude peptide hydrazides. Analytical RP-HPLC and ESI-MS of the desired peptide segments **E2b-f** are shown in Figure 16 to Figure 20. The yields of most of the modified variants were similar to the wild type (**E2a**) and were around 10 % from the 0.1 mmol synthesis scale. The variants mK12 (**E2d**) and mK21 (**E2e**) showed almost 20 % yield. All variants had a similar purity. Only mK23 (**E2f**) had a slightly higher proportion of impurities, which were, however, neglected for the further steps.

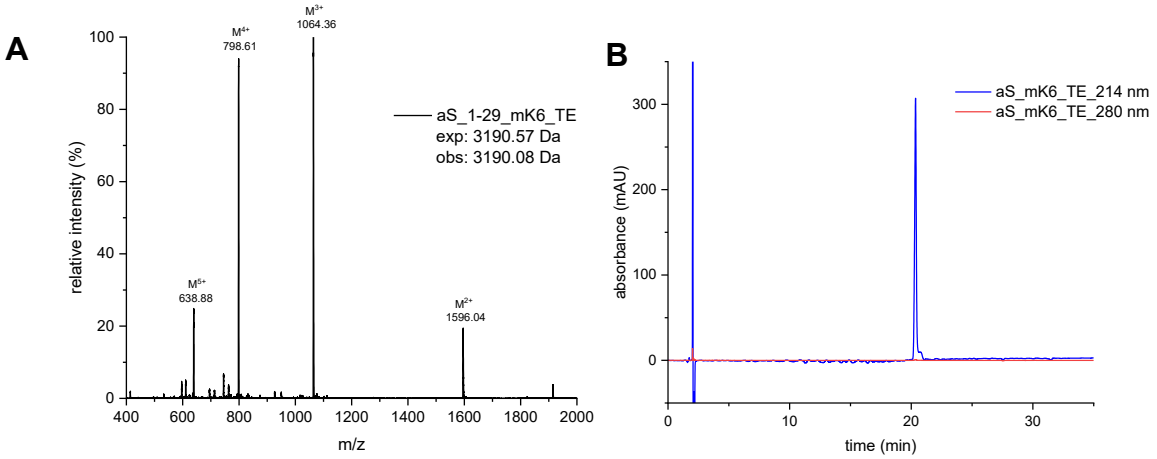

*Figure 16 Characterization of the N-terminal peptide thioester αS(1-29)^{mK6}-TE **E2b**. **A:** ESI-MS of the peptide thioester **E2b**; **B:** Analytical RP-HPLC at 214 nm and 280 nm of **E2b**.*

The yield for mK6 (**E2b**) was 36.4 mg (11 % from 0.1 mmol scale).

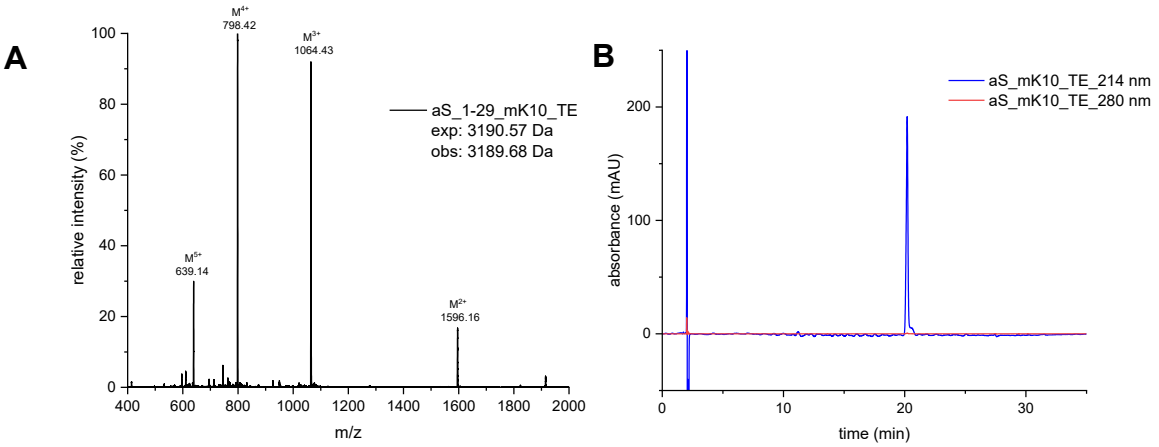

*Figure 17 n Characterization of the N-terminal peptide thioester αS(1-29)^{mK10}-TE **E2c**. **A:** ESI-MS of the peptide thioester **E2c**; **B:** Analytical RP-HPLC at 214 nm and 280 nm of **E2c**.*

The yield for mK10 (**E2c**) was 21 mg (7 % from 0.1 mmol scale).

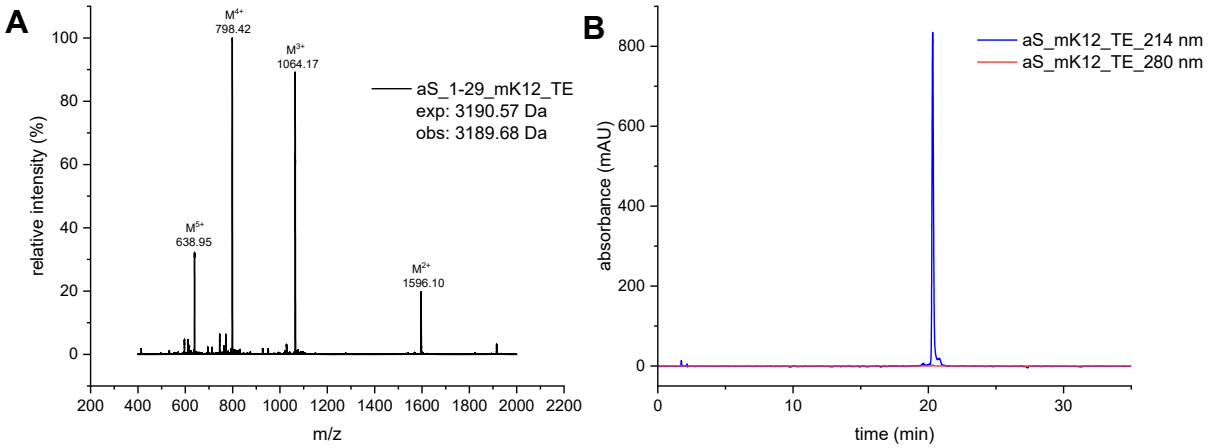

*Figure 18 n Characterization of the N-terminal peptide thioester αS(1-29)^{mK12}-TE **E2d**. **A:** ESI-MS of the peptide thioester **E2d**; **B:** Analytical RP-HPLC at 214 nm and 280 nm of **E2d**.*

The yield for mK12 (**E2d**) was 59.3 mg (19 % from 0.1 mmol scale).

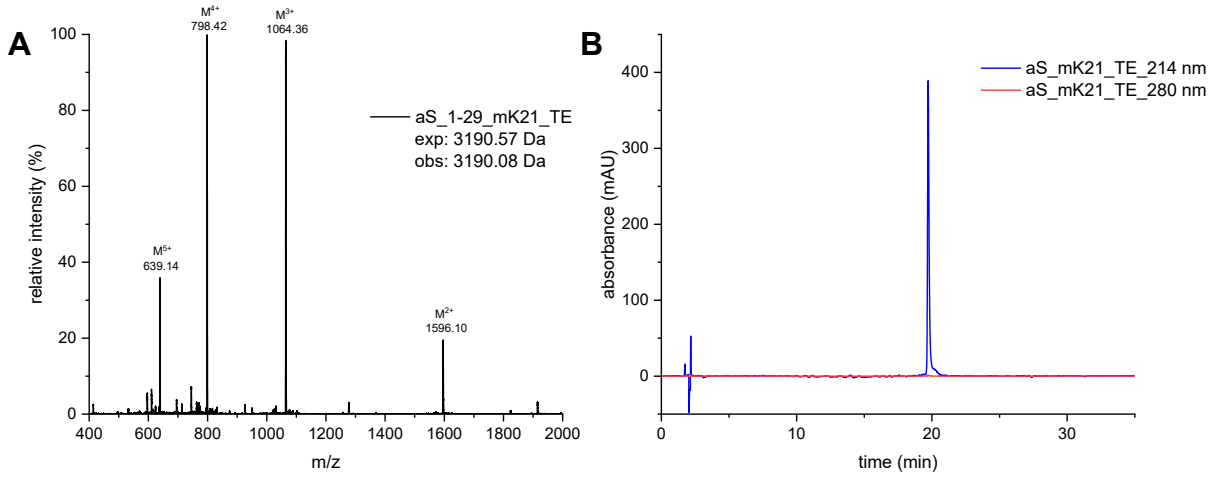

*Figure 19 n Characterization of the N-terminal peptide thioester αS(1-29)^{mK21}-TE **E2e**. **A:** ESI-MS of the peptide thioester **E2e**; **B:** Analytical RP-HPLC at 214 nm and 280 nm of **E2e**.*

The yield for mK21 (**E2e**) was 63.4 mg (20 % from 0.1 mmol scale).

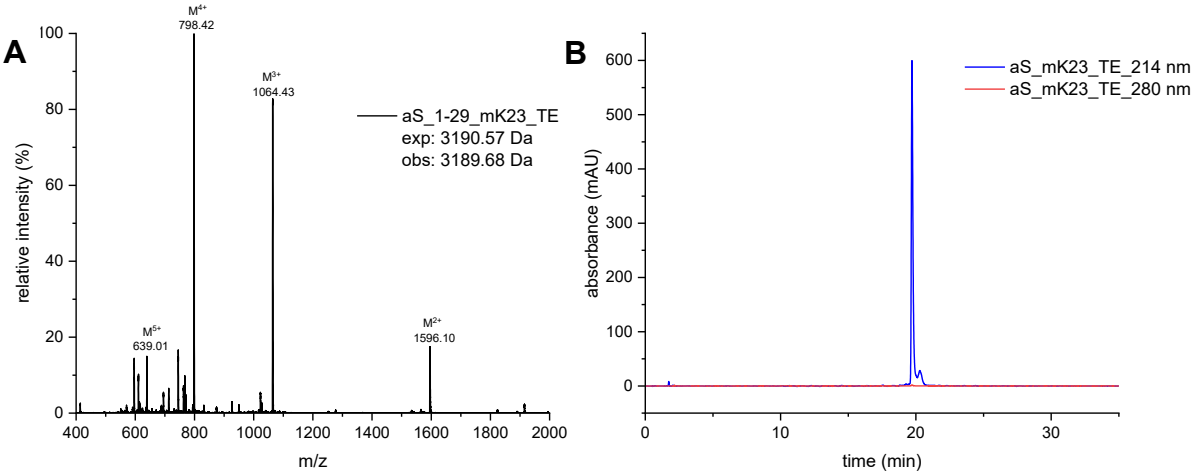

*Figure 20 Characterization of the N-terminal peptide thioester αS(1-29)^{mK23}-TE **E2f**. **A:** ESI-MS of the peptide thioester **E2f**; **B:** Analytical RP-HPLC at 214 nm and 280 nm of **E2f**.*

The yield for mK23 (**E2f**) was 31 mg (10 % from 0.1 mmol scale).

4.4 Ligations

4.4.1 Ligation of αS(1-29)^{wt}-TE and αS(30-140)

Ligation and purification of the desired wild type ligation product **G1a** was carried out under the conditions described in section 3.7.1. Therefore, 1 equivalent (5 mg) protein construct αS(30-140) (**F2**) was dissolved in degassed ligation buffer (200 mM NaPi, 6 M Gdn HCl, pH 7.2) containing 50 mM TCEP and 200 mM MPAA to reach a protein concentration of 1 mM. 2.1 equivalent (2.8 mg) of peptide thioester (**E2a**) was added and the mixture shaken at 600 rpm and 37°C for 5 h. The reaction progress was monitored via LCMS (Appendix; Figure 58), analytical RP-HPLC, and SDS-PAGE after 0.5 h, 2 h, and 5 h (Figure 21 and Figure 22).

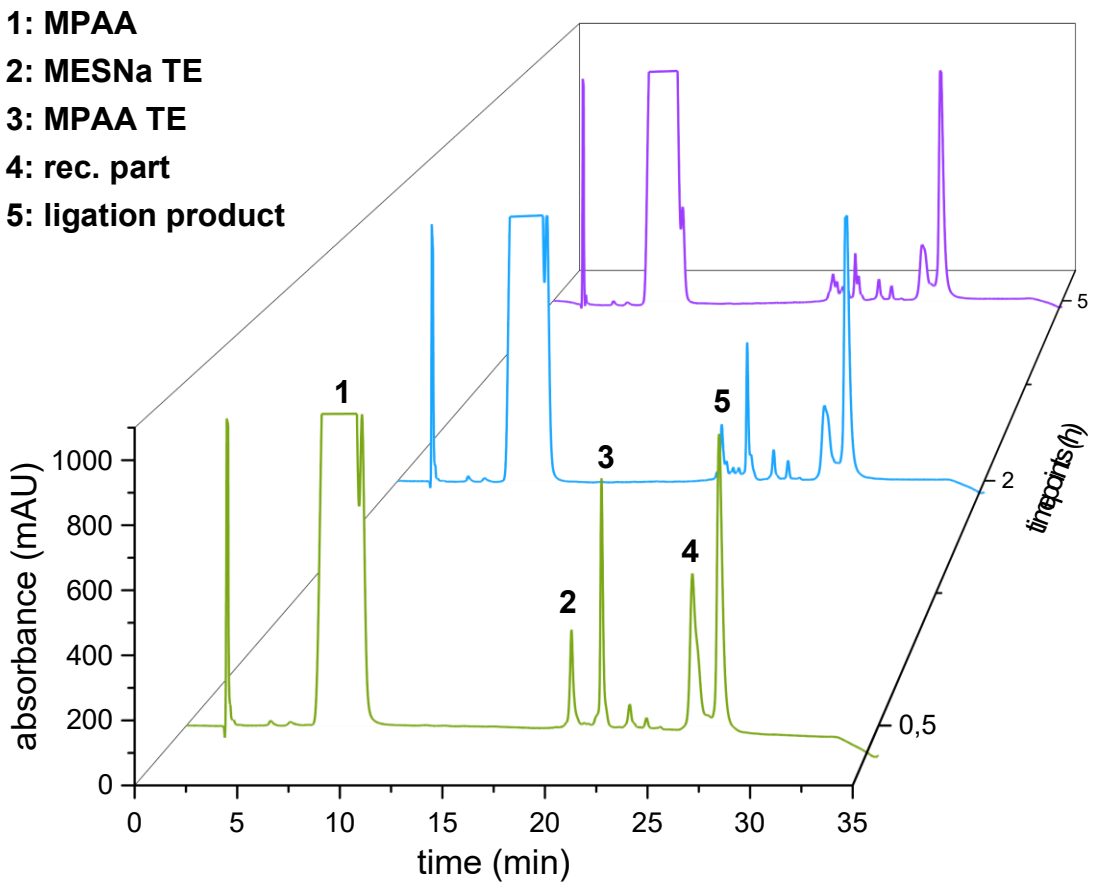

*Figure 21 Waterfall diagram of the monitoring of the ligation between the recombinant C-terminal protein segment αS (30-140) **F2** and the desired N-terminal peptide thioester αS (1-29) **E2a**.*

The ligation was monitored by analytical RP-HPLC (Figure 21). The following analytical RP-HPLC peaks were observed: MPAA (**1**, 10 min), MESNa thioester (**2**, 21 min), MPAA thioester (**3**, 23 min), recombinant part (**4**, 27 min), and ligation product (**5**, 28 min).

Hydrolysis was not a problem in this reaction. The peak of the ligation product (**5**) was already clearly visible after 0.5 h and was already higher than the peak of the recombinant part (**4**), which indicates a rapid reaction. Evaluation of the reaction progress was done by analysis of the decreasing starting material. The peak of starting material (**4**) diminished with the reaction time after the addition of thioester (**2**), but no significant difference could be seen between 2 h and 5 h of reaction time.

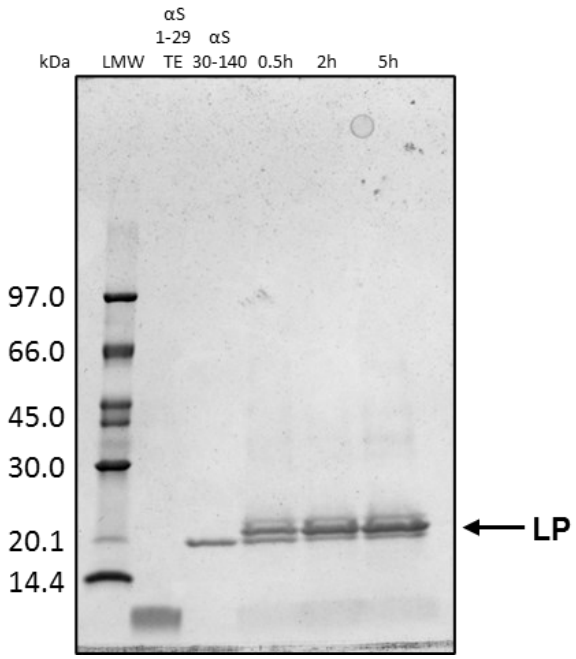

*Figure 22 Monitoring of the ligation of recombinant C-terminal protein segment αS (30-140) **F2** (calculated MW ≈ 11.5 kDa) with the desired N-terminal peptide thioester αS (1-29) **E2a** (calculated MW ≈ 3.2 kDa). The band of the ligation product LP (calculated MW ≈ 14.5 kDa) appeared at ca. 21.0 kDa. Comparison of the band for the ligation product with the band of starting material revealed a conversion of ca. 81% after 2h reaction time, which is similar to the conversion after 5h reaction time (78%).*

Comparison of the SDS-PAGE band for the ligation product with the band of starting material revealed a conversion of ca. 81 % after 2 h reaction time, which is similar to the conversion after 5 h reaction time (78 %) (Figure 22). Thus, the reaction was finished after 2 h of reaction time.

The ligation product was purified by semipreparative RP-HPLC. Yields for a ligation on a scale of 5 mg **F2** were 3.5 mg (56 %) of purified ligation product **G1a**. Data of the final characterization from the purified product by analytical RP-HPLC and ESI-MS are shown in Figure 23.

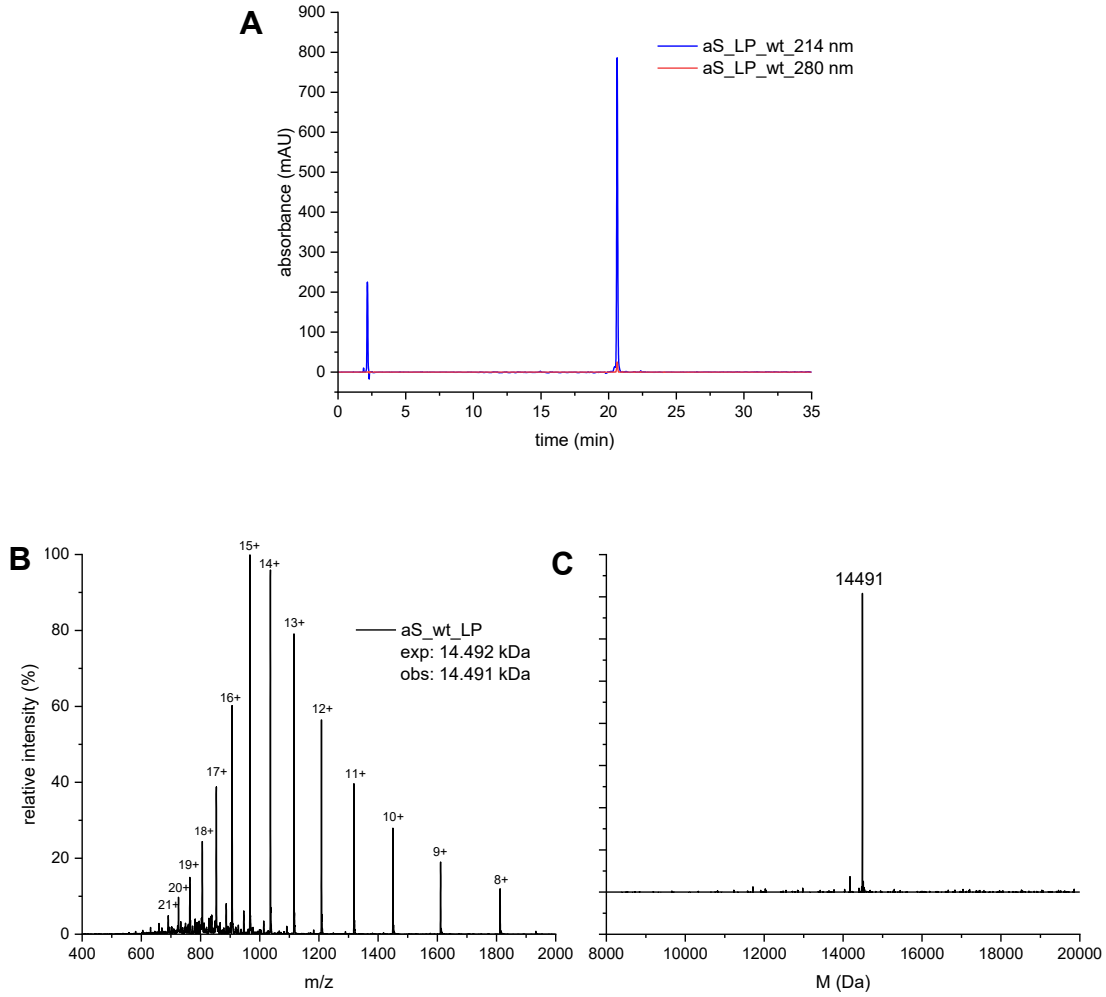

*Figure 23 Characterization of isolated ligation product **G1a**; **A:** RP-HPLC analysis at 214 nm and 280 nm; **B:** raw ESI-MS; **C:** deconvoluted mass spectrum.*

4.4.2 Ligation of αS(1-29)^{mK6,10,12,21,23}-TE and αS(30-140)

The ligation products (**G1b-f**) were obtained by ligation of the modified thioesters (**E2b-f**) with the protein construct αS(30-140) (**F2**). The ligation was carried out like described in section 3.7.1. The reaction time was reduced from 5 h to 2 h, as the ligation in case of the wild type variant (**G1a**) has shown to be finished in 2 h. The reaction progress was monitored via LCMS (Appendix; Figure 59 to Figure 63), analytical RP-HPLC, and SDS-PAGE after 0.5 h, 1 h, and 2 h (**G1e**: Figure 28 and Figure 29). Whereby, SDS-PAGE and analytical RP-HPLC data were only provided for the variant mK21 (**G1e**) as a representative for all modified variants.

The ligation product was purified by semipreparative RP-HPLC. Analytical RP-HPLC data was only provided for the variant mK21 (**G1e**) as a representative for all modified variants (Figure 27). ESI-MS and the deconvoluted mass of the desired ligation products **G1b-f** are shown in Figure 24 to Figure 27 and Figure 30. The purities of all

modified variants were similar to each other and to the wild type (**G1a**). The yields for many variants were between 80 and 90 %. For variants mK21 (**G1e**) and mK23 (**G1f**), the yields were lower and more similar to the wild type (**G1a**).

mK6:

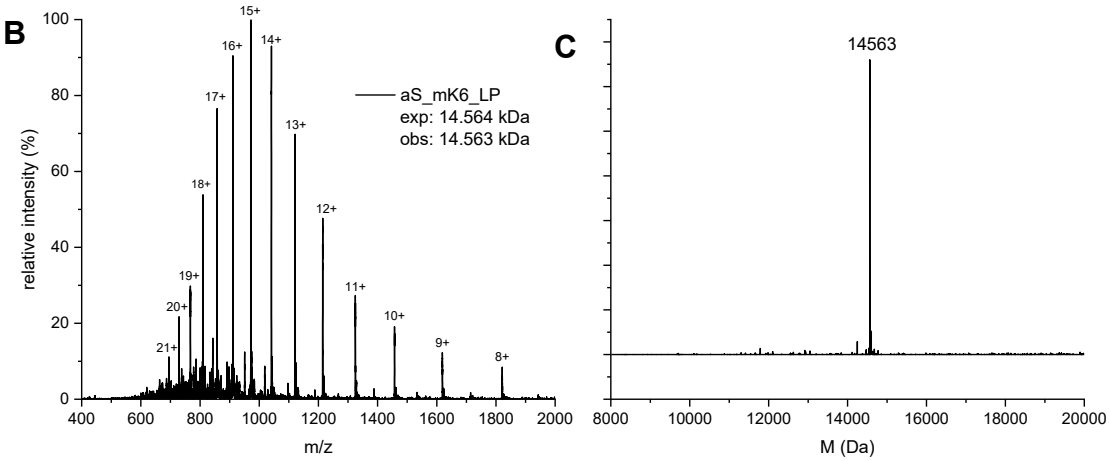

*Figure 24 Characterization of isolated ligation product **G1b**; **B:** raw ESI-MS; **C:** deconvoluted mass spectrum.*

The yield for mK6 (**G1b**) was 7.1 mg (112 %; product still wet).

mK10:

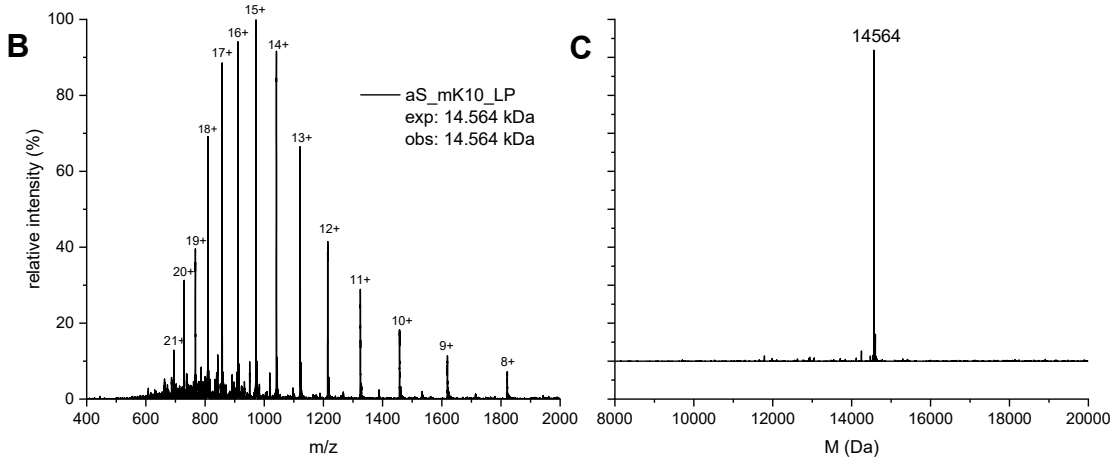

*Figure 25 Characterization of isolated ligation product **G1c**; **B:** raw ESI-MS; **C:** deconvoluted mass spectrum.*

The yield for mK10 (**G1c**) was 5.1 mg (81 %).

mK12:

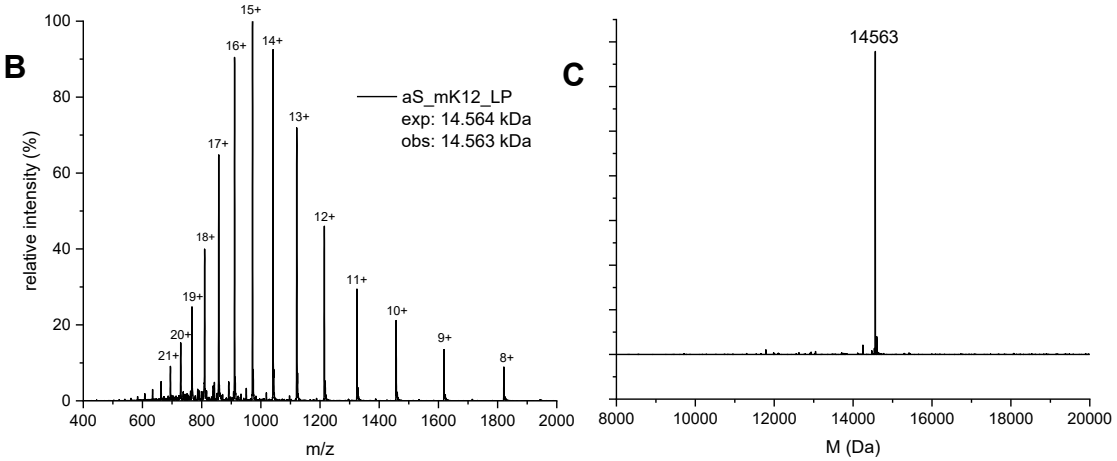

*Figure 26 Characterization of isolated ligation product **G1d**; **B:** raw ESI-MS; **C:** deconvoluted mass spectrum.*

The yield for mK12 (**G1d**) was 5.6 mg (89 %).

mK21:

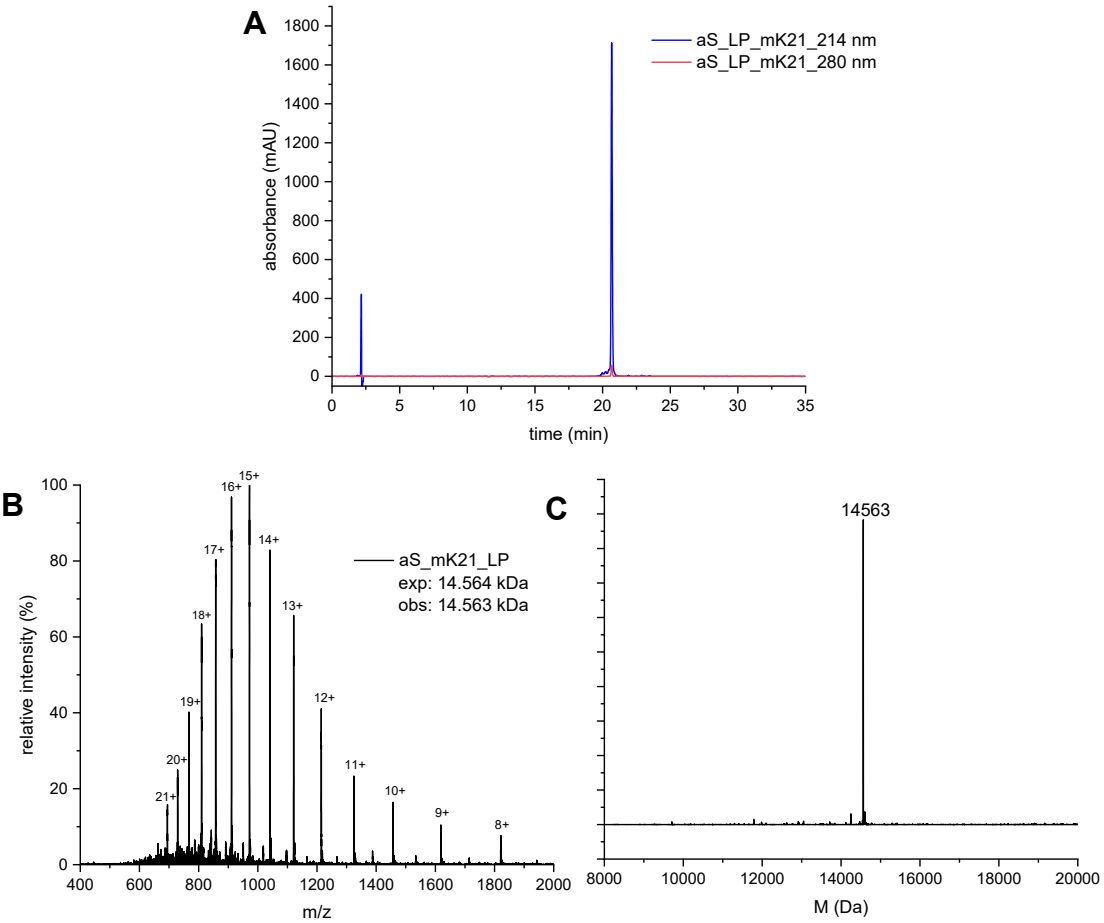

*Figure 27 Characterization of isolated ligation product **G1e**; **A:** RP-HPLC analysis at 214 nm and 280 nm; **B:** raw ESI-MS; **C:** deconvoluted mass spectrum.*

The yield for mK21 (**G1e**) was 4.2 mg (66 %).

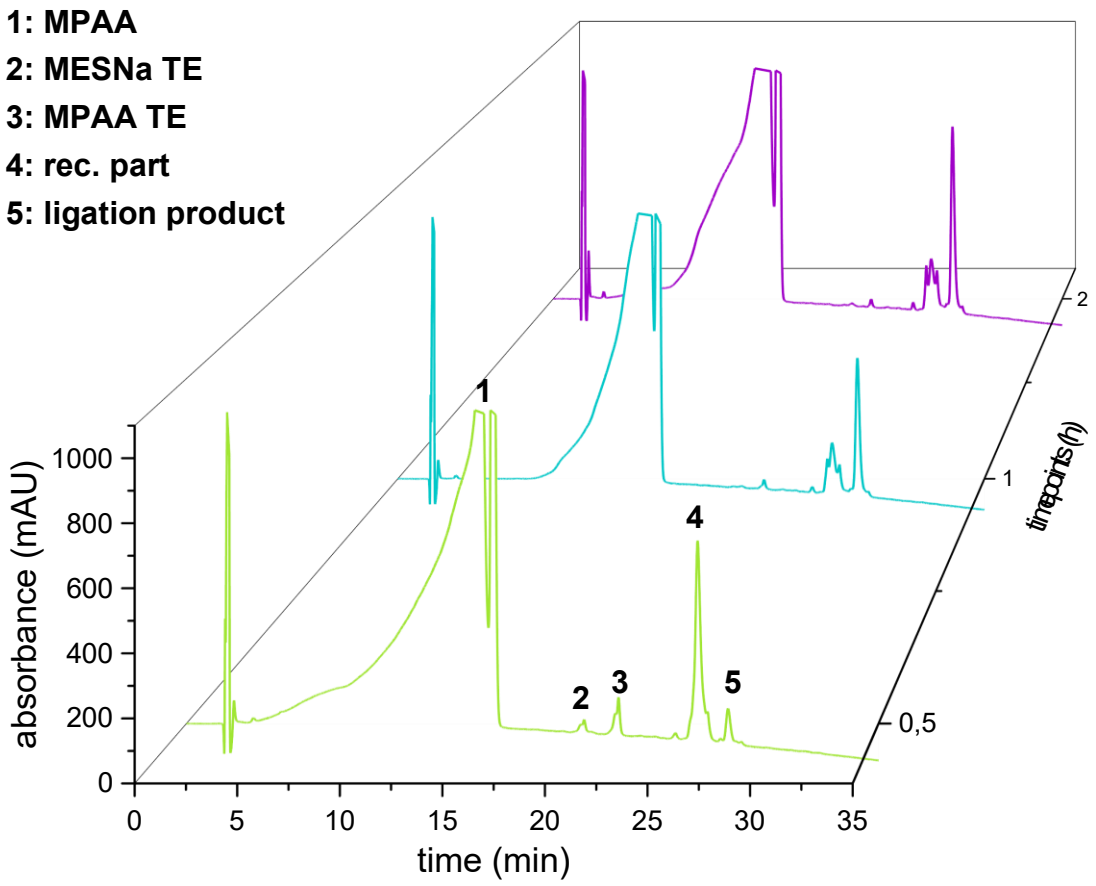

*Figure 28 Waterfall diagram of the monitoring of the ligation between the recombinant C-terminal protein segment αS (30-140) **F2** and the desired N-terminal peptide thioester αS (1-29) **E2e**, evaluation of the reaction progress had to be done by analysis of the decreasing starting material. The peak of starting material diminished with the reaction time after the addition of thioester. The reaction was considered to be finished after 2 h of reaction time.*

The ligation was monitored by analytical RP-HPLC (Figure 28). The following analytical RP-HPLC peaks were observed: MPAA (**1**, 15 min), MESNa thioester (**2**, 22 min), MPAA thioester (**3**, 23 min), recombinant part (**4**, 27 min), and ligation product (**5**, 28 min).

Evaluation of the reaction progress was done by analysis of the decreasing starting material (**4**). As with the wild type **G1a** (Figure 28), the reaction was completed after 2 hours. Hydrolysis did not seem to be a problem here either. After 0.5 h, the peak of the ligation product (**5**) was still much lower than the peak of the recombinant part (**4**), which indicates that the reaction proceeded more slowly at the beginning compared to the wild type **G1a**.

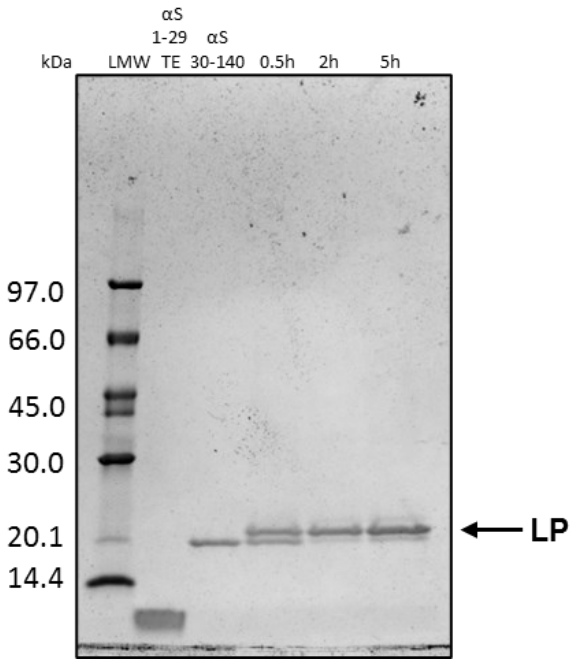

*Figure 29 Monitoring of the ligation of recombinant C-terminal protein segment αS (30-140) **F2** (calculated MW ≈ 11.5 kDa) with the desired N-terminal peptide thioester αS (1-29) **E2e** (calculated MW ≈ 3.2 kDa). The band of the ligation product LP (calculated MW ≈ 14.5 kDa) appeared at ca. 21.0 kDa. Comparison of the band for the ligation product with the band of starting material revealed a conversion of ca. 89% after 2h reaction time.*

Comparison of the SDS-PAGE band for the ligation product **G1e** with the band of starting material **F2** revealed a conversion of ca. 89 % after 2 h reaction time (Figure 29), which is similar to the wild type **G1a**.

mK23:

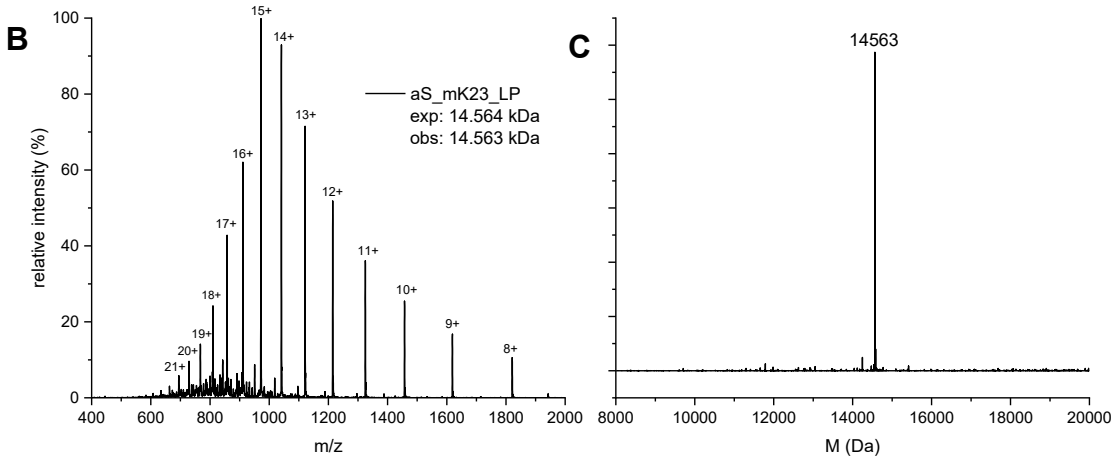

*Figure 30 Characterization of isolated ligation product **G1f**; **B:** raw ESI-MS; **C:** deconvoluted mass spectrum.*

The yield for mK23 (**G1f**) was 3.5 mg (55 %).

4.5 Desulfurization

4.5.1 Desulfurization of αS(1-140)^{wt}

Metal-free desulfurization was carried out for ligation product **G1a** like described in section 3.8.1. Generally, the reaction was performed in desulfurization buffer (200 mM NaPi, 6 M Gdn HCl, pH 6.8-7.2) (100 µL per mg). The same volume of neutralized TCEP solution (500 mM TCEP in DB, neutralized with 28 µL Et_3N per 100 µL DB, pH 6.5-7.0) was added. Then, MESNa (130 mM final concentration) and VA-044 (0.4 M in degassed water, diluted to 25 mM final concentration (6.7 µL stock solution / 100 µL reaction volume)) were added. The reaction progress was monitored by LCMS and the product was purified by semipreparative RP-HPLC. As the desulfurization took the first time more than 3 h, for the other desulfurizations instead of 25 mM 50 mM final concentration of VA-044 (radical initiator) was used.

Data of the final characterization of the pure product **G2a** by analytical RP-HPLC and ESI-MS are shown in Figure 31. The yield was 3 mg (48 %) and 2.4 mg (38 %) over ligation and desulfurization.

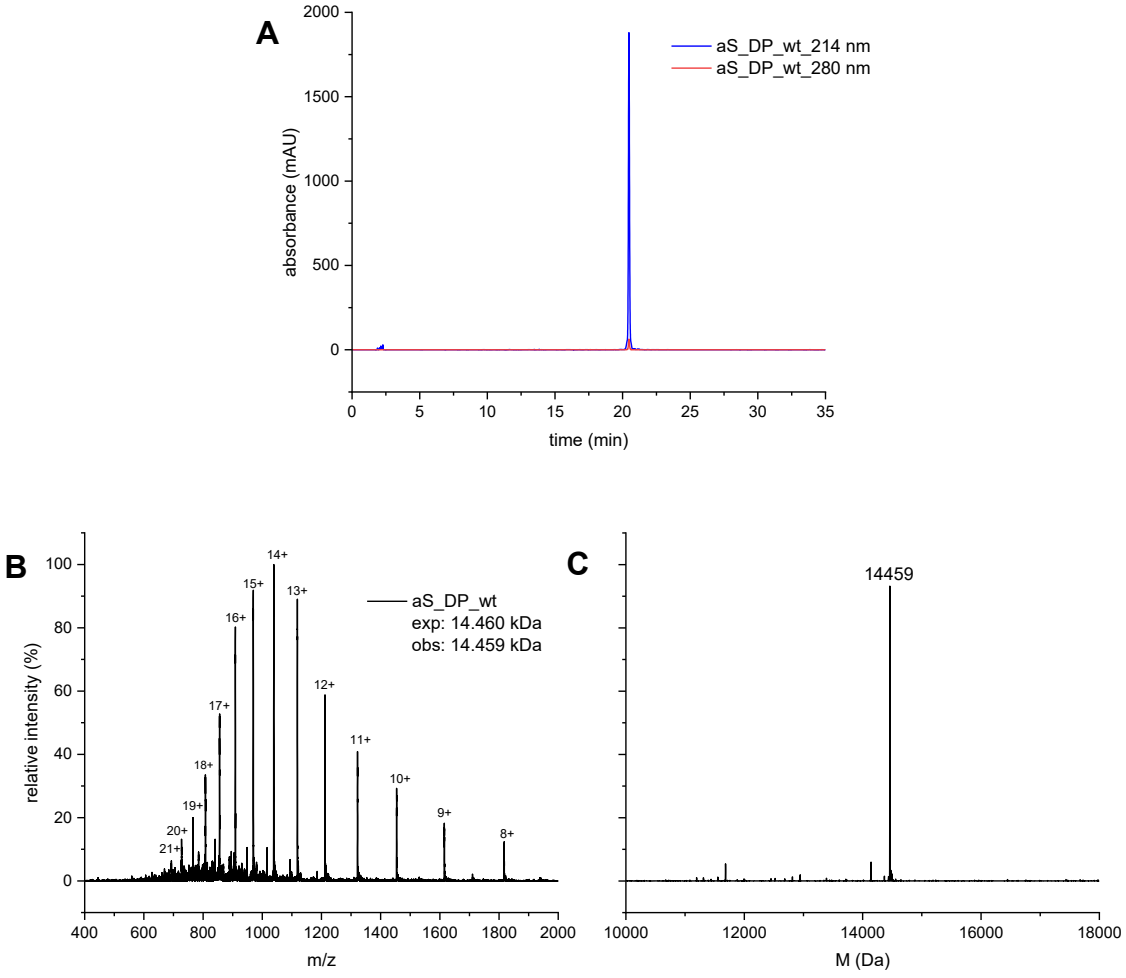

*Figure 31 Characterization of desulfurization product **G2a**; **A:** RP-HPLC analysis at 214 nm and 280 nm; **B:** raw ESI-MS; **C:** deconvoluted mass spectrum.*

4.5.2 Desulfurization of αS(1-140)^{mK6,10,12,21,23}

Metal-free desulfurization was carried out for ligation products **G1b-f** like described in section 3.8.1. A final concentration of 50 mM VA-044 was used.

Data of the final characterization of **G2b-f** by analytical RP-HPLC and ESI-MS are shown in Figure 32 to Figure 36. The purities of all modified variants were similar to the wild type. The yields of the variants mK12 (**G2d**) and 23 (**G2f**) were similar to the wild type **G2a** (36-38 %). The other variants showed higher yields (55-67 %).

mK6:

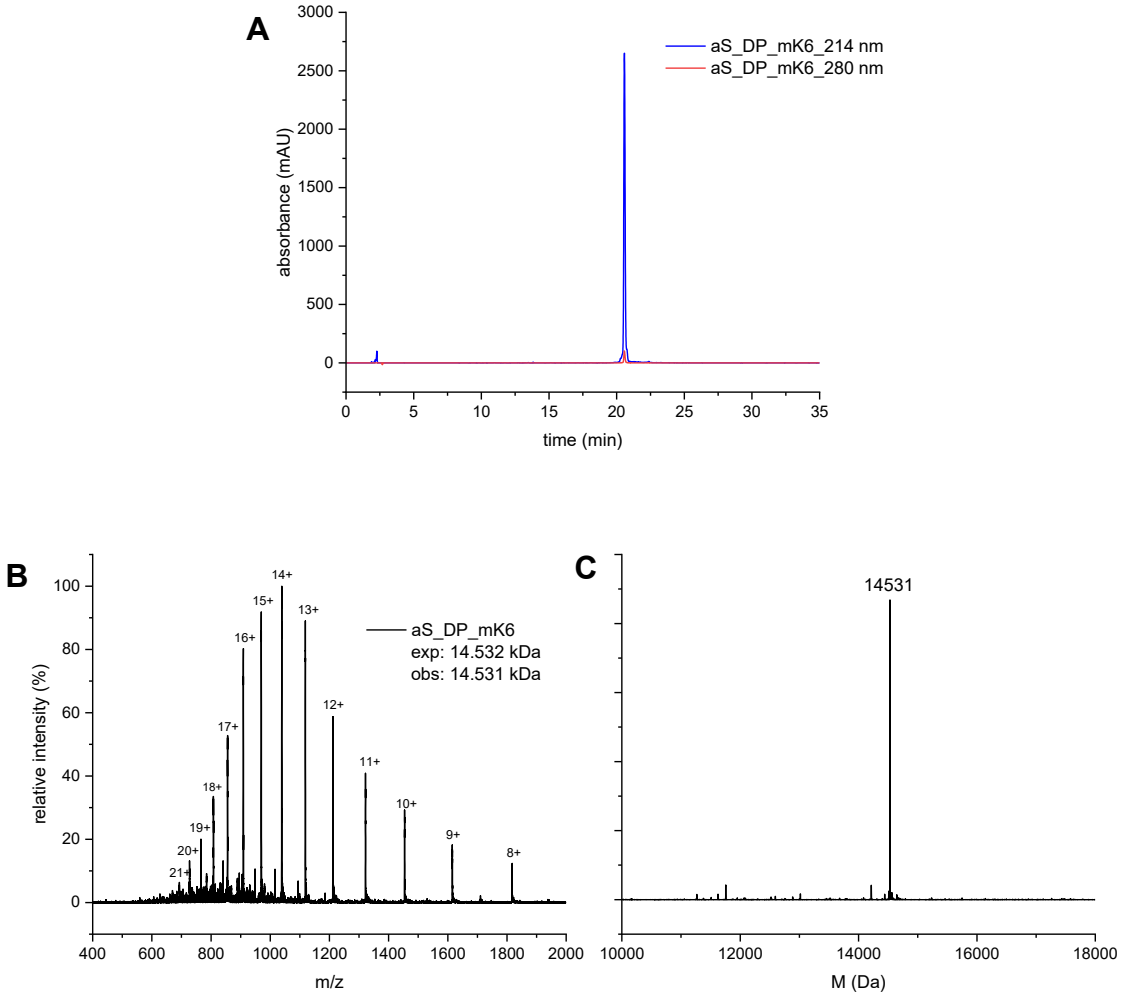

*Figure 32 Characterization of desulfurization product **G2b**; **A:** RP-HPLC analysis at 214 nm and 280 nm; **B:** raw ESI-MS; **C:** deconvoluted mass spectrum.*

The yield for mK6 (**G2b**) was 4.2 mg (67 %) over ligation and desulfurization.

mK10:

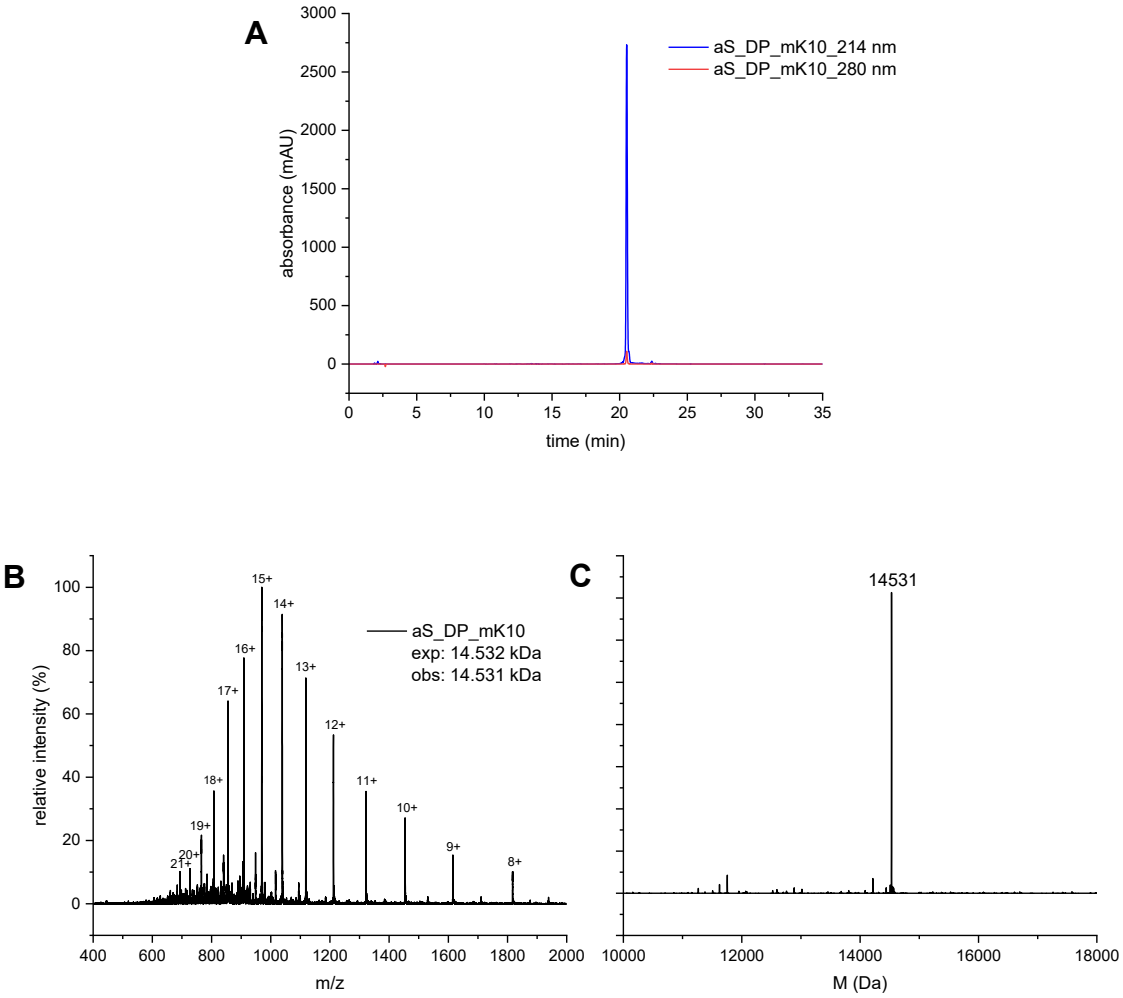

*Figure 33 Characterization of desulfurization product **G2c**; **A:** RP-HPLC analysis at 214 nm and 280 nm; **B:** raw ESI-MS; **C:** deconvoluted mass spectrum.*

The yield for mK10 (**G2c**) was 3.9 mg (62 %) over ligation and desulfurization.

mK12:

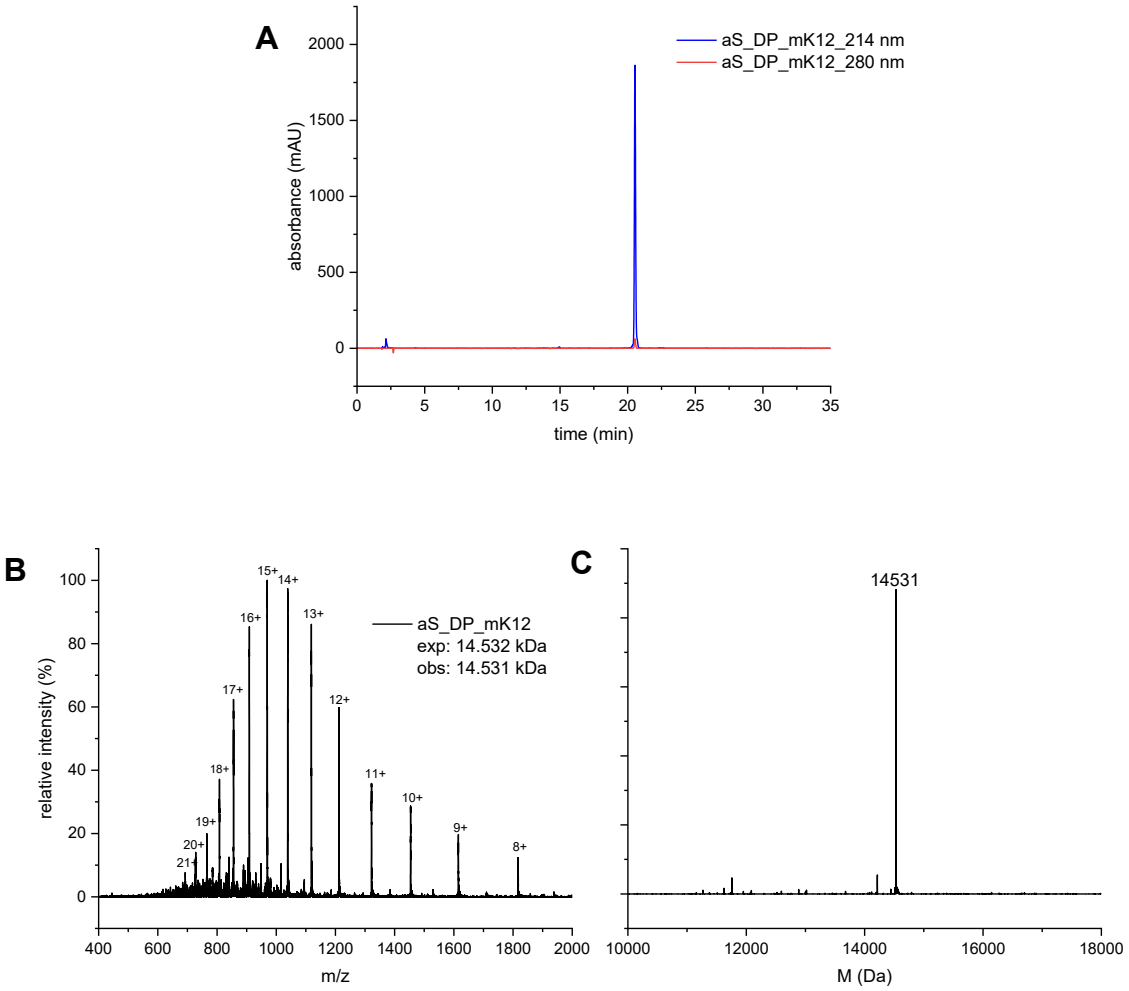

*Figure 34 Characterization of desulfurization product **G2d**; **A:** RP-HPLC analysis at 214 nm and 280 nm; **B:** raw ESI-MS; **C:** deconvoluted mass spectrum.*

The yield for mK12 (**G2d**) was 2.3 mg (36 %) over ligation and desulfurization.

mK21:

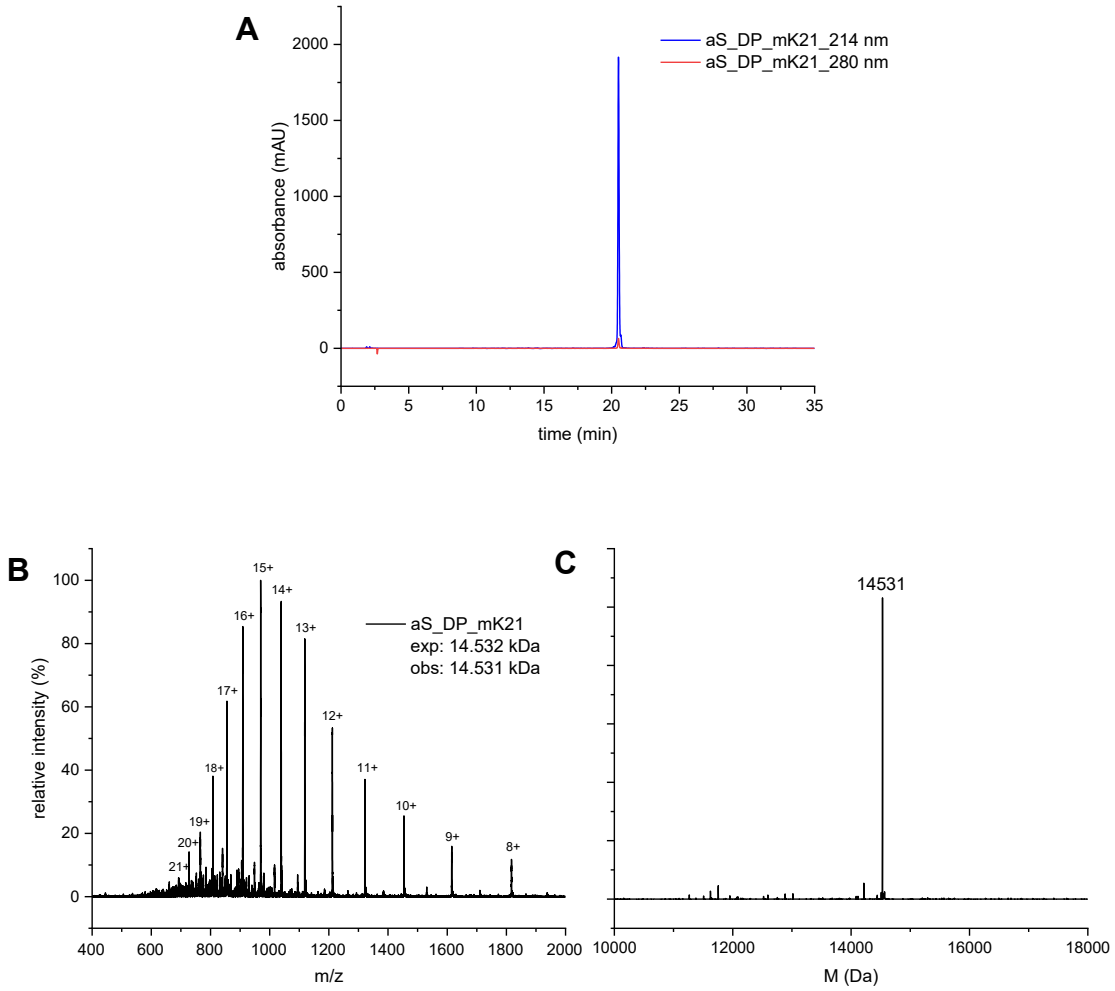

*Figure 35 Characterization of desulfurization product **G2e**; **A:** RP-HPLC analysis at 214 nm and 280 nm; **B:** raw ESI-MS; **C:** deconvoluted mass spectrum.*

The yield for mK21 (**G2e**) was 3.5 mg (55 %) over ligation and desulfurization.

mK23:

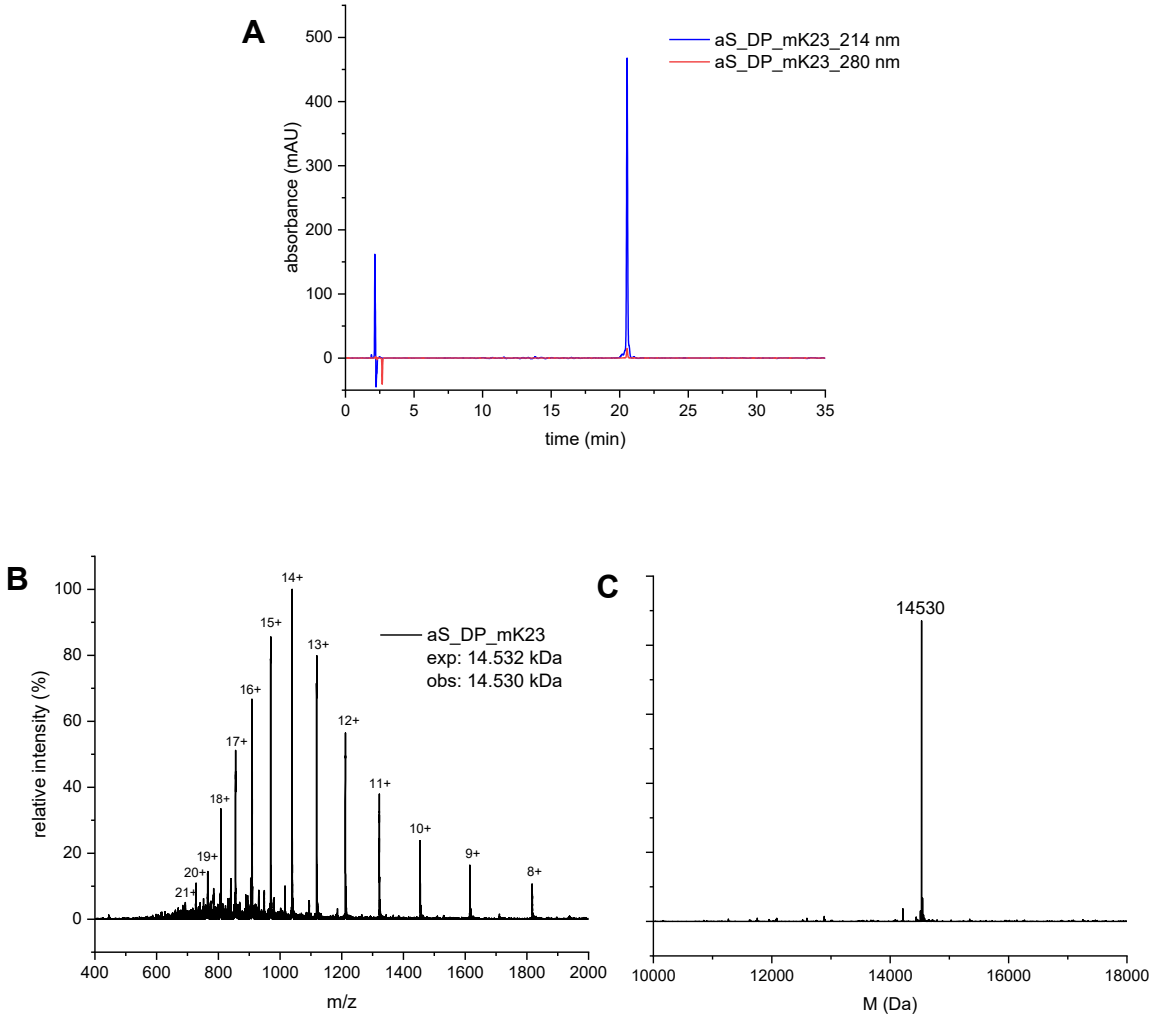

*Figure 36 Characterization of desulfurization product **G2f**; **A:** RP-HPLC analysis at 214 nm and 280 nm; **B:** raw ESI-MS; **C:** deconvoluted mass spectrum.*

The yield for mK23 (**G2f**) was 2.4 mg (38 %) over ligation and desulfurization.

HRMS:

From all full length αSyn variants **G2a-f** a HRMS (high resolution MS) analysis was performed (Figure 37; Appendix Figure 64 to Figure 66). The spectrum of **G2f** in Figure 37 is shown here as a representative for all variants. The spectrum consists mainly of the peak series of the desired protein, indicating a high purity.

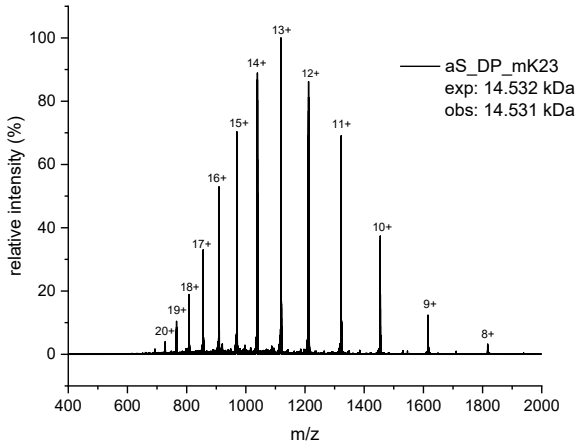

*Figure 37 HRMS after desulfurization of full-length αSyn variant **G2f**.*

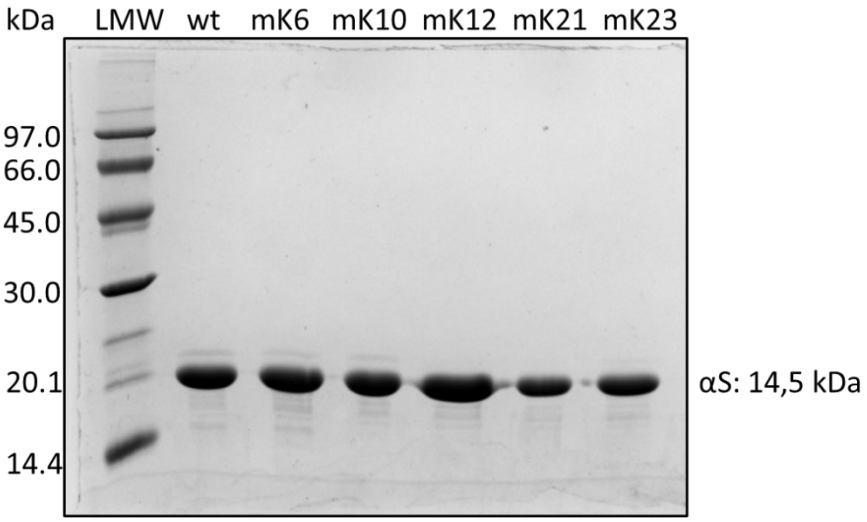

*Figure 38 SDS- PAGE of all full length αSyn variants **G2a-f**. High purity was achieved.*

The SDS-PAGE of all αSyn variants **G2a-f** can be seen in Figure 38. Only small bands of impurities could be seen. These probably came from the purification of the recombinant part but are negligible. In general, it can be said that the desired products were obtained in high purity. The band of alpha synuclein appeared at 21.0 kDa (calculated MW ≈ 14.5 kDa).

4.6 ThT Assay and SEM Measurements

4.6.1 ThT Assay

For the ThT (thioflavin T) assay, an approach was first followed in which the aggregation reaction was carried out for more than 7 days and the alpha synuclein aggregation of different time points was then quantified by thioflavin T fluorescence like described in section 3.9. The experiment was first only tested for the wild type alpha synuclein (**G2a**) with concentrations of 50 µM and 100 µM (Figure 39).

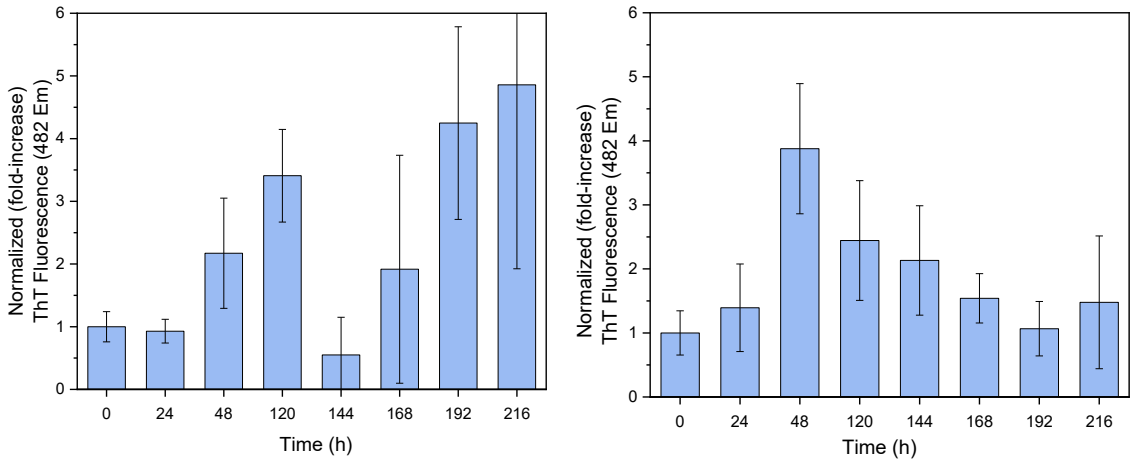

Figure 39 ThT Assay: aggregation reaction in Eppendorf tubes; left: 100µM αS(1-140)^{wt}; right: 50µM αS(1-140)^{wt}.

The ThT fluorescence was measured after the aggregation reaction in Eppendorf tubes. Figure 39 shows the results for αS_wt (**G2a**) with a concentration of 100 µM on the left and the results for αS_wt (**G2a**) with a concentration of 50 µM on the right. The ThT fluorescence increase can be better recognised for 100 µM. In general, it can be said that the results of the Eppendorf Tube approach are subject to very strong fluctuations. At the higher concentration, the increase in the ThT fluorescence signal, which is due to an aggregation of alpha synuclein, was more noticeable. Unfortunately, we could not draw any conclusion from this set of experiment.

To reduce the fluctuations and to collect more data points a combined approach was used. Therefore, the assay was repeated for both concentrations in a 96-well plate where aggregation reaction and ThT fluorescene measurment took place. The entire experiment was carried out as described in section 3.9.

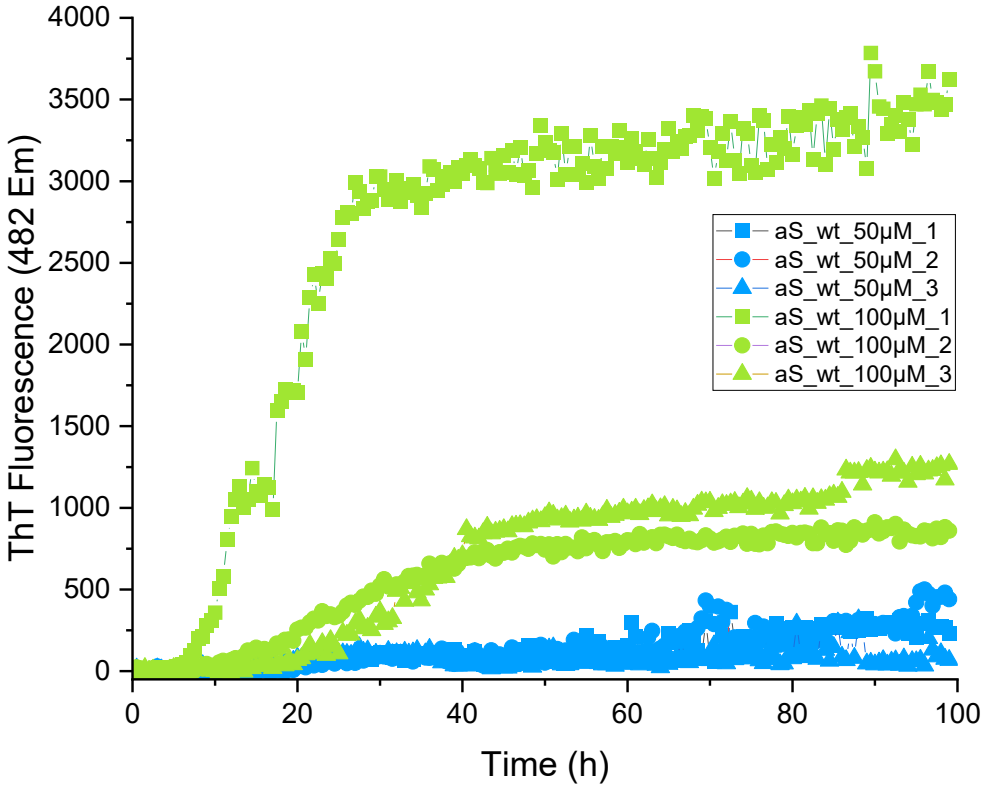

*Figure 40 ThT Assay: aggregation reaction in 96-well plate; 50 µM and 100 µM αS(1-140)^{wt} (**G2a**).*

Figure 40 shows the comparison of the ThT fluorescence of αS_wt (**G2a**) with a concentration of 50 µM and 100 µM. The 100 µM concentration showed higher ThT fluorescence and the increase was clearly more visible than for a concentration of 50 µM. The triplicates at 50 µM gave very similar results, while for 100 µM one curve showed significantly higher ThT fluorescence intensity. The fluctuations are generally less than for the Eppendorf Tube approach. The higher concentration provided more stable values and the graphs generally corresponded more closely to those in literature[86,87].

This approach was chosen for the experiment with all αSyn variants (**G2a-f**) and a concentration of 85 µM was used.

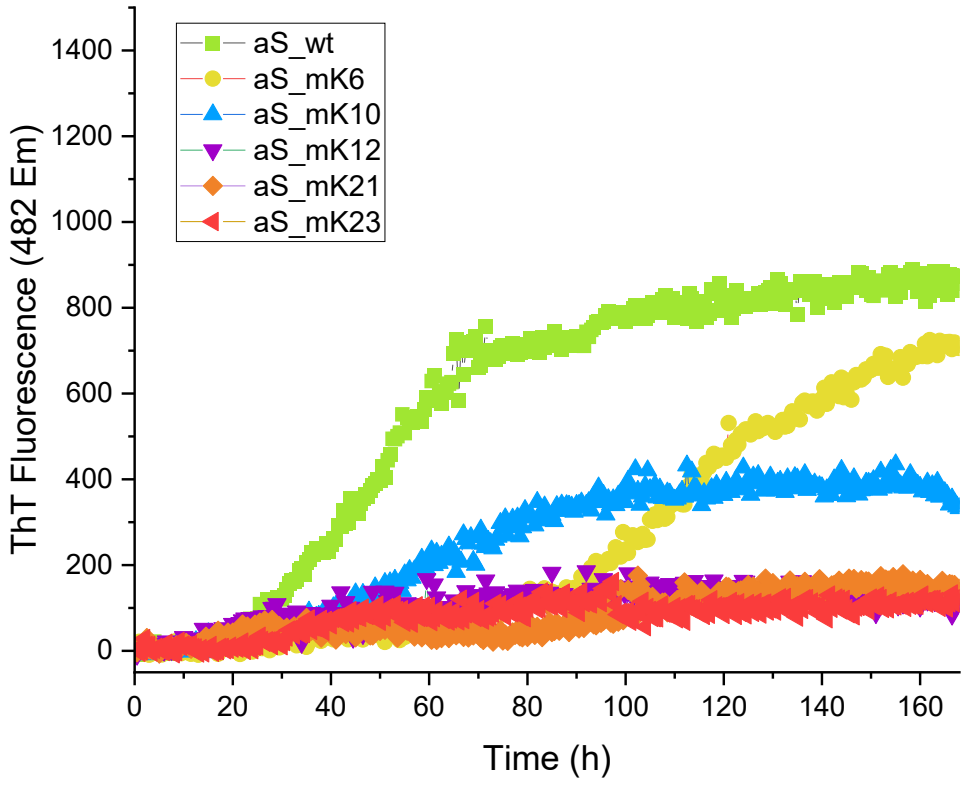

*Figure 41 ThT Assay: 96-well plate; all variants αS(1-140)^{wt,mK6,mK10,mK12,mK21,mK23} (**G2a-f**).*

All ThT fluorescence curves of the alpha synuclein variants (**G2a-f**) were plotted in Figure 41. If the mean values of each variant are compared, it can be seen that the curve of αS_wt (**G2a**) is most similar to literature. The fluorescence rises strongly and then reaches a plateau.[86,87] αS_wt (**G2a**) had the highest increase. αS_mK6 (**G2b**) also had a high increase in aggregation, whereby the start of the increase was significantly later than in the other variants (began 60 h later). αS_mK10 (**G2c**) produced a very similar curve to αS_wt (**G2a**), although the ThT fluorescence intensity was only half as high. The variants αS_mK12 (**G2d**), αS_mK21 (**G2e**) and αS_mK23 (**G2f**) had very similar curves. A slight increase was seen, but the ThT fluorescence intensity was very low. Compared to the other variants, they had significantly weaker increases. The ThT assay of all variants had shown that alpha synuclein aggregation has taken place in all of them (**G2a-f**). Looking at Figure 41 the CEL modification reduced the aggregation attributes of αSyn in general, the extent was variable though. Regarding the stochastic nature[86] of the fibril formation in the ThT assay itself and due to the fact that the assay was only carried out once with triplicates it is hard to distinguish significant differences of the aggregation between the variants.

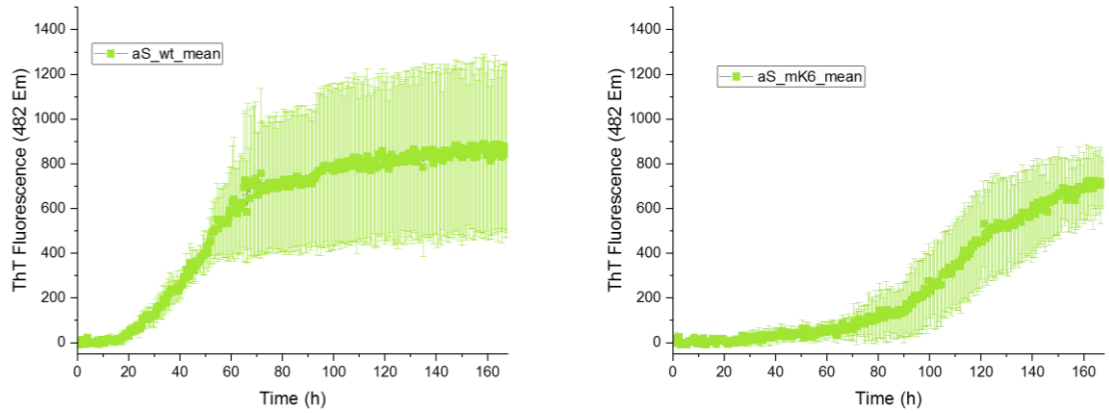

*Figure 42 ThT Assay of αS(1-140)^{wt} (**G2a**) (left) and αS(1-140)^{mK6} (**G2b**) (right); mean value and standard deviation.*

Both αS_wt (**G2a**) (Figure 42; left) and αS_mK6 (**G2b**) (Figure 42; right) showed high ThT fluorescence. The increase was clearly recognisable. For αS_wt (G2a), the ThT fluorescence values of the triplicates were further apart, which is why the standard deviation is larger. mK6 (**G2b**) has a significantly delayed fluorescence increase compared to the other variants.

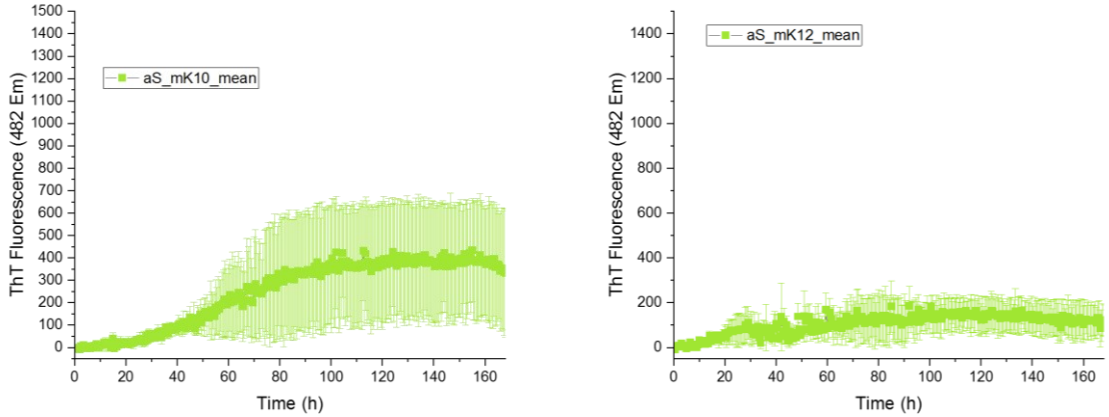

*Figure 43 ThT Assay of αS(1-140)^{mK10} (**G2c**) (left) and αS(1-140)^{mK12} (**G2d**) (right); mean value and standard deviation.*

Figure 43 shows the ThT fluorescence of αS_mK10 (**G2c**) (left) and αS_mK12 (**G2d**) (right). Both have curves with very low intensity, but an increase is visible in both. The standard deviation for αS_mK10 (**G2c**) is larger. For αS_mK10 (**G2c**), the standard deviation compared to the absolute fluorescence is the highest of all variants.

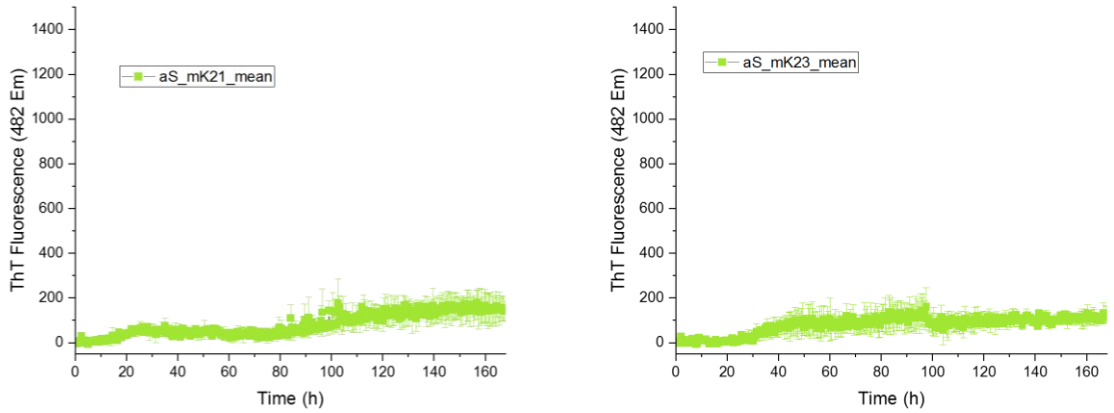

*Figure 44 ThT Assay of αS(1-140)^{mK21} (**G2e**) (left) and αS(1-140)^{mK23} (**G2f**) (right); mean value and standard deviation.*

The ThT fluorescence of αS_mK21 (**G2e**) (Figure 44; left) and αS_mK23 (**G2f**) (Figure 44; right) is very similar. The intensity is not very high, but an increase can still be recognised.

The standard deviations are very high for all variants (Figure 42 to Figure 44), especially from the area in which the fluorescence increases. For αS_mK12 (**G2d**), αS_mK21 (**G2e**) and αS_mK23 (**G2f**) the standard deviation looks low at first glance, as the fluorescence is generally low. On closer inspection, however, it can be seen that the values there also scatter widely. For those variants only a very slight increase was recognisable. The curves of the triplicates from each variant, from which mean values and standard deviation were calculated, can be found in the appendix (Figure 67 to Figure 69). The discussion of the outcome of ThT assay can be found in section 4.6.3.

4.6.2 SEM imaging

A scanning electron microscope (SEM) was utilized for the imaging of samples of the final ThT assay with all alpha synuclein variants **G2a-f** to ensure that the increase in ThT fluorescence is caused by the formation of fibrils. For imaging of protein aggregates, the volume of each desired well was mixed, a 10 µL (85 µM concentration) droplet from each desired aggregation experiment was deposited on formvar coated copper TEM (transmission electron microscopy) grid (3.05 mm, 200 mesh, Plano GmbH, glued on a sample holder). The grids were prepared like described in section 3.9, sputter-coated with gold and imaged using a scanning electron microscope operated with different magnification values. For SEM imaging magnification values of 40000X and 10000X were used. The fibril length was determined for all variants. Therefore, in general an attempt was made to use fibrils that are exposed.

Blank

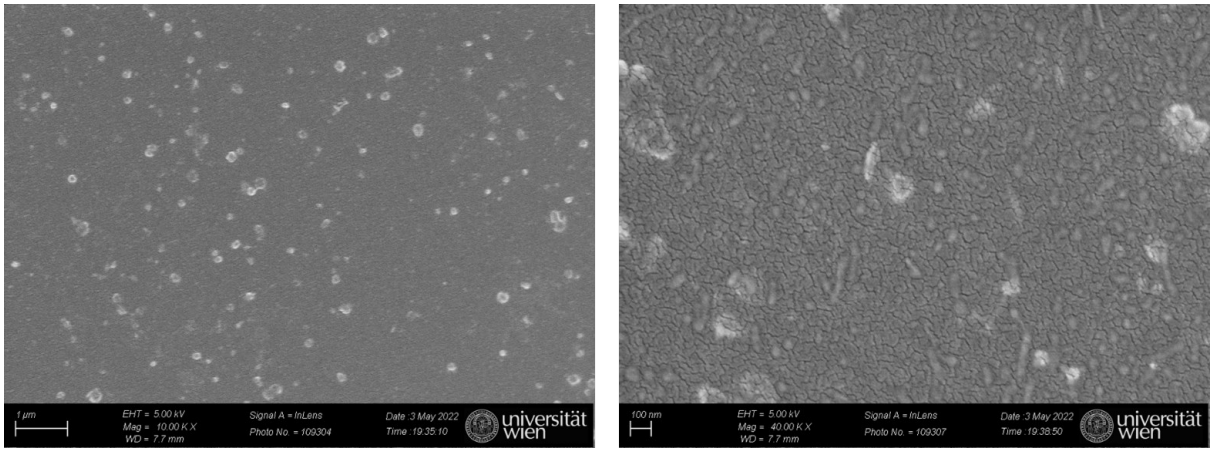

Figure 45 SEM imaging of blank; left: magnification 10 kx; right: magnification 40 kx.

The images of the blank are shown in Figure 45. No fibrils can be seen, only salt residue.

Wt

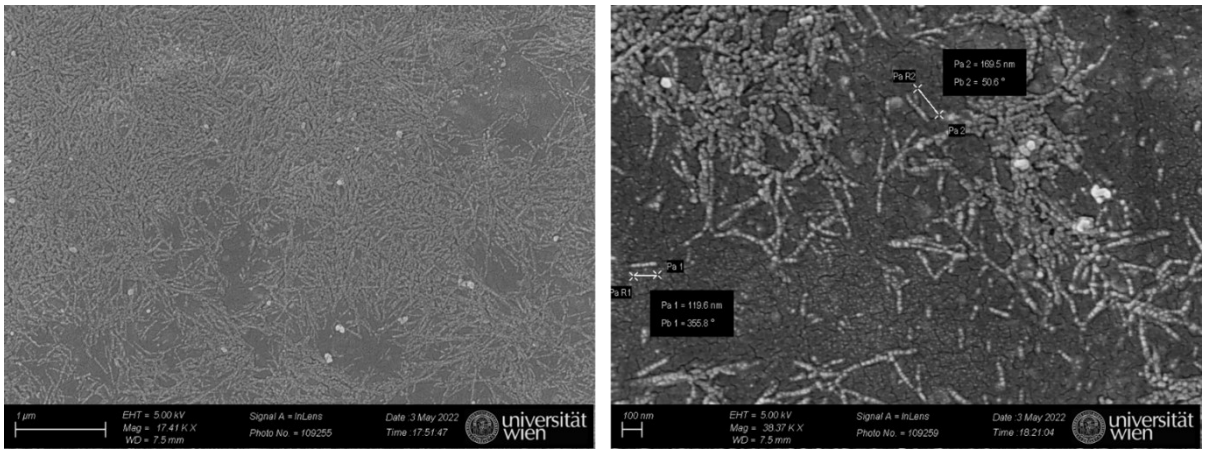

*Figure 46 SEM imaging of αS(1-140)^{wt}(**G2a**); magnification 10 kx (left) and 40 kx (right); fibril length: 120nm and 170nm.*

The SEM imaging of αS_wt (**G2a**) (Figure 46) showed a widespread presence of fibrils. The two measured fibrils had a length of 120 nm and 170 nm.

mK6

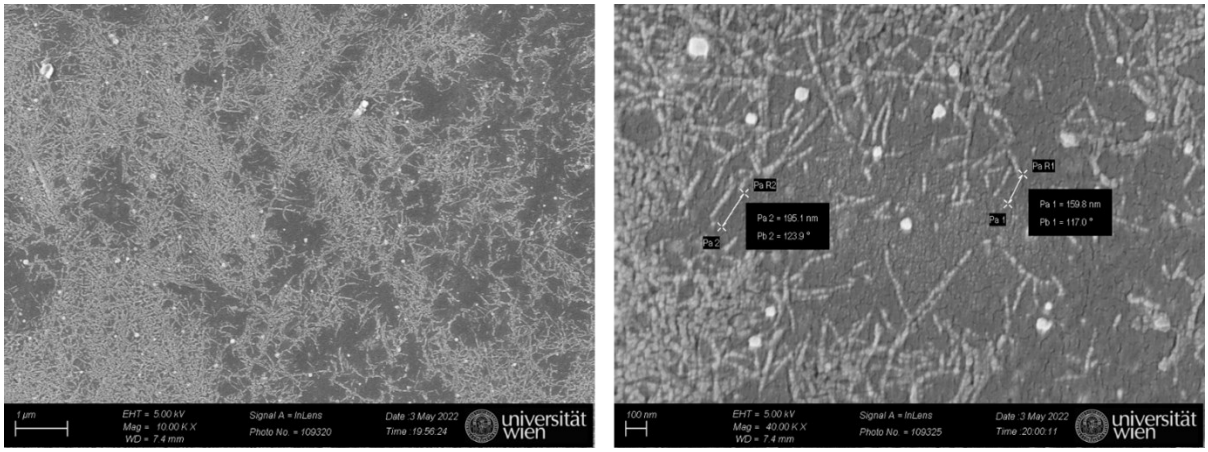

*Figure 47 SEM imaging of αS(1-140)^{mK6}(**G2b**); magnification 10 kx (left) and 40 kx (right); fibril length: 195nm and 160nm.*

αS_mK6 (**G2b**) also showed area-wide fibrils (Figure 47). The fibril length was 195 nm and 160 nm.

mK10

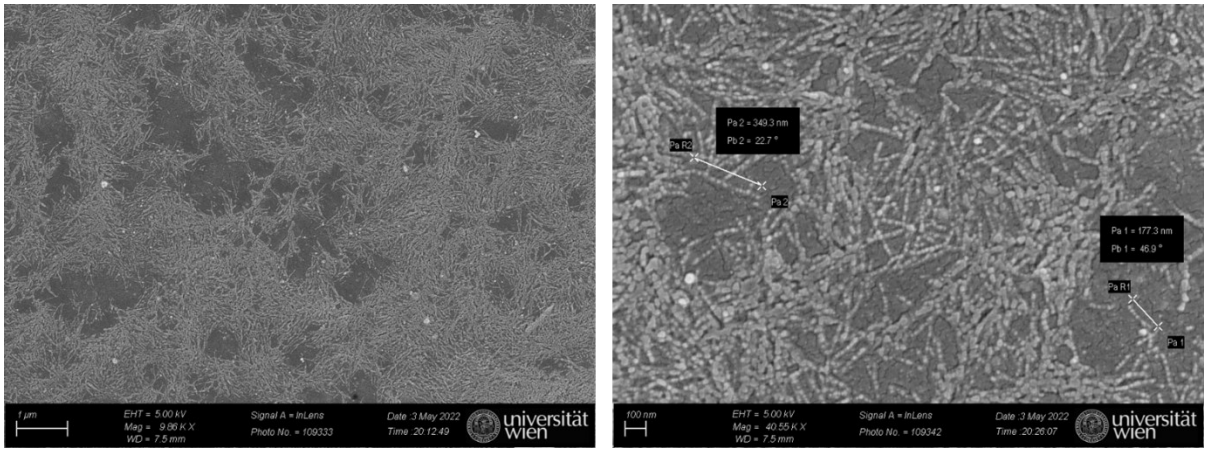

*Figure 48 SEM imaging of αS(1-140)^{mK10}(**G2c**); magnification 10 kx (left) and 40 kx (right); fibril length: 349nm and 177nm.*

Figure 48 (αS_mK10 (**G2c**)) showed fibrils covering the entire surface, with a length of 349 nm and 177 nm.

mK12

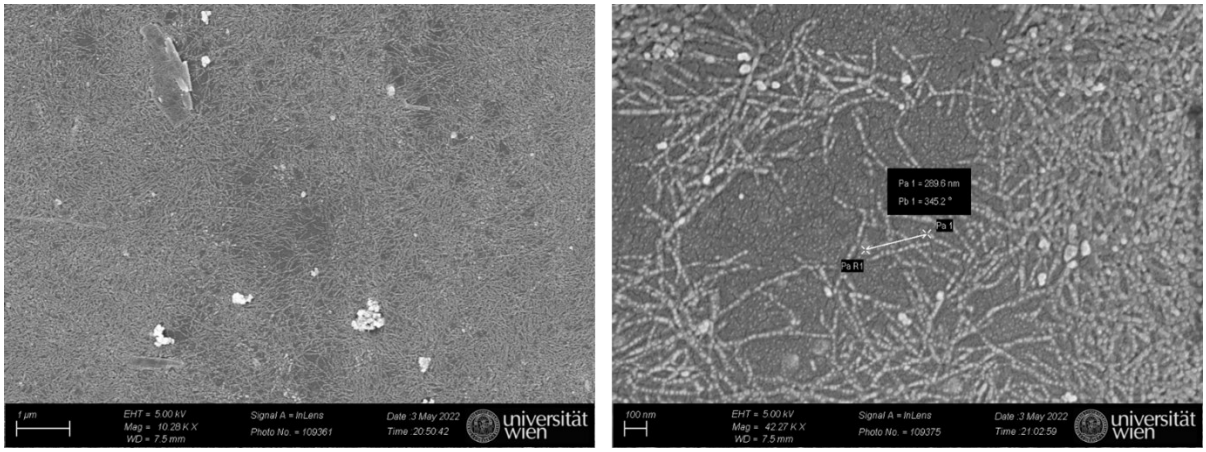

*Figure 49 SEM imaging of αS(1-140)^{mK12}(**G2d**); magnification 10 kx (left) and 40 kx (right); fibril length: 290nm.*

For αS_mK12 (**G2d**), fibrils could be seen on the entire surface of the grid (Figure 49) with a fibril length of 290 nm.

mK21

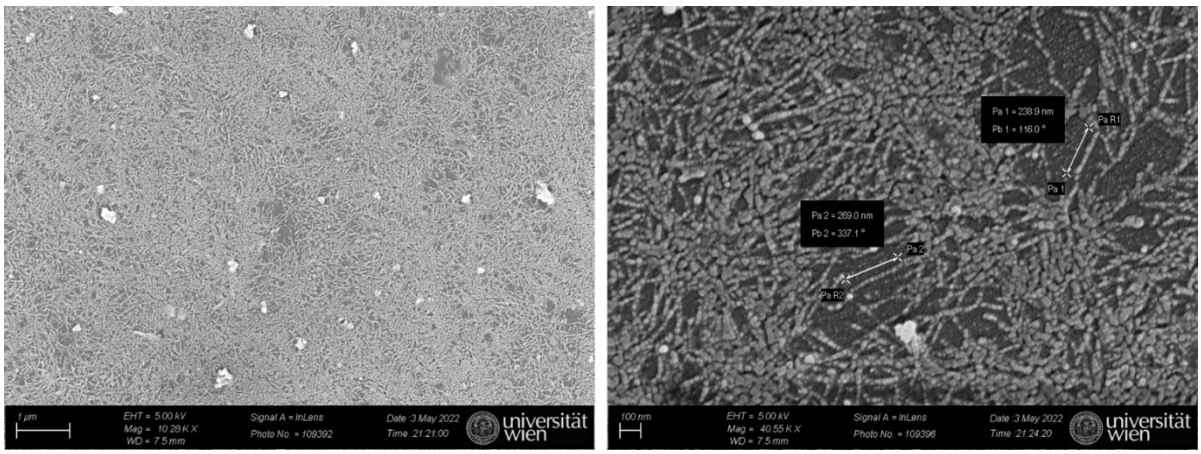

*Figure 50 SEM imaging of αS(1-140)^{mK21}(**G2e**); magnification 10 kx (left) and 40 kx (right); fibril length: 269nm and 239nm.*

The fibrils of αS_mK21 (**G2e**) had a length of 269 nm and 239 nm. The fibril formation was extensive (Figure 50).

mK23

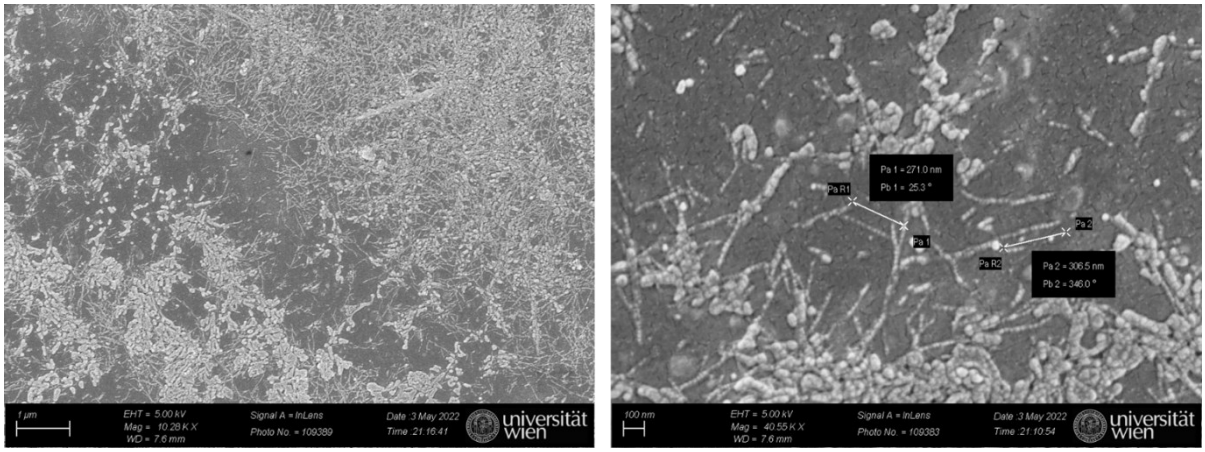

*Figure 51 SEM imaging of αS(1-140)^{mK23}(**G2f**); magnification 10 kx (left) and 40 kx (right); fibril lenght: 271nm and 307nm.*

For αS_mK23 (**G2*f***) fibril formation was extensive with a fibril length of 271 nm and 307 nm. However, in Figure 51 a lot of salt residues were still visible, apparently the buffer was not sufficiently washed away during sample preparation.

A high number of fibrils is clearly recognisable in all pictures of alpha synuclein variants **G2a-f** (Figure 46 to Figure 51). The length of the fibrils (Figure 52) varies greatly (wt: 120 nm and 170 nm; mk6: 195 nm and 160 nm; mK10: 350 nm and 177 nm; mK12: 290 nm; mK21: 270 nm and 239 nm; mK23: 271 nm and 307 nm). As only one sample per variant was analysed, we only have a rough overview of the fibril formation. As only 2 fibrils were randomly selected per variant, no clear inferences can be drawn about the differences between the variants. For mK12 (**G2d**) only the length of one fibril was determined, as no other fibril was exposed in the selected area. The fibrils that were selected were shorter for wt (**G2a**) and mK6 (**G2b**) compared to the other variants. The discussion of the outcome of SEM imaging can be found in section 4.6.3.

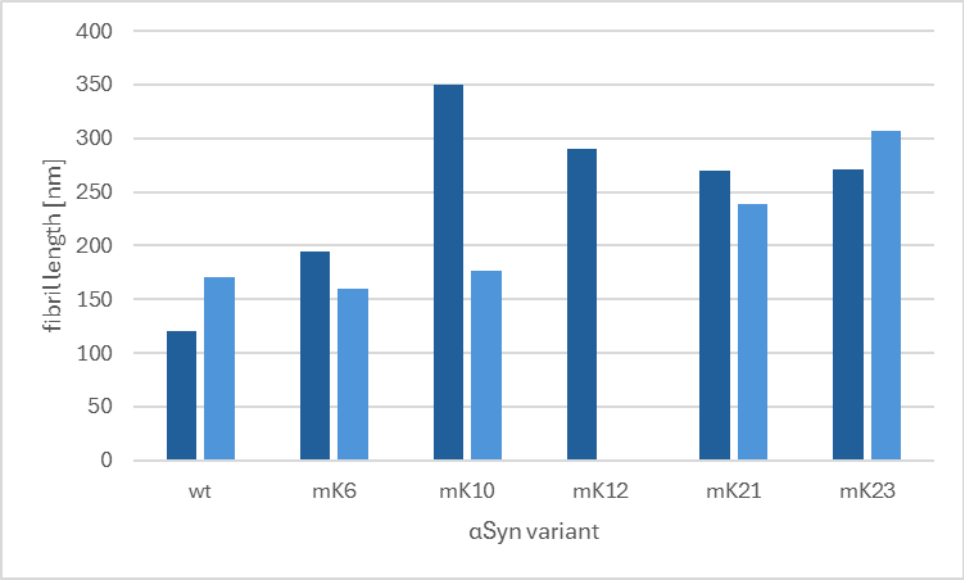

*Figure 52 Fibril length of αSyn variants **G2a-f**.*

4.6.3 Discussion of ThT Assay and SEM imaging

Looking at the ThT assay of all alpha synuclein variants (**G2a-f**) (section 4.6), it can be seen that all of them aggregate. Clear differences in the aggregation process of the variants can be recognised and large deviations can be seen in all triplicates (high standard deviation). This can be explained since aggregation is generally a very slow process, and aggregation tests have poor reproducibility because they are subject to a large number of modulating factors and because fibril formation is stochastic in nature.[86]

The reproducibility of the combined approach was significantly better than in the first experiment in the Eppendorf Tubes. This is due to the fact that glass beads were added to each well to improve mixing and homogeneity[88]. To prevent adsorption of amyloid fibrils to the well surface, which is known to be a process that can cause aberrant readings in ThT assays[89], non-binding 96-well plates were also used.

To further improve reproducibility, the following steps could be considered.

The reproducibility of aggregation in ThT assays is increased by N-terminal acetylation of α-synuclein[90]. It is known that *in vivo* the N-terminus of αSyn is acetylated and has an impact on aggregation into amyloid fibrils[90]. However, it must be taken into account that since an N-terminal de-acetyltransferase (Ndat) does not exist in eukaryotic cells or has not yet been discovered, this post-translational modification is considered irreversible.[91]

Aggregation can also be dramatically accelerated by the use of α-synuclein preformed fibrils (PFFs).[87] This would be a possible approach to accelerate the process and thereby reduce the fluctuations. The use of higher concentrations should also have a positive effect on the deviations.

SEM imaging showed that all alpha synuclein variants **G2a-f** exhibited fibrils covering the entire surface. The SEM data cannot be compared directly with the data from the ThT assay because these are two different phases of the same process examined with two different methods.

The different αSyn variants had large differences in ThT fluorescence intensities (Figure 42 to Figure 44). In SEM imaging (Figure 46 to Figure 51), no significant differences could be seen between the different variants, as all variants had very similar amounts of fibrils. A possible explanation could be that αSyn variants form different types of fibrils into which thioflavin T can be incorporated to different degrees. In order to confirm this theory, further experiments on fibril structure elucidation (morphology) would have to be carried out.

This theory is very likely because experiments have shown that alpha synuclein can form more than one type of fibrils with different secondary structures and morphologies, in fact it is possible that alpha synuclein aggregates into up to four distinct types of fibrils under identical conditions.[92] This of course has a major impact on the outcome of the ThT assay, as different fibrils may exhibit different levels of ThT fluorescence intensity. Even with similar secondary structures of the fibrils, strong differences in ThT fluorescence intensity could be observed. In the case of alpha synuclein, it is not possible to estimate aggregation concentration by ThT fluorescence. The complex nature of fibril formation in alpha synuclein could also have an influence on the pathogenesis of Parkinson's disease and other synucleinopathies.[92]

4.7 Ubiquitination

Here, a protocol provided by Dr. Luca Ferrari (Max Perutz Labs, Vienna, Austria) described in section 3.10 was used. The ubiquitin-activating enzyme UBA1 (E1), the ubiquitin-conjugating enzyme UbcH5B (E2) and the ubiquitin-protein ligase Nedd4 (E3) were used. These are frequently used enzymes in the ubiquitination of alpha synuclein.[93]

The SDS PAGEs of the ubiquitination assay from wild type (**G2a**) with and without E3 (Nedd4), with and without ATP (Table 1-3) described in section 3.10 were stained via Coomassie and can be found in the appendix (Figure 70 and Figure 71).

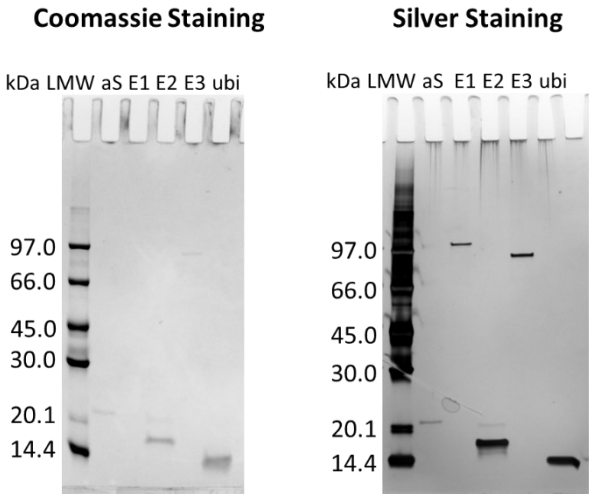

*Figure 53 Ubiquitination; comparison between Coomassie staining (left) and silver staining (right); aS: alpha synuclein (**G2a**); E1: ubiquitin-activating enzyme (UBA1); E2: ubiquitin-conjugating enzyme (UbcH5B); E3: ubiquitin-protein ligase (Nedd4); ubi: ubiquitin; left: Coomassie staining; right: silver staining; silver staining was the better option as the bands were much more clearly recognisable.*

Figure 53 shows the comparison between Coomassie staining and silver staining of the SDS PAGEs. The intensity of the bands was too weak with Coomassie staining, so silver staining was used for the ubiquitination reactions. In the gel (right) alpha synuclein (**G2a**), the three enzymes and ubiquitin are labelled next to each other. This

serves as a guide for the subsequent gels. It can be seen that the ubiquitin-conjugating enzyme UbcH5B (E2) used has a slight impurity (band at 20 kDa and bands below 16 kDa), but this is negligible for this experiment. The band of alpha synuclein appears at 21.0 kDa (calculated MW ≈ 14.5 kDa). E1 has a mass of 114.3 kDa[94], E2 has a mass of 16.7 kDa[95] and E3 has a mass of 88 kDa[96]. Ubiquitin has a mass of 8.5 kDa and the band appears at 15 kDa[97].

The disadvantage of the silver staining was that the development had to be stopped very quickly and it was therefore difficult to stain all the gels to exactly the same degree. In addition, the bands of the low molecular weight ladder (LMW) are very strongly coloured compared to the much less concentrated reaction sample bands. This problem could be solved via using lower volume of the LMW ladder (e.g. 1-2 µL). Nevertheless, silver staining was assumed as the best option for this experiment.

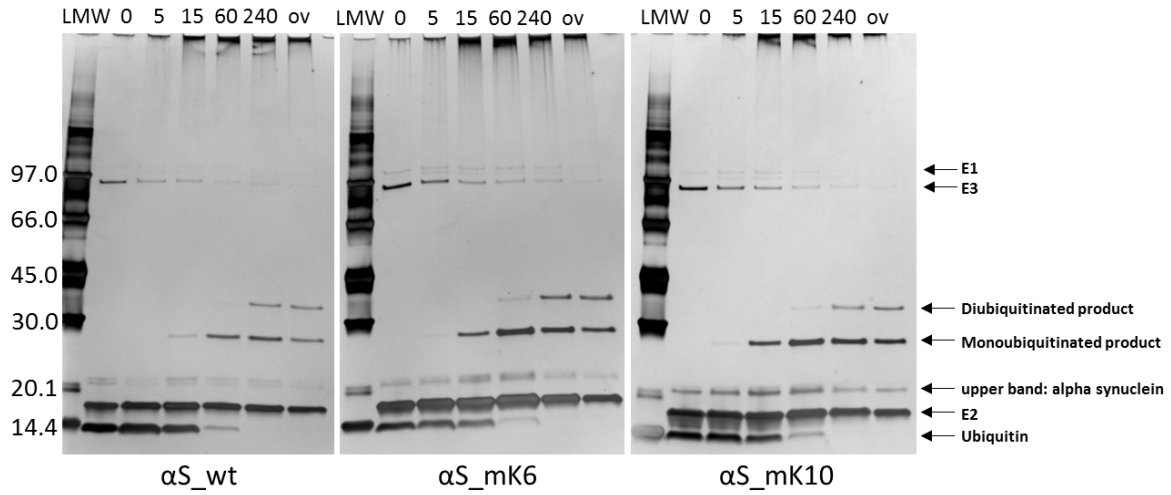

*Figure 54 Ubiquitination reaction of alpha synuclein variants **G2a-c**; LMW: Low molecular weight ladder; samples of the reaction mixture were taken after 0, 5, 15, 60, 240 minutes, and overnight; Monoubiquitinated and Diubiquitinated product could be seen in all variants.*

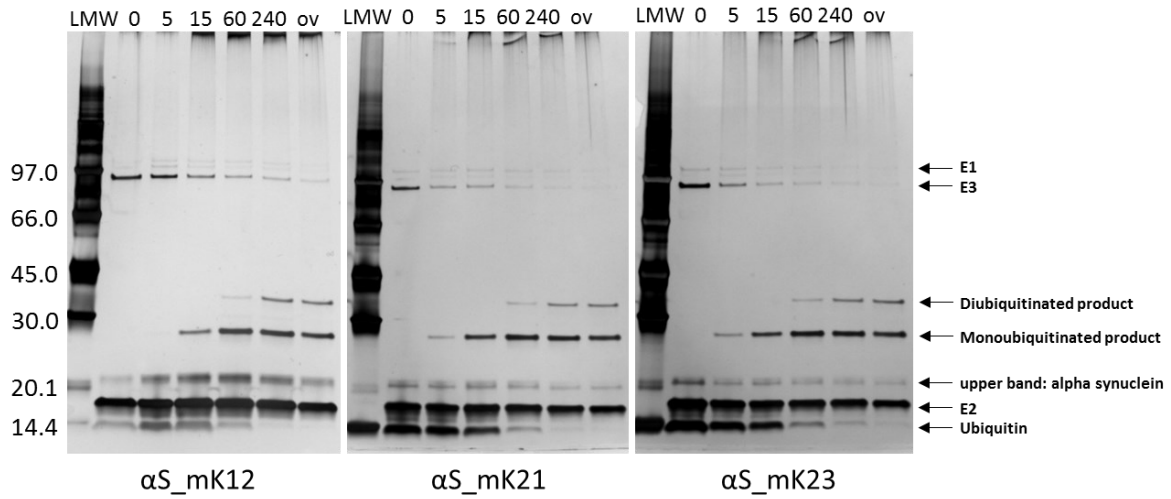

*Figure 55 Ubiquitination reaction of alpha synuclein variants **G2d-f**; LMW: Low molecular weight ladder; samples of the reaction mixture were taken after 0, 5, 15, 60, 240 minutes, and overnight; Monoubiquitinated and Diubiquitinated product could be seen in all variants.*

The protocol in section 3.10 was followed and the ubiquitination experiment was performed for all alpha synuclein variants (**G2a-f**). Samples were taken after 0, 5, 15, 60, 240 minutes, and overnight. Figure 54 and Figure 55 show the SDS PAGEs rendered with silver staining. It can be seen that all variants lose ubiquitin and alpha synuclein intensities over time (bands become paler) as both monoubiquitinated and diubiquitinated product is formed (bands become stronger). The formation of the monoubiquitinated product already starts after 5 min reaction time, while the diubiquitinated product can only be recognised after 60 min. The intensity of the colouring of the gels is different for all variants. The gel from αS_wt (**G2a**), for example, has the weakest colouring. The outcome of the ubiquitination reaction of all alpha synuclein variants (**G2a-f**) was similar to the gels found in literature.[93] The bands were analysed, and the results shown in Figure 56 and Figure 57. Therefore, the quantifications were done with the gel imager software from BioRad.

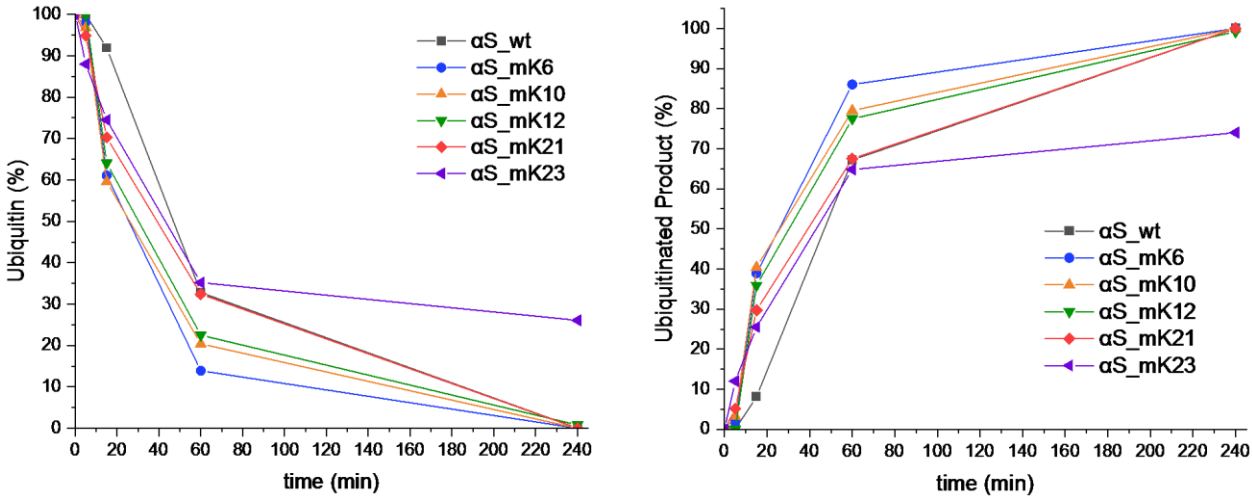

Figure 56 Ubiquitination reaction; left: Ubiquitin [%]; right: Ubiquitinated product [%].

Figure 56 shows the relative proportion [%] of the intensity of the band of ubiquitin (left) or ubiquitinated product (right) on the gel. The intensity of monoubiquitinated product, diubiquitinated product and ubiquitin is in total 100 %.

As the results, shown in the gels (Figure 54 and Figure 55), are the same after 240 min and overnight, the reaction was considered complete after 240 min and the graphs in Figure 56 were only created for 0 to 240 min. The left graph of Figure 56 shows that the amount of ubiquitin decreases with time and has fallen to 0 % after 240 min for all variants except αS_mK23 (**G2f**). For αS_mK23 (**G2f**), the ubiquitin intensity fell to 30 % after 240 min. However, a closer look at the gels (Figure 54 and Figure 55) shows that the gel of αS_mK23 (**G2f**) is the most strongly stained of all. The other gels also show minor bands after 240 min, but they are too weakly coloured to be recognised by the evaluation tool. In all variants, the ubiquitin band becomes weaker and weaker

during the ubiquitination reaction, which represents a consumption of ubiquitin. The amount of ubiquitin does not drop to 0 %. The graph on the right (Figure 56) shows how the amount of ubiquitylated products increases over time. The maximum is reached after 240 min. For αS_mK23 (**G2f**), the amount of ubiquitylated products only reaches 70 %, as the ubiquitin amount is taken into account for the calculation and as already mentioned, this was taken into account here by the evaluation tool due to the more strongly coloured bands. In general, it should also be noted here that if the colouring of the gels is considered, all alpha synuclein variants generally provide very similar results.

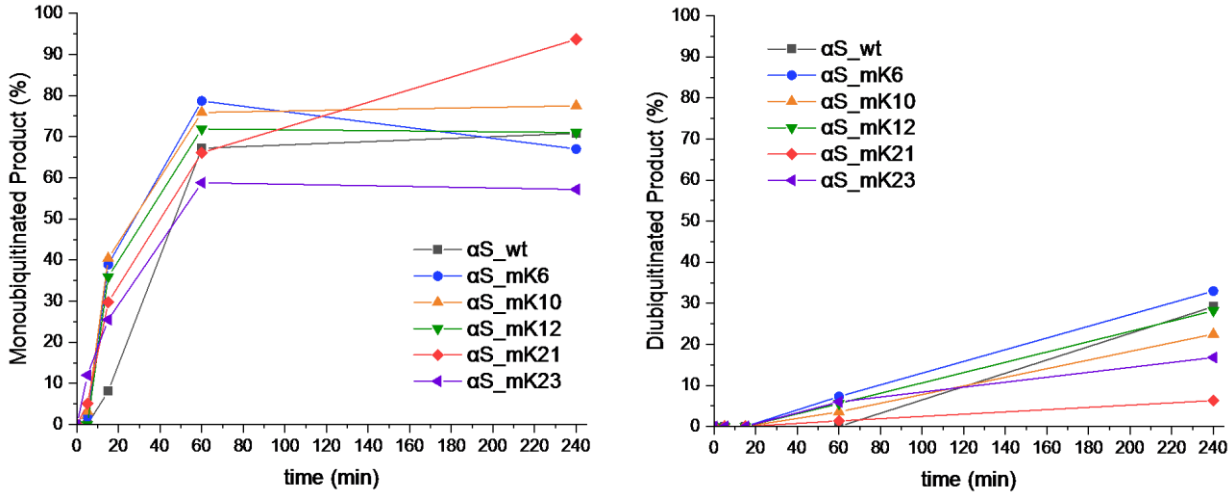

Figure 57 Ubiquitination reaction; left: Monoubiquitinated product [%]; right: Diubiquitinated product [%].

Figure 57 shows the relative proportion [%] of the intensity of the band of monoubiquitinated product (left) or diubiquitinated product (right) on the gel. The intensity of monoubiquitinated product, diubiquitinated product and ubiquitin is in total 100 %.

It can be seen that the formation of monoubiquitinated product was much faster and in greater quantities than the formation of diubiquitinated product. For monoubiquitinated product, the maximum is already reached after 60 min. For the variants αS_wt (**G2a**), αS_mK10 (**G2c**), αS_mK12 (**G2d**) and αS_mK23 (**G2f**), the amount of monoubiquitinated product remains the same from 60 min to 240 min. For αS_mK6 (**G2b**), the amount decreases from 80 % to 65 % from 60 min to 240 min. This is due to the fact that more diubiquitinated product is formed during this time. For αS_mK21 (**G2e**), the amount increases from 65 % to 95 % from 60 min to 240 min. This is due to the fact that the integral area was calculated incorrectly during evaluation because the limits of the bands were set incorrectly. As for all other variants, it is assumed that there is hardly any change between the samples after 240 min and overnight. αS_mK21 (**G2e**) has overnight values of 73.6 % monoubiquitinated product and 26.4 % diubiquitinated product. Looking at these values, the result would be similar to all other variants. The amount of monoubiquitinated product was after 240 min between 60 and

80 %. The amount of diubiquitinated product was after 240 min between 15 and 30 %. Again, the different colouring of the gels should be mentioned. αS_mK10 (**G2c**) had the largest amount of monoubiquitinated product. αS_mK23 (**G2f**) had the least amount of monoubiquitinated product. The largest amount of diubiquitinated product was found in αS_mK6 (**G2b**) and the smallest in αS_mK23 (**G2f**) (taking the overnight values for mK21 into account). The discussion of the ubiquitination assay can be found in section 4.7.1.

4.7.1 Discussion Ubiquitination

The lysines at position 21 and 96 of alpha synuclein are the most important ubiquitination sites by the ubiquitin-protein ligase Nedd4 (E3).[93] Figure 54 and Figure 55 show no difference between the αS_mK21 (**G2e**) variant and the other variants. Since the lysine at position 96 is not modified in any variant, this position is freely available for ubiquitination in all variants. This leads to the conclusion that the ubiquitination of alpha synuclein would also take place despite modification of a single lysine residue, which could also be shown in this experiment.

The results (Figure 56 to Figure 57) do not show any major differences between the alpha synuclein variants with the used method of analysis. The slight differences are probably due to the different staining efficacy of the gels. It is very difficult to obtain gels of exactly the same colour intensity with sliver staining, as colour development must be stopped very quickly during silver staining. Consequently, even small differences in colouring make it difficult to evaluate and compare the gels with each other. In addition to SDS PAGE with silver staining, Western blotting with anti-α-synuclein antibodies (Anti-αSyn LB509 and Anti-αSyn Syn-1) could be used, which would make all bands (with alpha synuclein) even more clearly visible due to the specific antigen antibody binding and make possible differences easier to recognise.[93] A silver stained SDS PAGE gel could also be made with all 240 min samples of all alpha synuclein variants. As the colouring would then be uniform for this gel, the outcome of the ubiquitination reaction of all variants after 240 min could be better compared. However, strong differences are not to be expected. These would have already been seen with the gels in Figure 54 and Figure 55. In addition, to be able to draw real conclusions, several repetitions per variant would have to be carried out in order to include a standard deviation. However, this experiment still provides an overview and suggests that there are hardly any differences between the variants. Since several lysine residues per variant are always unmodified, there is always enough freely accessible lysine left over for ubiquitination, so that a ubiquitination reaction can still take place.

All alpha-synuclein variants (**G2a-f**) were ubiquitinated by Nedd4, with both monoubiquitinated and diubiquitinated product found. Since monoubiquitinated alpha-synuclein undergoes proteasomal degradation, it can be concluded that this should happen with all variants.[98] It is also known that polyubiquitination accelerates the endocytic transport process and proteins linked to poly-Ub are mainly delivered to and degraded by the 26S proteasome (Ubiquitin-proteasome system).[77,98] However, polyubiquitination could not be detected in this experiment.

Using SDS PAGE, no significant differences between the variants could be detected. Further analytical methods such as detailed MS measurements could provide more precise information about the changes in the Ub pattern.[99]

In general, it must also be said that there are major differences in experiments depending on whether they are carried out *in vitro* or *in vivo*. Consequently, the modified alpha synuclein variants can lead to different results *in vivo*, as experiments *in vivo* are subject to more factors. For example, protein sequence analysis revealed that *in vitro* Lys21, Lys23, Lys32 and Lys34 are the most important ubiquitination sites. While *in vivo* mainly Lys6, Lys10 and Lys12 are ubiquitinated.[100]

5 Conclusion

Alpha synuclein wild type **G2a** and variants containing a CEL modification (K6, K10, K12, K21, K23) **G2b-f** were generated utilizing traceless semisynthesis. All variants were obtained in a high quality with no detected side products. With respect to aggregation properties, it can be said that all variants formed fibrils as proven by SEM imaging. Modified αSyn variants **G2b-f** showed, on average, a lower ThT fluorescence than the wild type **G2a**. Since the ThT assay is stochastic in nature[86] and literature[92] showed that different forms of fibrils (with different ThT intensities) could be formed within one setup, the results are currently not sufficiently meaningful to point out significant differences between αSyn variants. In turn, the ubiquitination assay showed also no significant differences between the variants. Which leads to the assumption that only one lysine position blocked by CEL does not have a big influence on the ubiquitination as ubiquitin has still enough other positions to attach. More detailed evaluation by MS could be used to detect changes in the Ub pattern. This method of analysis could be used for further investigation.[99] To point out significant differences of specific positions for the ubiquitination a possible way would be to block all lysine positions at the N-terminus of αSyn with CEL except of the one of interest. All variants **G2a-f** were ubiquitinated, with monoubiquitination and diubiquitination as the main species visible on the gel. Monoubiquitination can lead to proteasomal degradation[98], which leads to the assumption that all modified αSyn variants can be degraded (prior to aggregation). To see if this assumption is correct further experiments need to be carried out. In addition, to see if the variants lead to different ubiquitin degradation *in vivo*, other assays could be used.

6 References

(1) Bendor, J. T.; Logan, T. P.; Edwards, R. H. The Function of α-Synuclein. *Neuron* **2013**, *79* (6), 1044–1066. https://doi.org/10.1016/j.neuron.2013.09.004.

(2) Maroteaux, L.; Campanelli, J.; Scheller, R. Synuclein: A Neuron-Specific Protein Localized to the Nucleus and Presynaptic Nerve Terminal. *J. Neurosci.* **1988**, *8* (8), 2804–2815. https://doi.org/10.1523/JNEUROSCI.08-08-02804.1988.

(3) Stefanis, L. -Synuclein in Parkinson's Disease. *Cold Spring Harbor Perspectives in Medicine* **2012**, *2* (2), a009399–a009399. https://doi.org/10.1101/cshperspect.a009399.

(4) Vicente Miranda, H.; Chegão, A.; Oliveira, M. S.; Fernandes Gomes, B.; Enguita, F. J.; Outeiro, T. F. Hsp27 Reduces Glycation-induced Toxicity and Aggregation of Alpha-synuclein. *FASEB j.* **2020**, *34* (5), 6718–6728. https://doi.org/10.1096/fj.201902936R.

(5) Soto, C. Unfolding the Role of Protein Misfolding in Neurodegenerative Diseases. *Nat Rev Neurosci* **2003**, *4* (1), 49–60. https://doi.org/10.1038/nrn1007.

(6) Forloni, G. Alpha Synuclein: Neurodegeneration and Inflammation. *IJMS* **2023**, *24* (6), 5914. https://doi.org/10.3390/ijms24065914.

(7) El-Agnaf, O. M. A.; Irvine, G. B. Aggregation and Neurotoxicity of α-Synuclein and Related Peptides. *Biochemical Society Transactions* **2002**, *30* (4), 559–565. https://doi.org/10.1042/bst0300559.

(8) Plotegher, N.; Bubacco, L. Lysines, Achilles' Heel in Alpha-Synuclein Conversion to a Deadly Neuronal Endotoxin. *Ageing Research Reviews* **2016**, *26*, 62–71. https://doi.org/10.1016/j.arr.2015.12.002.

(9) Vicente Miranda, H.; El-Agnaf, O. M. A.; Outeiro, T. F. G Lycation in P Arkinson's Disease and Alzheimer's Disease. *Movement Disorders* **2016**, *31* (6), 782–790. https://doi.org/10.1002/mds.26566.

(10) Weinreb, P. H.; Zhen, W.; Poon, A. W.; Conway, K. A.; Lansbury, P. T. NACP, A Protein Implicated in Alzheimer's Disease and Learning, Is Natively Unfolded. *Biochemistry* **1996**, *35* (43), 13709–13715. https://doi.org/10.1021/bi961799n.

(11) Davidson, W. S.; Jonas, A.; Clayton, D. F.; George, J. M. Stabilization of α-Synuclein Secondary Structure upon Binding to Synthetic Membranes. *Journal of Biological Chemistry* **1998**, *273* (16), 9443–9449. https://doi.org/10.1074/jbc.273.16.9443.

(12) Lashuel, H. A.; Overk, C. R.; Oueslati, A.; Masliah, E. The Many Faces of α-Synuclein: From Structure and Toxicity to Therapeutic Target. *Nat Rev Neurosci* **2013**, *14* (1), 38–48. https://doi.org/10.1038/nrn3406.

(13) Bordbar, S.; Alijanzadeh, D.; Samieefar, N.; Khazeei Tabari, M. A.; Pourbakhtyaran, E.; Rezaei, N. The Role of Alpha-Synuclein in Neurodevelopmental Diseases. *Mol Neurobiol* **2024**. https://doi.org/10.1007/s12035-024-04305-2.

(14) Lavedan, C. The Synuclein Family. *Genome Res.* **1998**, *8* (9), 871–880. https://doi.org/10.1101/gr.8.9.871.

(15) Bonini, N. M.; Giasson, B. I. Snaring the Function of α-Synuclein. *Cell* **2005**, *123* (3), 359–361. https://doi.org/10.1016/j.cell.2005.10.017.

(16) Emamzadeh, F. Alpha-Synuclein Structure, Functions, and Interactions. *J Res Med Sci* **2016**, *21* (1), 29. https://doi.org/10.4103/1735-1995.181989.

(17) Béraud, D.; Hathaway, H. A.; Trecki, J.; Chasovskikh, S.; Johnson, D. A.; Johnson, J. A.; Federoff, H. J.; Shimoji, M.; Mhyre, T. R.; Maguire-Zeiss, K. A. Microglial Activation and Antioxidant Responses Induced by the Parkinson's Disease Protein α-Synuclein. *J Neuroimmune Pharmacol* **2013**, *8* (1), 94–117. https://doi.org/10.1007/s11481-012-9401-0.

(18) Mariño, L.; Ramis, R.; Casasnovas, R.; Ortega-Castro, J.; Vilanova, B.; Frau, J.; Adrover, M. Unravelling the Effect of *N* (ε)-(Carboxyethyl)Lysine on the Conformation, Dynamics and Aggregation Propensity of α-Synuclein. *Chem. Sci.* **2020**, *11* (12), 3332–3344. https://doi.org/10.1039/D0SC00906G.

(19) Schmid, A. W.; Fauvet, B.; Moniatte, M.; Lashuel, H. A. Alpha-Synuclein Post-Translational Modifications as Potential Biomarkers for Parkinson Disease and Other Synucleinopathies. *Molecular & Cellular Proteomics* **2013**, *12* (12), 3543–3558. https://doi.org/10.1074/mcp.R113.032730.

(20) Oueslati, A.; Fournier, M.; Lashuel, H. A. Role of Post-Translational Modifications in Modulating the Structure, Function and Toxicity of α-Synuclein. In *Progress in Brain Research*; Elsevier, 2010; Vol. 183, pp 115–145. https://doi.org/10.1016/S0079-6123(10)83007-9.

(21) Vicente Miranda, H.; Szegő, É. M.; Oliveira, L. M. A.; Breda, C.; Darendelioglu, E.; De Oliveira, R. M.; Ferreira, D. G.; Gomes, M. A.; Rott, R.; Oliveira, M.; Munari, F.; Enguita, F. J.; Simões, T.; Rodrigues, E. F.; Heinrich, M.; Martins, I. C.; Zamolo, I.; Riess, O.; Cordeiro, C.; Ponces-Freire, A.; Lashuel, H. A.; Santos, N. C.; Lopes, L. V.; Xiang, W.; Jovin, T. M.; Penque, D.; Engelender, S.; Zweckstetter, M.; Klucken, J.; Giorgini, F.; Quintas, A.; Outeiro, T. F. Glycation Potentiates α-Synuclein-Associated Neurodegeneration in Synucleinopathies. *Brain* **2017**, *140* (5), 1399–1419. https://doi.org/10.1093/brain/awx056.

(22) Abeywardana, T.; Lin, Y. H.; Rott, R.; Engelender, S.; Pratt, M. R. Site-Specific Differences in Proteasome-Dependent Degradation of Monoubiquitinated α-Synuclein. *Chemistry & Biology* **2013**, *20* (10), 1207–1213. https://doi.org/10.1016/j.chembiol.2013.09.009.

(23) Luk, K. C.; Kehm, V.; Carroll, J.; Zhang, B.; O'Brien, P.; Trojanowski, J. Q.; Lee, V. M.-Y. Pathological α-Synuclein Transmission Initiates Parkinson-like Neurodegeneration in Nontransgenic Mice. *Science* **2012**, *338* (6109), 949–953. https://doi.org/10.1126/science.1227157.

(24) Chartier-Harlin, M.-C.; Kachergus, J.; Roumier, C.; Mouroux, V.; Douay, X.; Lincoln, S.; Levecque, C.; Larvor, L.; Andrieux, J.; Hulihan, M.; Waucquier, N.; Defebvre, L.; Amouyel, P.; Farrer, M.; Destée, A. α-Synuclein Locus Duplication as a Cause of Familial Parkinson's Disease. *The Lancet* **2004**, *364* (9440), 1167–1169. https://doi.org/10.1016/S0140-6736(04)17103-1.

(25) Desplats, P.; Lee, H.-J.; Bae, E.-J.; Patrick, C.; Rockenstein, E.; Crews, L.; Spencer, B.; Masliah, E.; Lee, S.-J. Inclusion Formation and Neuronal Cell Death through Neuron-to-Neuron Transmission of α-Synuclein. *Proc. Natl. Acad. Sci. U.S.A.* **2009**, *106* (31), 13010–13015. https://doi.org/10.1073/pnas.0903691106.

(26) Wales, P.; Pinho, R.; Lázaro, D. F.; Outeiro, T. F. Limelight on Alpha-Synuclein: Pathological and Mechanistic Implications in Neurodegeneration. *Journal of Parkinson's Disease* **2013**, *3* (4), 415–459. https://doi.org/10.3233/JPD-130216.

(27) Postuma, R. B.; Aarsland, D.; Barone, P.; Burn, D. J.; Hawkes, C. H.; Oertel, W.; Ziemssen, T. Identifying Prodromal Parkinson's Disease: Pre-Motor Disorders in Parkinson's Disease. *Movement Disorders* **2012**, *27* (5), 617–626. https://doi.org/10.1002/mds.24996.

(28) De Nuccio, F.; Kashyrina, M.; Serinelli, F.; Laferrière, F.; Lofrumento, D. D.; De Giorgi, F.; Ichas, F. Oligodendrocytes Prune Axons Containing α-Synuclein Aggregates In Vivo: Lewy Neurites as Precursors of Glial Cytoplasmic Inclusions in Multiple System Atrophy? *Biomolecules* **2023**, *13* (2), 269. https://doi.org/10.3390/biom13020269.

(29) Hamilton, R. L. Lewy Bodies in Alzheimer's Disease: A Neuropathological Review of 145 Cases Using α-Synuclein Immunohistochemistry. *Brain Pathology* **2000**, *10* (3), 378–384. https://doi.org/10.1111/j.1750-3639.2000.tb00269.x.

(30) Rott, R.; Szargel, R.; Haskin, J.; Shani, V.; Shainskaya, A.; Manov, I.; Liani, E.; Avraham, E.; Engelender, S. Monoubiquitylation of α-Synuclein by Seven in Absentia Homolog (SIAH) Promotes Its Aggregation in Dopaminergic Cells. *Journal of Biological Chemistry* **2008**, *283* (6), 3316–3328. https://doi.org/10.1074/jbc.M704809200.

(31) Castellani, R.; Smith, M. A.; Richey, G. L.; Perry, G. Glycoxidation and Oxidative Stress in Parkinson Disease and Diffuse Lewy Body Disease. *Brain Research* **1996**, *737* (1–2), 195–200. https://doi.org/10.1016/0006-8993(96)00729-9.

(32) Rosano, G. L.; Ceccarelli, E. A. Recombinant Protein Expression in Escherichia Coli: Advances and Challenges. *Front. Microbiol.* **2014**, *5*. https://doi.org/10.3389/fmicb.2014.00172.

(33) Hannig, G.; Makrides, S. C. Strategies for Optimizing Heterologous Protein Expression in Escherichia Coli. *Trends in Biotechnology* **1998**, *16* (2), 54–60. https://doi.org/10.1016/S0167-7799(97)01155-4.

(34) Sharp, P. M.; Li, W.-H. The Codon Adaptation Index-a Measure of Directional Synonymous Codon Usage Bias, and Its Potential Applications. *Nucl Acids Res* **1987**, *15* (3), 1281–1295. https://doi.org/10.1093/nar/15.3.1281.

(35) Calderone, T. L.; Stevens, R. D.; Oas, T. G. High-Level Misincorporation of Lysine for Arginine at AGA Codons in a Fusion Protein Expressed inEscherichia Coli. *Journal of Molecular Biology* **1996**, *262* (4), 407–412. https://doi.org/10.1006/jmbi.1996.0524.

(36) Hatfield, G. W.; Roth, D. A. Optimizing Scaleup Yield for Protein Production: Computationally Optimized DNA Assembly (CODA) and Translation Engineering™. In *Biotechnology Annual Review*; Elsevier, 2007; Vol. 13, pp 27–42. https://doi.org/10.1016/S1387-2656(07)13002-7.

(37) Francis, D. M.; Page, R. Strategies to Optimize Protein Expression in *E. Coli*. *CP Protein Science* **2010**, *61* (1). https://doi.org/10.1002/0471140864.ps0524s61.

(38) Tegel, H.; Steen, J.; Konrad, A.; Nikdin, H.; Pettersson, K.; Stenvall, M.; Tourle, S.; Wrethagen, U.; Xu, L.; Yderland, L.; Uhlén, M.; Hober, S.; Ottosson, J. High-throughput Protein Production – Lessons from Scaling up from 10 to 288 Recombinant Proteins per Week. *Biotechnology Journal* **2009**, *4* (1), 51–57. https://doi.org/10.1002/biot.200800183.

(39) Kent, S. B. H. Total Chemical Synthesis of Proteins. *Chem. Soc. Rev.* **2009**, *38* (2), 338–351. https://doi.org/10.1039/B700141J.

(40) Xie, J.; Schultz, P. G. Adding Amino Acids to the Genetic Repertoire. *Current Opinion in Chemical Biology* **2005**, *9* (6), 548–554. https://doi.org/10.1016/j.cbpa.2005.10.011.

(41) Merrifield, R. B. Solid Phase Peptide Synthesis. I. The Synthesis of a Tetrapeptide. *J. Am. Chem. Soc.* **1963**, *85* (14), 2149–2154. https://doi.org/10.1021/ja00897a025.

(42) Frederick, M. O.; Boyse, R. A.; Braden, T. M.; Calvin, J. R.; Campbell, B. M.; Changi, S. M.; Coffin, S. R.; Condon, C.; Gowran, O.; McClary Groh, J.; Groskreutz, S. R.; Harms, Z. D.; Humenik, A. A.; Kallman, N. J.; Klitzing, N. D.; Kopach, M. E.; Kretsinger, J. K.; Lambertus, G. R.; Lampert, J. T.; Maguire, L. M.; Moynihan, H. A.; Mullane, N. S.; Murphy, J. D.; O'Mahony, M. E.; Richey, R. N.; Seibert, K. D.; Spencer, R. D.; Strege, M. A.; Tandogan, N.; Torres Torres, F. L.; Tsukanov, S. V.; Xia, H. Kilogram-Scale GMP Manufacture of Tirzepatide Using a Hybrid SPPS/LPPS Approach with Continuous Manufacturing. *Org. Process Res. Dev.* **2021**, *25* (7), 1628–1636. https://doi.org/10.1021/acs.oprd.1c00108.

(43) Tam, J. P.; Yu, Q.; Miao, Z. Orthogonal Ligation Strategies for Peptide and Protein. *Biopolymers* **1999**, *51* (5), 311–332. https://doi.org/10.1002/(SICI)1097-0282(1999)51:5<311::AID-BIP2>3.0.CO;2-A.

(44) Dawson, P. E.; Muir, T. W.; Clark-Lewis, I.; Kent, S. B. H. Synthesis of Proteins by Native Chemical Ligation. *Science* **1994**, *266* (5186), 776–779. https://doi.org/10.1126/science.7973629.

(45) Conibear, A. C.; Watson, E. E.; Payne, R. J.; Becker, C. F. W. Native Chemical Ligation in Protein Synthesis and Semi-Synthesis. *Chem. Soc. Rev.* **2018**, *47* (24), 9046–9068. https://doi.org/10.1039/C8CS00573G.

(46) Wang, Z. A.; Cole, P. A. Methods and Applications of Expressed Protein Ligation. In *Expressed Protein Ligation*; Vila-Perelló, M., Ed.; Methods in Molecular Biology; Springer US: New York, NY, 2020; Vol. 2133, pp 1–13. https://doi.org/10.1007/978-1-0716-0434-2_1.

(47) Shah, N. H.; Muir, T. W. Inteins: Nature's Gift to Protein Chemists. *Chem. Sci.* **2014**, *5* (2), 446–461. https://doi.org/10.1039/C3SC52951G.

(48) Paulus, H. Protein Splicing and Related Forms of Protein Autoprocessing. *Annu. Rev. Biochem.* **2000**, *69* (1), 447–496. https://doi.org/10.1146/annurev.biochem.69.1.447.

(49) Flavell, R. R.; Muir, T. W. Expressed Protein Ligation (EPL) in the Study of Signal Transduction, Ion Conduction, And Chromatin Biology. *Acc. Chem. Res.* **2009**, *42* (1), 107–116. https://doi.org/10.1021/ar800129c.

(50) Muir, T. W.; Sondhi, D.; Cole, P. A. Expressed Protein Ligation: A General Method for Protein Engineering. *Proc. Natl. Acad. Sci. U.S.A.* **1998**, *95* (12), 6705–6710. https://doi.org/10.1073/pnas.95.12.6705.

(51) Sun, Z.; Ma, W.; Cao, Y.; Wei, T.; Mo, X.; Chow, H. Y.; Tan, Y.; Cheung, C. H. P.; Liu, J.; Lee, H. K.; Tse, E. C. M.; Liu, H.; Li, X. Superfast Desulfurization for Protein Chemical Synthesis and Modification. *Chem* **2022**, *8* (9), 2542–2557. https://doi.org/10.1016/j.chempr.2022.07.017.

(52) Vinther, T. N.; Ribel, U.; Åskov Pedersen, T.; Kjeldsen, T. B.; Jensen, K. J.; Hubálek, F. Identification of Anchor Points for Chemical Modification of a Small Cysteine-Rich Protein by Using a Cysteine Scan. *ChemBioChem* **2011**, *12* (16), 2448–2455. https://doi.org/10.1002/cbic.201100464.

(53) Yan, L. Z.; Dawson, P. E. Synthesis of Peptides and Proteins without Cysteine Residues by Native Chemical Ligation Combined with Desulfurization. *J. Am. Chem. Soc.* **2001**, *123* (4), 526–533. https://doi.org/10.1021/ja003265m.

(54) Wan, Q.; Danishefsky, S. J. Free-Radical-Based, Specific Desulfurization of Cysteine: A Powerful Advance in the Synthesis of Polypeptides and Glycopolypeptides. *Angewandte Chemie* **2007**, *119* (48), 9408–9412. https://doi.org/10.1002/ange.200704195.

(55) Wan, Q.; Danishefsky, S. J. Free-Radical-Based, Specific Desulfurization of Cysteine: A Powerful Advance in the Synthesis of Polypeptides and Glycopolypeptides. *Angew Chem Int Ed* **2007**, *46* (48), 9248–9252. https://doi.org/10.1002/anie.200704195.

(56) Haase, C.; Rohde, H.; Seitz, O. Native chemische Verknüpfung mit Valin. *Angewandte Chemie* **2008**, *120* (36), 6912–6915. https://doi.org/10.1002/ange.200801590.

(57) Haase, C.; Rohde, H.; Seitz, O. Native Chemical Ligation at Valine. *Angew Chem Int Ed* **2008**, *47* (36), 6807–6810. https://doi.org/10.1002/anie.200801590.

(58) Siman, P.; Blatt, O.; Moyal, T.; Danieli, T.; Lebendiker, M.; Lashuel, H. A.; Friedler, A.; Brik, A. Chemical Synthesis and Expression of the HIV-1 Rev Protein. *ChemBioChem* **2011**, *12* (7), 1097–1104. https://doi.org/10.1002/cbic.201100033.

(59) Dawson, P. E. Native Chemical Ligation Combined with Desulfurization and Deselenization: A General Strategy for Chemical Protein Synthesis. *Israel Journal of Chemistry* **2011**, *51* (8–9), 862–867. https://doi.org/10.1002/ijch.201100128.

(60) Jin, K.; Li, X. Advances in Native Chemical Ligation–Desulfurization: A Powerful Strategy for Peptide and Protein Synthesis. *Chemistry A European J* **2018**, *24* (66), 17397–17404. https://doi.org/10.1002/chem.201802067.

(61) Diemer, V.; Melnyk, O. Protein Desulfurization: Sodium Tetraethylborate Makes It Fast. *Chem* **2022**, *8* (10), 2571–2573. https://doi.org/10.1016/j.chempr.2022.09.011.

(62) Thompson, R. E.; Muir, T. W. Chemoenzymatic Semisynthesis of Proteins. *Chem. Rev.* **2020**, *120* (6), 3051–3126. https://doi.org/10.1021/acs.chemrev.9b00450.

(63) Berrade, L.; Camarero, J. A. Expressed Protein Ligation: A Resourceful Tool to Study Protein Structure and Function. *Cell. Mol. Life Sci.* **2009**, *66* (24), 3909–3922. https://doi.org/10.1007/s00018-009-0122-3.

(64) Durek, T.; Becker, C. F. W. Protein Semi-Synthesis: New Proteins for Functional and Structural Studies. *Biomolecular Engineering* **2005**, *22* (5–6), 153–172. https://doi.org/10.1016/j.bioeng.2005.07.004.

(65) Muir, T. W. Semisynthesis of Proteins by Expressed Protein Ligation. *Annu. Rev. Biochem.* **2003**, *72* (1), 249–289. https://doi.org/10.1146/annurev.biochem.72.121801.161900.

(66) Zheng, J.-S.; Tang, S.; Qi, Y.-K.; Wang, Z.-P.; Liu, L. Chemical Synthesis of Proteins Using Peptide Hydrazides as Thioester Surrogates. *Nat Protoc* **2013**, *8* (12), 2483–2495. https://doi.org/10.1038/nprot.2013.152.

(67) Fang, G.; Wang, J.; Liu, L. Convergent Chemical Synthesis of Proteins by Ligation of Peptide Hydrazides. *Angew Chem Int Ed* **2012**, *51* (41), 10347–10350. https://doi.org/10.1002/anie.201203843.

(68) Khan, S.; Bhat, A. A. Nonenzymatic Posttranslational Protein Modifications: Mechanism and Associated Disease Pathologies. In *Protein Modificomics*; Elsevier, 2019; pp 229–280. https://doi.org/10.1016/B978-0-12-811913-6.00010-2.

(69) Baldensperger, T.; Eggen, M.; Kappen, J.; Winterhalter, P. R.; Pfirrmann, T.; Glomb, M. A. Comprehensive Analysis of Posttranslational Protein Modifications in Aging of Subcellular Compartments. *Sci Rep* **2020**, *10* (1), 7596. https://doi.org/10.1038/s41598-020-64265-0.

(70) Vistoli, G.; De Maddis, D.; Cipak, A.; Zarkovic, N.; Carini, M.; Aldini, G. Advanced Glycoxidation and Lipoxidation End Products (AGEs and ALEs): An Overview of Their Mechanisms of Formation. *Free Radical Research* **2013**, *47* (sup1), 3–27. https://doi.org/10.3109/10715762.2013.815348.

(71) Cho, S.-J.; Roman, G.; Yeboah, F.; Konishi, Y. The Road to Advanced Glycation End Products: A Mechanistic Perspective. *CMC* **2007**, *14* (15), 1653–1671. https://doi.org/10.2174/092986707780830989.

(72) Bobalova, J.; Strouhalova, D.; Bobal, P. Common Post-Translational Modifications (PTMs) of Proteins: Analysis by Up-to-Date Analytical Techniques with an Emphasis on Barley. *J. Agric. Food Chem.* **2023**, *71* (41), 14825–14837. https://doi.org/10.1021/acs.jafc.3c00886.

(73) Ahmed, M. U.; Thorpe, S. R.; Baynes, J. W. Identification of N Epsilon-Carboxymethyllysine as a Degradation Product of Fructoselysine in Glycated Protein. *J Biol Chem* **1986**, *261* (11), 4889–4894.

(74) Li, J.; Liu, D.; Sun, L.; Lu, Y.; Zhang, Z. Advanced Glycation End Products and Neurodegenerative Diseases: Mechanisms and Perspective. *Journal of the Neurological Sciences* **2012**, *317* (1–2), 1–5. https://doi.org/10.1016/j.jns.2012.02.018.

(75) Uchiki, T.; Weikel, K. A.; Jiao, W.; Shang, F.; Caceres, A.; Pawlak, D.; Handa, J. T.; Brownlee, M.; Nagaraj, R.; Taylor, A. Glycation-altered Proteolysis as a Pathobiologic Mechanism That Links Dietary Glycemic Index, Aging, and Age-related Disease (in Nondiabetics). *Aging Cell* **2012**, *11* (1), 1–13. https://doi.org/10.1111/j.1474-9726.2011.00752.x.

(76) Ramazi, S.; Zahiri, J. Post-Translational Modifications in Proteins: Resources, Tools and Prediction Methods. *Database* **2021**, *2021*, baab012. https://doi.org/10.1093/database/baab012.

(77) Hwang, J.-T.; Lee, A.; Kho, C. Ubiquitin and Ubiquitin-like Proteins in Cancer, Neurodegenerative Disorders, and Heart Diseases. *IJMS* **2022**, *23* (9), 5053. https://doi.org/10.3390/ijms23095053.

(78) Abeywardana, T.; Pratt, M. R. Using Chemistry to Investigate the Molecular Consequences of Protein Ubiquitylation. *ChemBioChem* **2014**, *15* (11), 1547–1554. https://doi.org/10.1002/cbic.201402117.

(79) Henneberg, L. T.; Schulman, B. A. Decoding the Messaging of the Ubiquitin System Using Chemical and Protein Probes. *Cell Chemical Biology* **2021**, *28* (7), 889–902. https://doi.org/10.1016/j.chembiol.2021.03.009.

(80) Gui, W.; Davidson, G. A.; Zhuang, Z. Chemical Methods for Protein Site-Specific Ubiquitination. *RSC Chem. Biol.* **2021**, *2* (2), 450–467. https://doi.org/10.1039/D0CB00215A.

(81) Popovic, D.; Vucic, D.; Dikic, I. Ubiquitination in Disease Pathogenesis and Treatment. *Nat Med* **2014**, *20* (11), 1242–1253. https://doi.org/10.1038/nm.3739.

(82) Schmidt, M. F.; Gan, Z. Y.; Komander, D.; Dewson, G. Ubiquitin Signalling in Neurodegeneration: Mechanisms and Therapeutic Opportunities. *Cell Death Differ* **2021**, *28* (2), 570–590. https://doi.org/10.1038/s41418-020-00706-7.

(83) Sirangelo, I.; Iannuzzi, C. Understanding the Role of Protein Glycation in the Amyloid Aggregation Process. *IJMS* **2021**, *22* (12), 6609. https://doi.org/10.3390/ijms22126609.

(84) Balana, A. T.; Levine, P. M.; Mukherjee, S.; Pedowitz, N. J.; Moon, S. P.; Takahashi, T. T.; Becker, C. F. W.; Pratt, M. R. O-GlcNAcylation of Small Heat Shock Proteins Enhances Their Anti-Amyloid Chaperone Activity. December 10, 2019. https://doi.org/10.1101/869909.

(85) Levine, P. M.; Galesic, A.; Balana, A. T.; Mahul-Mellier, A.-L.; Navarro, M. X.; De Leon, C. A.; Lashuel, H. A.; Pratt, M. R. α-Synuclein O-GlcNAcylation Alters Aggregation and Toxicity, Revealing Certain Residues as Potential Inhibitors of Parkinson's Disease. *Proc. Natl. Acad. Sci. U.S.A.* **2019**, *116* (5), 1511–1519. https://doi.org/10.1073/pnas.1808845116.

(86) Wördehoff, M.; Hoyer, W. α-Synuclein Aggregation Monitored by Thioflavin T Fluorescence Assay. *BIO-PROTOCOL* **2018**, *8* (14). https://doi.org/10.21769/BioProtoc.2941.

(87) Chakroun, T.; Evsyukov, V.; Nykänen, N.-P.; Höllerhage, M.; Schmidt, A.; Kamp, F.; Ruf, V. C.; Wurst, W.; Rösler, T. W.; Höglinger, G. U. Alpha-Synuclein Fragments Trigger Distinct Aggregation Pathways. *Cell Death Dis* **2020**, *11* (2), 84. https://doi.org/10.1038/s41419-020-2285-7.

(88) Giehm, L.; Otzen, D. E. Strategies to Increase the Reproducibility of Protein Fibrillization in Plate Reader Assays. *Analytical Biochemistry* **2010**, *400* (2), 270–281. https://doi.org/10.1016/j.ab.2010.02.001.

(89) Murray, A. N.; Palhano, F. L.; Bieschke, J.; Kelly, J. W. Surface Adsorption Considerations When Working with Amyloid Fibrils in Multiwell Plates and Eppendorf Tubes. *Protein Science* **2013**, *22* (11), 1531–1541. https://doi.org/10.1002/pro.2339.

(90) Iyer, A.; Roeters, S. J.; Schilderink, N.; Hommersom, B.; Heeren, R. M. A.; Woutersen, S.; Claessens, M. M. A. E.; Subramaniam, V. The Impact of N-Terminal Acetylation of α-Synuclein on Phospholipid Membrane Binding and Fibril Structure. *Journal of Biological Chemistry* **2016**, *291* (40), 21110–21122. https://doi.org/10.1074/jbc.M116.726612.

(91) Iyer, A.; Sidhu, A.; Subramaniam, V. How Important Is the N-Terminal Acetylation of Alpha-Synuclein for Its Function and Aggregation into Amyloids? *Front. Neurosci.* **2022**, *16*, 1003997. https://doi.org/10.3389/fnins.2022.1003997.

(92) Ziaunys, M.; Sakalauskas, A.; Mikalauskaite, K.; Smirnovas, V. Polymorphism of Alpha-Synuclein Amyloid Fibrils Depends on Ionic Strength and Protein Concentration. *IJMS* **2021**, *22* (22), 12382. https://doi.org/10.3390/ijms222212382.

(93) Tofaris, G. K.; Kim, H. T.; Hourez, R.; Jung, J.-W.; Kim, K. P.; Goldberg, A. L. Ubiquitin Ligase Nedd4 Promotes α-Synuclein Degradation by the Endosomal–Lysosomal Pathway. *Proc. Natl. Acad. Sci. U.S.A.* **2011**, *108* (41), 17004–17009. https://doi.org/10.1073/pnas.1109356108.

(94) *P22515 · UBA1_YEAST*. UniProt. https://www.uniprot.org/uniprotkb/P22515/entry (accessed 2024-07-15).

(95) *P62837 · UB2D2_HUMAN*. UniProt. https://www.uniprot.org/uniprotkb/P62837/entry (accessed 2024-07-15).

(96) *Recombinant Human His6-NEDD4 Protein, CF*. Bio-Techne Ltd. https://www.rndsystems.com/products/recombinant-human-his6-nedd4-protein-cf_e3-290 (accessed 2024-07-15).

(97) *Ubiquitin*. Chemie.de. https://www.chemie.de/lexikon/Ubiquitin.html (accessed 2024-07-15).

(98) Rott, R.; Szargel, R.; Haskin, J.; Bandopadhyay, R.; Lees, A. J.; Shani, V.; Engelender, S. α-Synuclein Fate Is Determined by USP9X-Regulated Monoubiquitination. *Proc. Natl. Acad. Sci. U.S.A.* **2011**, *108* (46), 18666–18671. https://doi.org/10.1073/pnas.1105725108.

(99) Sun, M.; Zhang, X. Current Methodologies in Protein Ubiquitination Characterization: From Ubiquitinated Protein to Ubiquitin Chain Architecture. *Cell Biosci* **2022**, *12* (1), 126. https://doi.org/10.1186/s13578-022-00870-y.

(100) Nonaka, T.; Iwatsubo, T.; Hasegawa, M. Ubiquitination of α-Synuclein. *Biochemistry* **2005**, *44* (1), 361–368. https://doi.org/10.1021/bi0485528.

7 Appendix

Ligation:

The Ligation reaction of all variants was monitored via LCMS (Figure 58 to Figure 63).

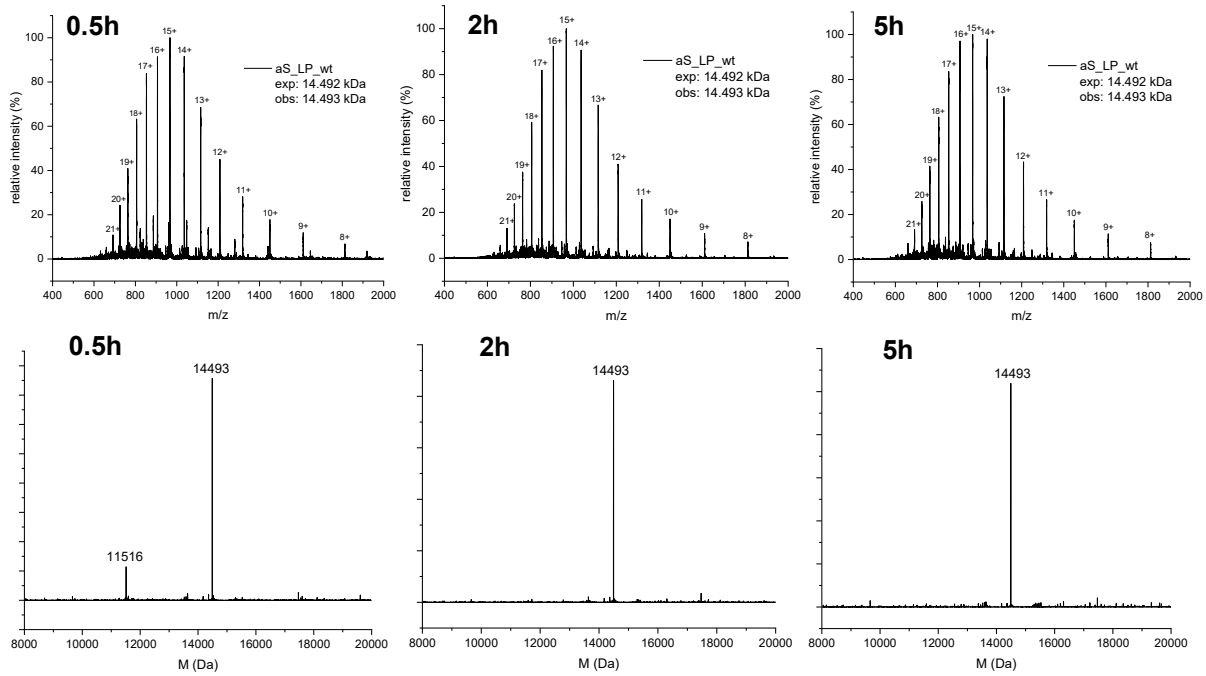

*Figure 58 Ligation reaction monitoring of **G1a** via LCMS after 0.5h, 2h, and 5h.*

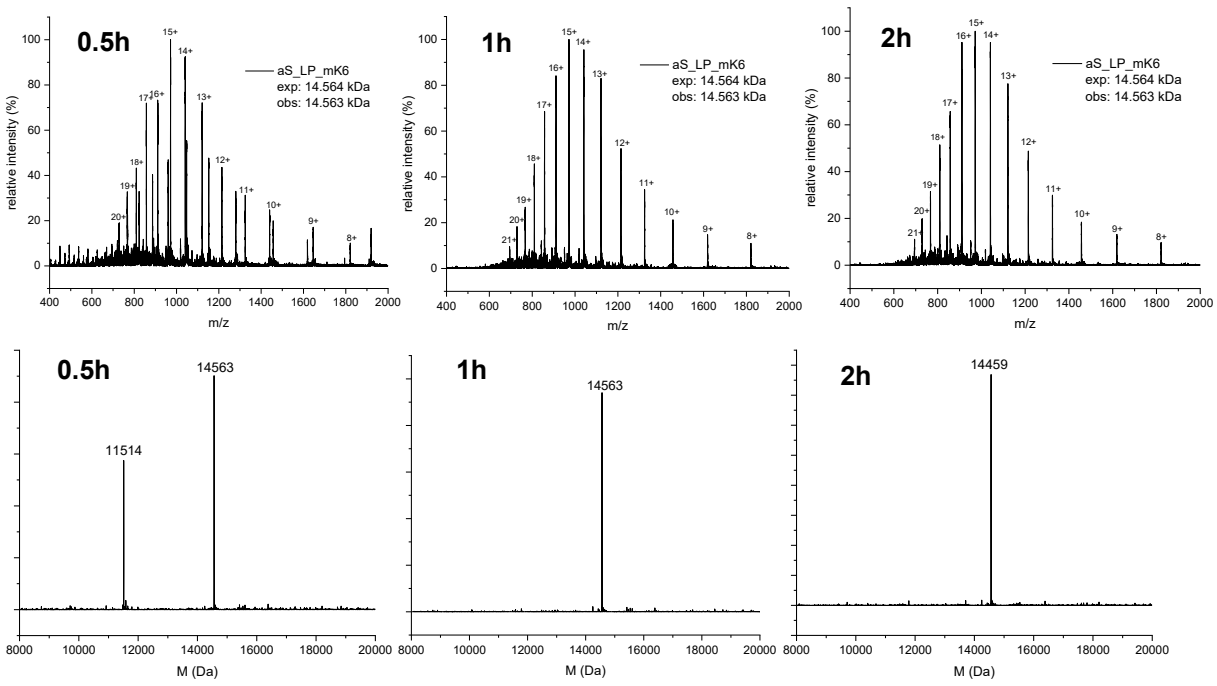

*Figure 59 Ligation reaction monitoring of **G1b** via LCMS after 0.5h, 1h, and 2h.*

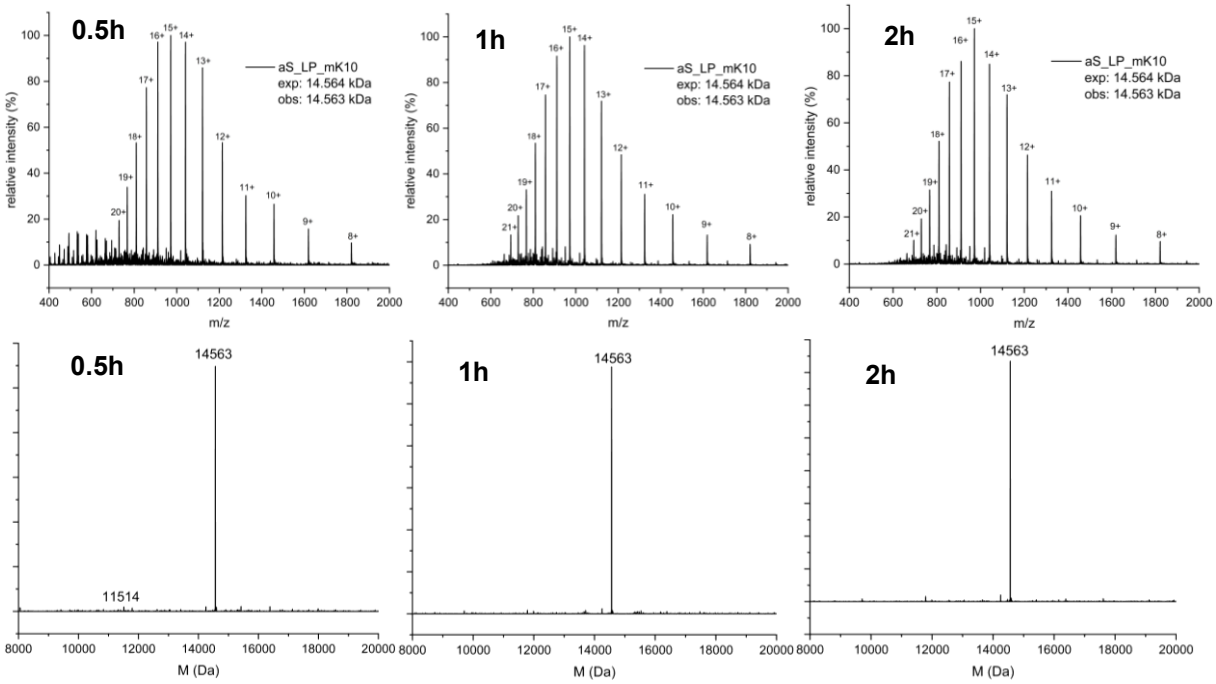

*Figure 60 Ligation reaction monitoring of **G1c** via LCMS after 0.5h, 1h, and 2h.*

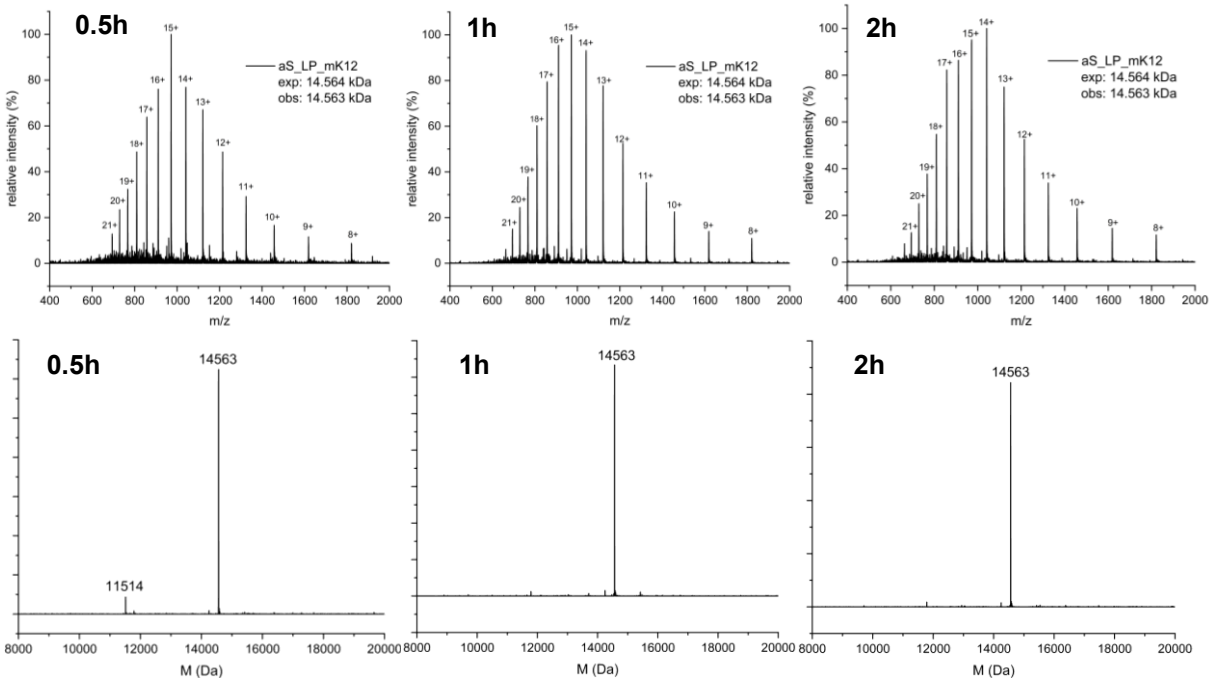

*Figure 61 Ligation reaction monitoring of **G1d** via LCMS after 0.5h, 1h, and 2h.*

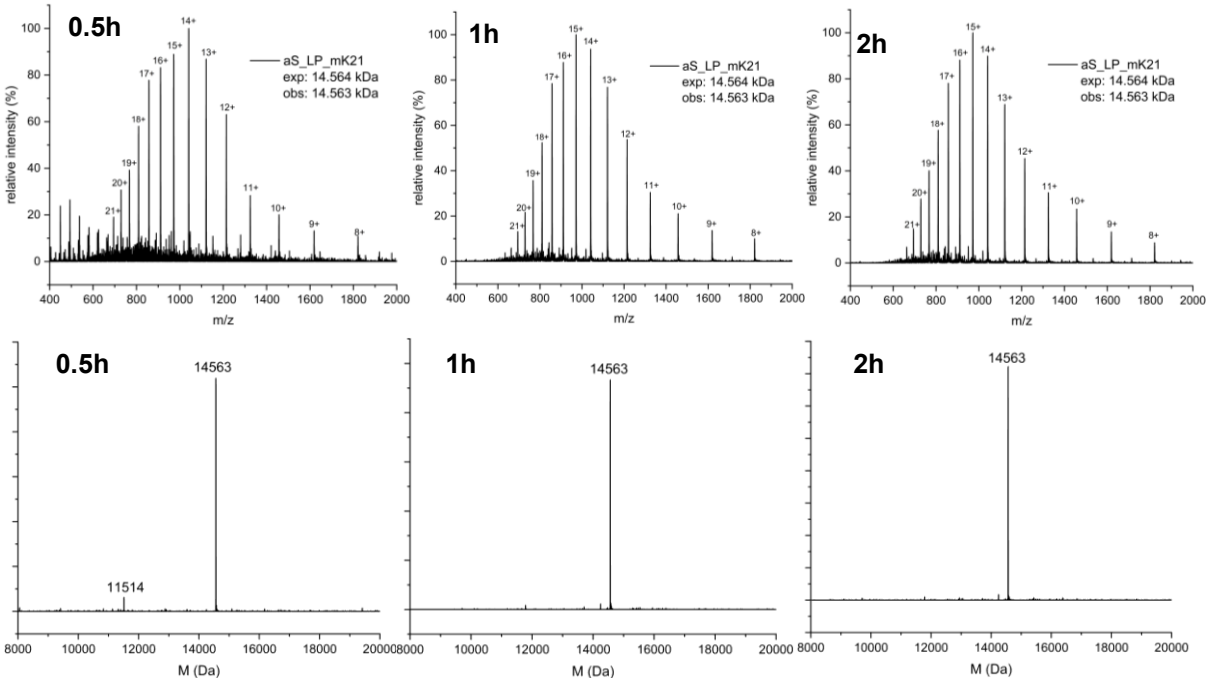

*Figure 62 Ligation reaction monitoring of **G1e** via LCMS after 0.5h, 1h, and 2h.*

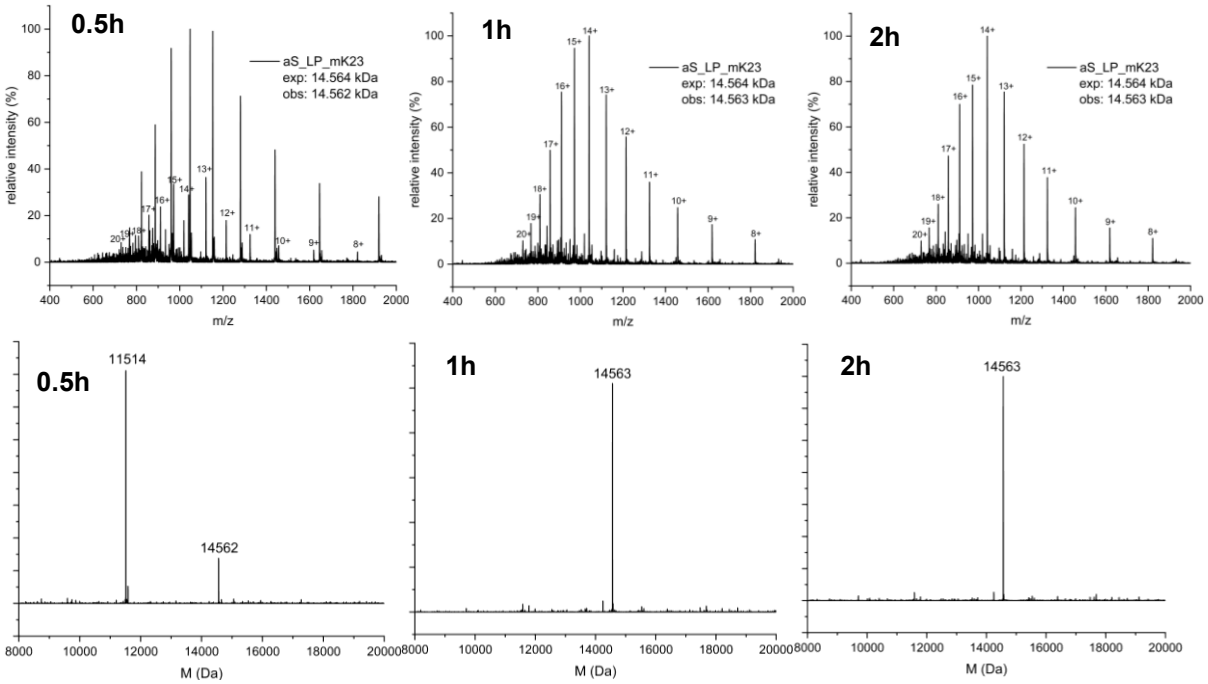

*Figure 63 Ligation reaction monitoring of **G1f** via LCMS after 0.5h, 1h, and 2h.*

HRMS:

The HRMS measurements of **G2a-e** (Figure 64 to Figure 66) were performed at a time interval to **G2f**. Other substances were also analysed at the institute, so the spectra are probably contaminated by another substance. Since the variants are otherwise very similar and the previously measured ESI-MS are also very similar to each other, this most likely explains why the spectrum of **G2f** (Figure 37) looks much purer.

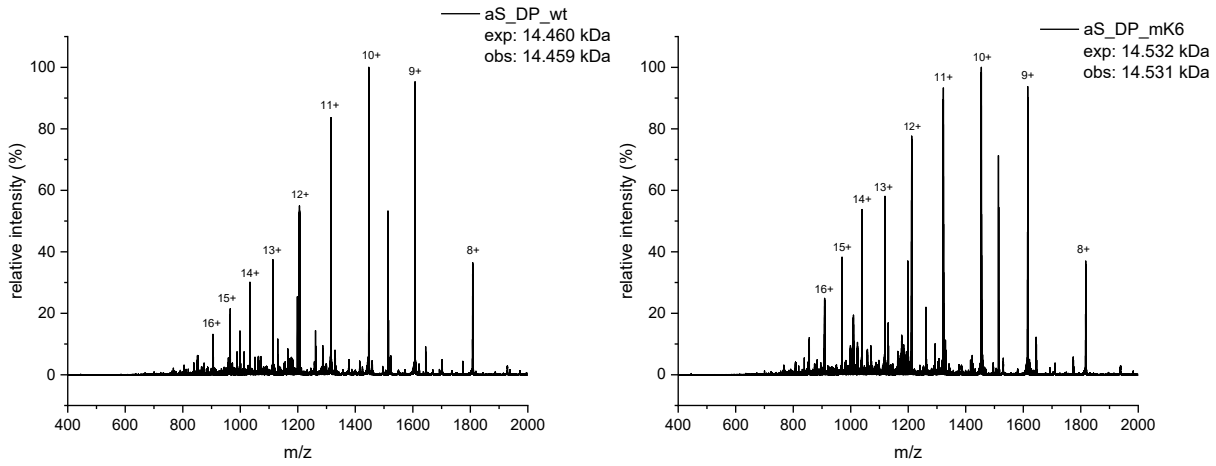

*Figure 64 HRMS after desulfurization of full-length αS variants **G2a** (left) and **G2b** (right).*

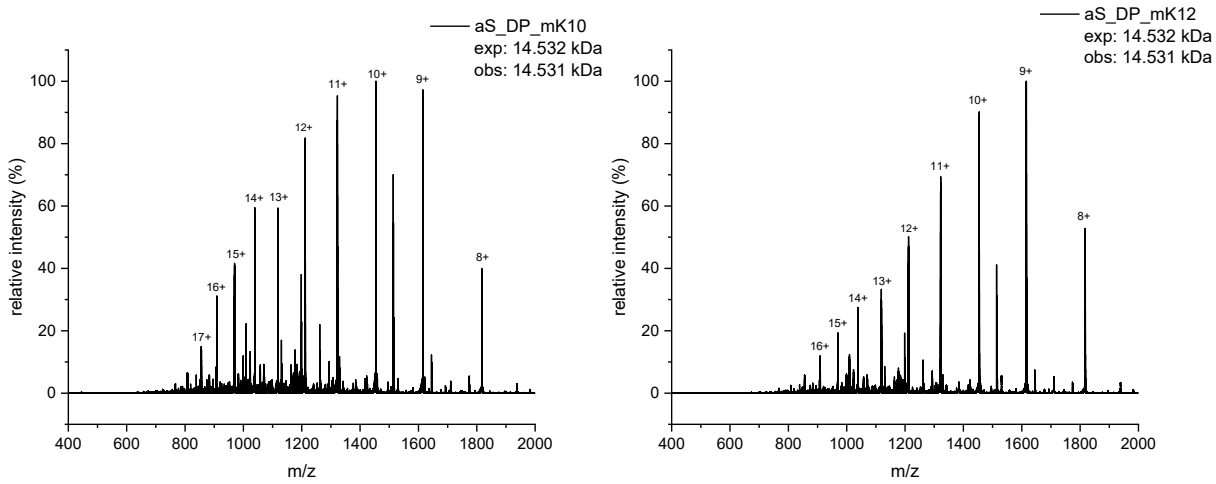

*Figure 65 HRMS after desulfurization of full-length αS variants **G2c** (left) and **G2d** (right).*

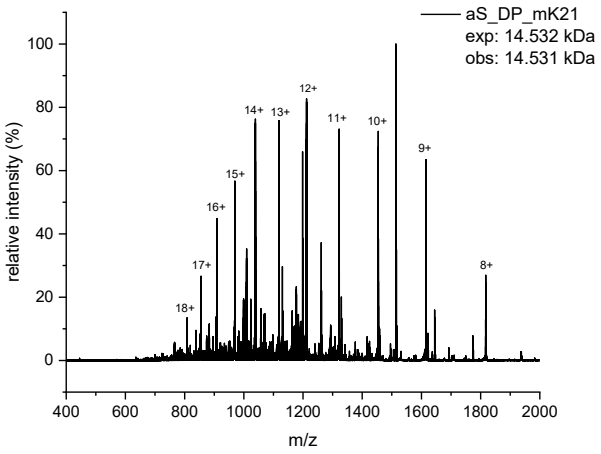

Figure 66 HRMS after desulfurization of full-length αS variant ***G2e****.*

ThT Assay:

In Figure 67 to Figure 69 the ThT assay triplicate measurements of all variants **G2a-f** can be seen.

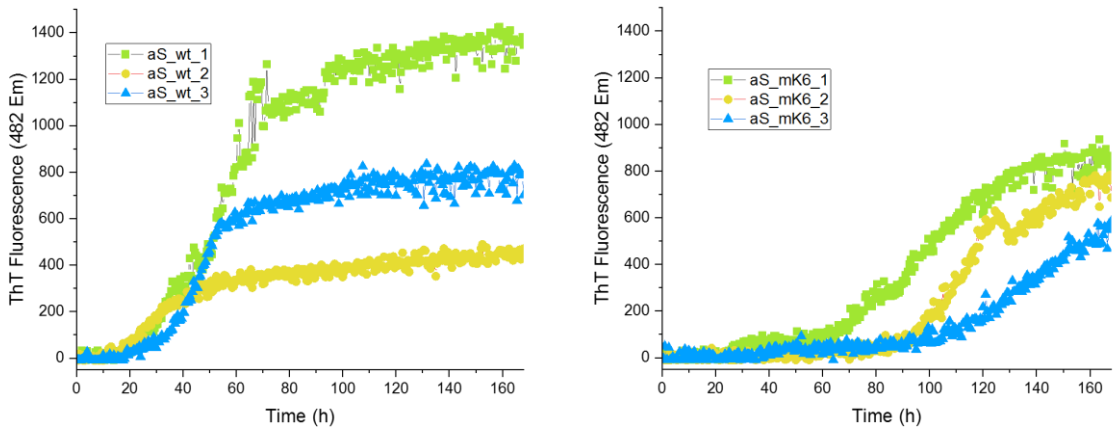

*Figure 67 ThT Assay: Triplicates of αS(1-140)^{wt} (**G2a**) (left) and αS(1-140)^{mK6} (**G2b**) (right).*

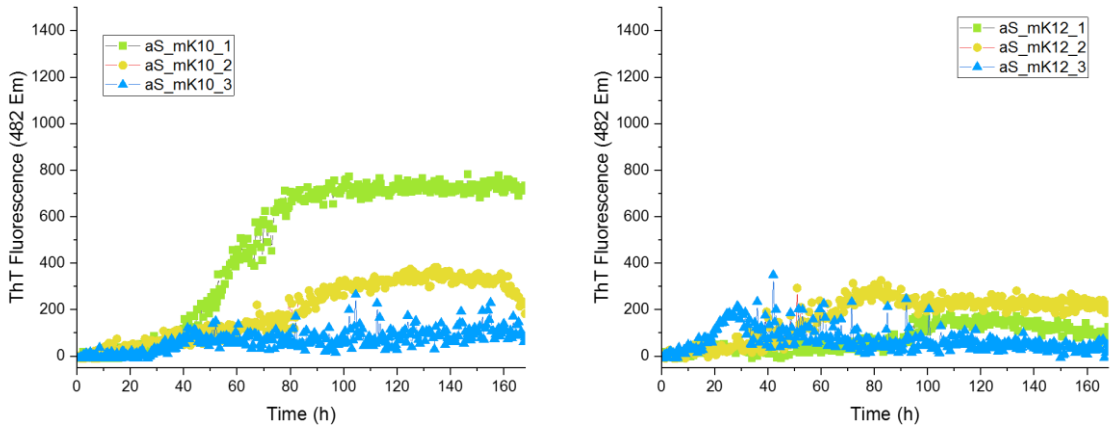

*Figure 68 ThT Assay: Triplicates of αS(1-140)^{mK10} (**G2c**) (left) and αS(1-140)^{mK12} (**G2d**) (right).*

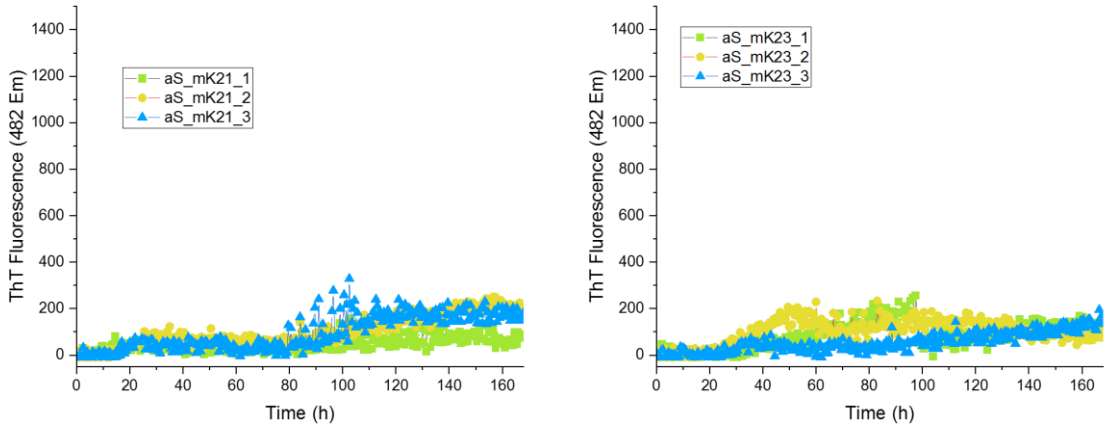

*Figure 69 ThT Assay: Triplicates of αS(1-140)^{mK21} (**G2e**) (left) and αS(1-140)^{mK23} (**G2f**) (right).*

Ubiquitination Assay:

The SDS PAGEs of the ubiquitination assay from wild type (**G2a**) without E3 with and without ATP are shown in Figure 70. In Figure 71 the results for the ubiquitination assay with E3 with and without ATP are shown. They were stained with Coomassie.

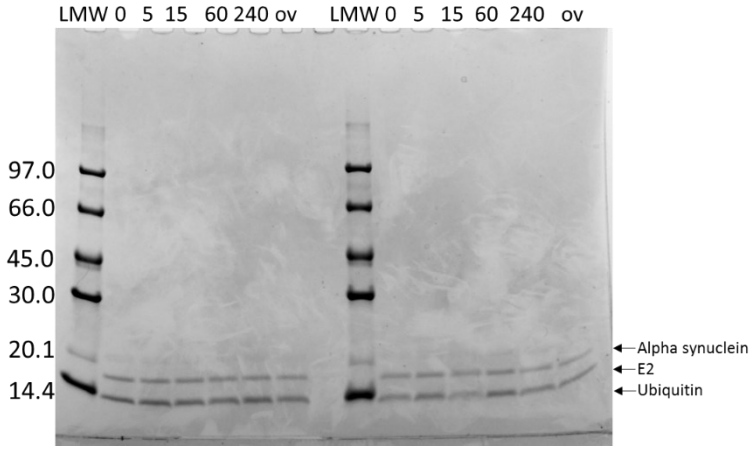

Figure 70 Ubiquitination assay without E3: without ATP (left) and with ATP (right).

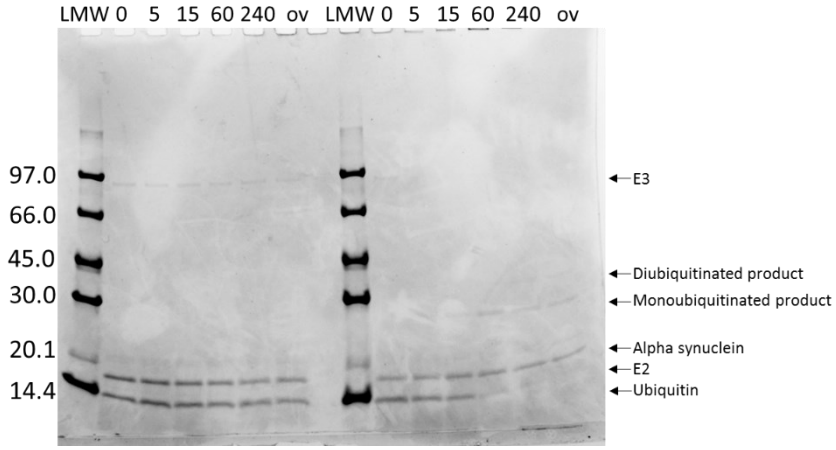

Figure 71 Ubiquitination assay with E3: without ATP (left) and with ATP (right).